THE UNIVERSITY OF MICHIGAN

COLLEGE OF ENGINEERING
Department of Chemical and Metallurgical Engineering
Department of Mechanical Engineering

INVESTIGATION OF LIQUID METAL BOILING HEAT TRANSFER

Richard E. Balzhiser
Project Director

Robert E. Barry
Bruce F. Caswell
Herman Merte, Jr.
Andrew Padilla, Jr.
Lowell R. Smith

ORA Project 05750

under contract with:

FLIGHT ACCESSORIES LABORATORY
AERONAUTICAL SYSTEMS DIVISION
AIR FORCE SYSTEMS COMMAND
UNITED STATES AIR FORCE
WRIGHT-PATTERSON AIR FORCE BASE, OHIO
CONTRACT NO. AF 33(657)-11548

administered through:

OFFICE OF RESEARCH ADMINISTRATION ANN ARBOR

February 1965

FOREWORD

This report summarizes progress on Contract AF 33(657)-11548 from its inception to December 1964. This contract provides for continuation of the experimental programs initiated under the original contract between the University of Michigan and ASD. The investigation is being conducted in the Liquid Metals Laboratory of the Department of Chemical and Metallurgical Engineering. Professor Richard E. Balzhiser is serving as Project Director at the University of Michigan. Messrs. Barry, Caswell, Padilla and Smith, all graduate students in chemical engineering are responsible for specific portions of the program.

Progress on the agravic studies with boiling mercury will be summarized in these reports. This work is being conducted by Professor Herman Merte, Jr. and Mr. Samuel Walker in the Mechanical Engineering Department.

Mr. Charles L. Delaney is project engineer for ASD.

ABSTRACT

Critical heat flux determinations have been completed for sodium and rubidium. Values fall above the predictions based on hydrodynamic considerations just as the earlier potassium results did. A modified design for the film boiling apparatus has been completed which avoids the difficulties encountered with the use of condensing liquid metals as a heat source.

Forced circulation studies were terminated after obtaining additional two phase flow data (reported herein) to repair the ruptured bellows in the test section. The difficulties in obtaining continuous flow since that time are discussed and conclusions reached regarding the use of zirconium as a hot trapping medium are cited. Recent cold filtering procedures, excluding the hot trap, have provided encouraging results and prolonged operation is now projected for late February.

Agravic results for mercury have been obtained in the nucleate and film boiling regimes. Accelerations up to 15 times that of normal gravity have been studied with definite effects on the heat transfer coefficient observed.

TABLE OF CONTENTS

LIST OF FIGURES

SYMBOLS

C	Constant in equation for Fanning friction factor, used in Equation (11)
C_p	Heat capacity
D	Tube inside diameter, ft.
f	Two-phase friction factor defined by Equation (6)
f_1	Fanning friction factor for single phase flow
f_g	Moody single-phase friction factor for all-vapor flow at conditions of same total flow rate and temperature as two-phase flow
f_I	Two-phase friction factor for isothermal flow
G	Total mass velocity, lbm/hr/sq ft
g	Acceleration of gravity, ft/sec/sec
g_c	Gravitational conversion constant, 32.17 lbm ft/lbf/sec/sec
h	Heat transfer coefficient
k	Thermal conductivity
L	Length along flow channel, ft.
N	Gamma-ray count rate for two-phase flow, counts/min
N_ℓ	Gamma-ray count rate for all-liquid flow, counts/min
N_g	Gamma-ray count rate for all-vapor flow, counts/min
N_μ	Ros(50) dimensionless liquid viscosity influence number, defined by Equation (20)
Nu	Nusselt Number
P	Absolute pressure, lbf/sq in
Pe	Peclet Number
$-dP_a$	Differential pressure drop due to acceleration effects, lbf/sq in
$-dP_f$	Differential pressure drop due to friction, lbf/sq in

$\Delta P/\Delta L$	Two-phase pressure gradient, lbf/sq in/ft
$(\Delta P/\Delta L)_{\ell(\text{or } g)}$	Pressure gradient that would occur if the liquid (or vapor) were passed through the tube at its own flow rate, lbf/sq in/ft
q	Local heat flux
q_w	Heat flux at wall
R	Tube radius
r	Radial distance from center line
Re_g	Vapor phase Reynolds number based on pipe diameter
S	Velocity slip ratio, given by Equation (8)
T	Local fluid temperature
T_b	Bulk temperature of fluid
T_w	Wall temperature
U	Local fluid velocity
U_b	Bulk velocity
V	Local superficial two-phase mixture velocity, ft/sec
V_g	Average vapor velocity, based on cross-sectional area occupied by vapor, ft/sec
V_ℓ	Average liquid velocity, based on cross-sectional area occupied by liquid, ft/sec
X	Lockhart-Martinelli (35) two-phase flow parameter defined by Equation (9)
X_{tt}	Lockhart-Martinelli X parameter for liquid turbulent-vapor turbulent flow, given by Equation (10)
X_{vt}	Lockhart-Martinelli X parameter for liquid viscous-vapor turbulent flow, given by Equation (11)
x	Quality (vapor mass fraction)
y	Distance from tube wall
α	Void fraction (volume fraction vapor)
θ	Angle of inclination of flow channel from horizontal, degrees

μ	Viscosity, lbm/ft/hr
ρ	Density, lbm/cu ft
σ	Surface tension, dynes/cm
τ	Local shear stress in fluid
τ_w	Shear stress at wall
ϵ_m	Coefficient of eddy diffusivity for momentum
ϵ_h	Coefficient of eddy diffusivity for heat transfer

SUBSCRIPTS

g	Vapor phase
ℓ	Liquid phase

SUPERSCRIPT

-	Average value

POOL BOILING STUDIES

Bruce F. Caswell

The burnout heat flux was measured for water, sodium and rubidium. These data are presented and compared with the results of other investigators and with some published correlations.

EXPERIMENTAL APPARATUS

The equipment used is somewhat modified from that described by Colver (13). The system was completely repiped as shown in Figure 1. The new piping system is of 316 stainless steel tubing with welded connections wherever possible. All threaded connections are made with Teflon tape. Jamesbury high vacuum ball valves are used as shown in Figure 1. The pressure gauge is an Ashcroft laboratory test gauge with an accuracy of 1/2% of full scale. It has been calibrated against a mercury column with increments of one inch of mercury. The helium supply has a combined oxygen and water content of less than 5 ppm.

The piping system was checked for leaks while under vacuum with a Consolidated Electrodynamics type 24-210 helium leak detector which is sensitive to 1 part helium in 300,000 parts of air and which will measure a leak rate of 10^{-8} atm. cc/sec. For this system this corresponds to a leak rate of 0.01 micron/hour at 1 micron system pressure. The system was checked at the most sensitive setting on the detector and all detectable leaks have been eliminated. The system can be evacuated to 0.1 micron (10^{-4} mm) pressure. While under vacuum the system was heated and outgassed for several days in order to remove adsorbed gases. A flame was applied to the vacuum manifold and other lines to promote desorption. The system was flushed several times with helium. Some difficulty

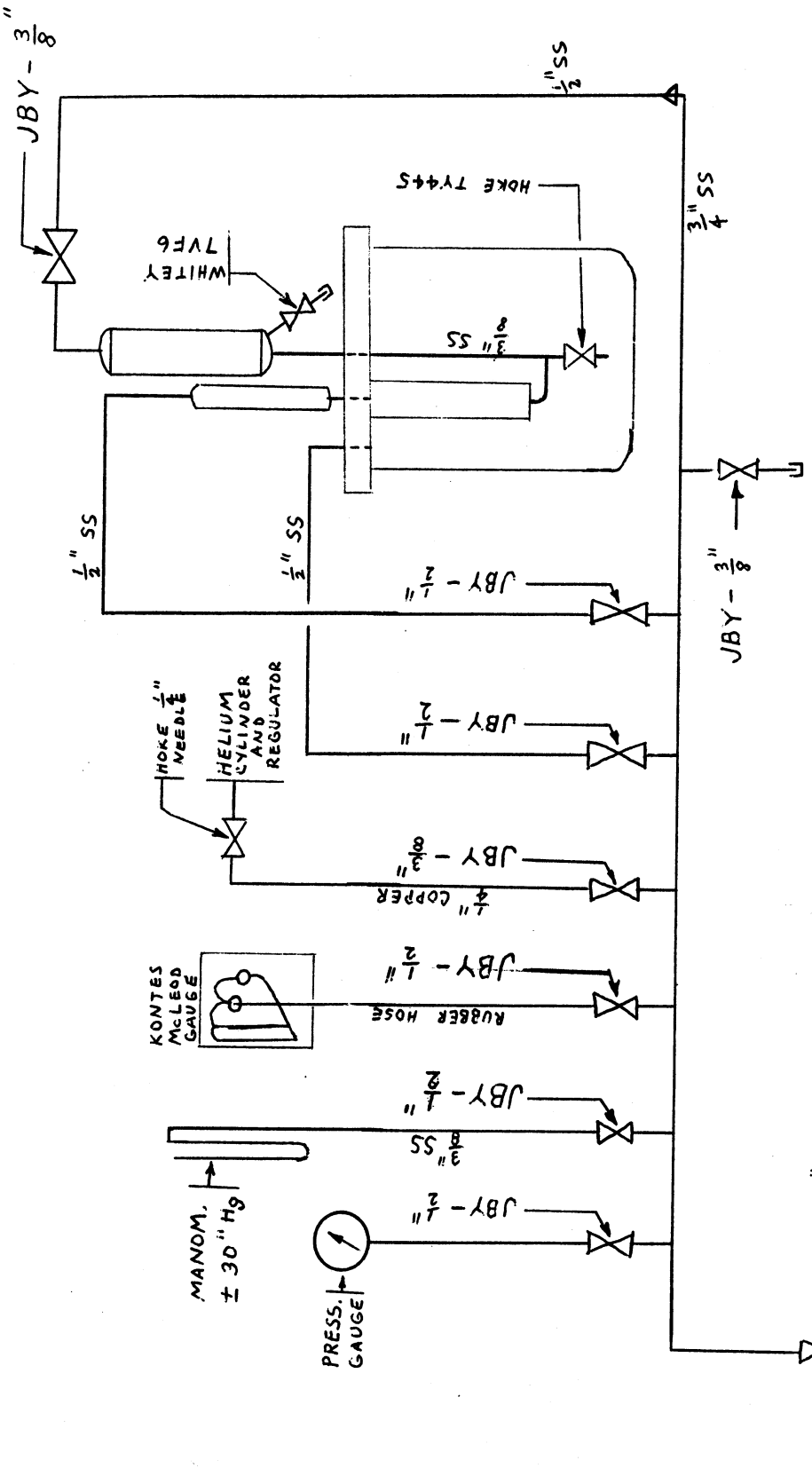

Figure 1. Piping Details

was encountered in sealing the 3/8-inch NPT connection at the boiling tube. Several sealing compounds were tried and a pipe dope called Silver Goop (Crawford Fitting Company, Cleveland, Ohio) was found to be satisfactory.

Five guard heaters were installed around the boiling vessel as shown in Figure 2. These are made of Hevi-Duty type 505 KSP heating coils, useable up to 2200°F, wrapped in 1/8-inch thick asbestos. Each heater is 500 watts capacity. Each is controlled independently with a variable transformer which is adjusted during a run to minimize heat losses from the boiling vessel.

Nine chromel-alumel thermocouples were located around the boiling vessel as shown in Figure 3. These were recorded on a Leeds and Northrup 16 point temperature recorder with a range of 200-2000°F. These readings are used as bases for controlling the guard heaters.

Three chromel-alumel thermocouples on the surface of the boiling tube each were connected to a Leeds and Northrup Speedomax H recorder which has a response time of one second full scale. Each recorder has an alarm circuit which will shut off the power to the boiling tube if a temperature excursion occurs. The alarm circuits are wired in series so that any single one can shut down the main power.

A modified charging system was installed as shown in Figure 4. As shown, the shipping container is connected to the bottom of the boiling vessel. After charging, the shipping container and valves B and C are disconnected from the system. Valve A remains inside the outer jacket of the system during the burnout runs. If desired, due to some difficulty with the system, the contents of the boiling vessel can be transferred to the vessel above the flange without removing the outer jacket or making any connections to the system.

A chromel-alumel thermocouple in a 3/16-inch OD stainless steel sheath was used to measure the bulk liquid temperature. Its vertical position can be adjusted by sliding it through a Conax tube gland. It has been calibrated against a platinum-platinum rhodium (10%) thermocouple which was calibrated by NBS.

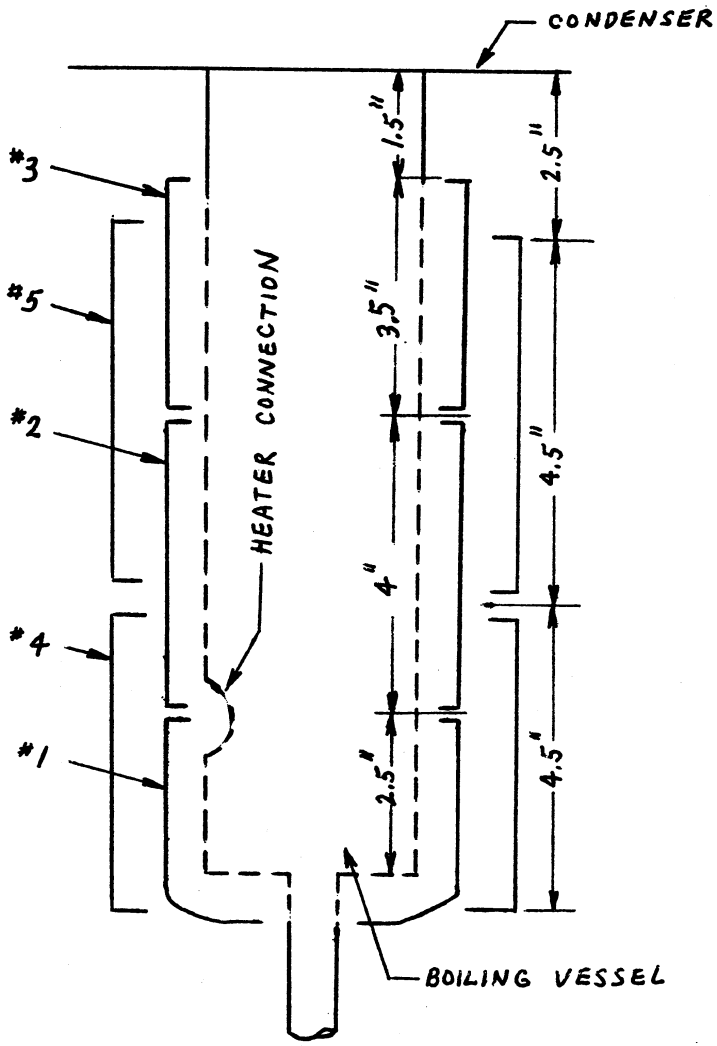

Figure 2. Location of Guard Heaters #1 - #5

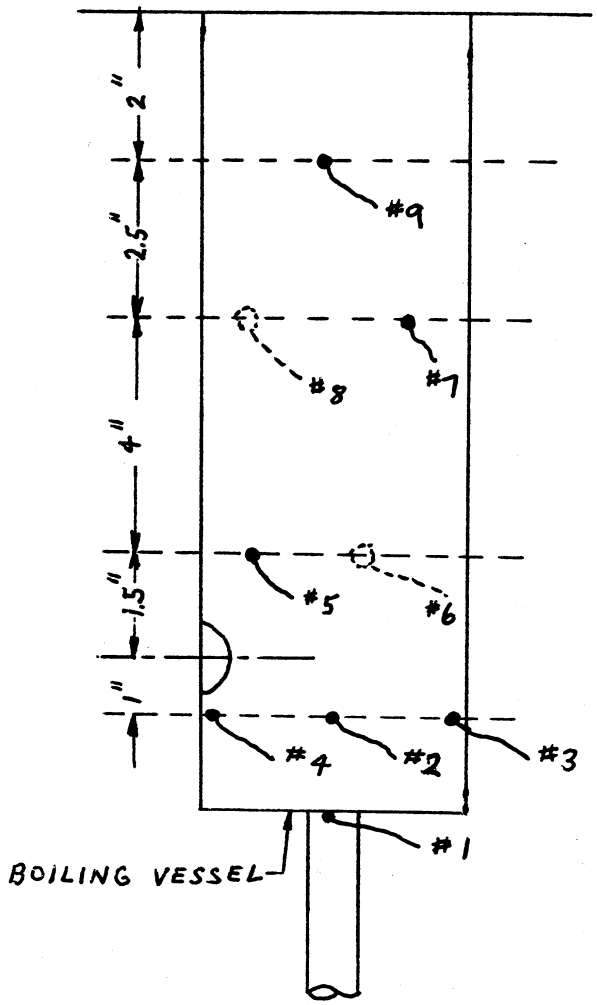

Figure 3. Location of Thermocouples #1 - #9

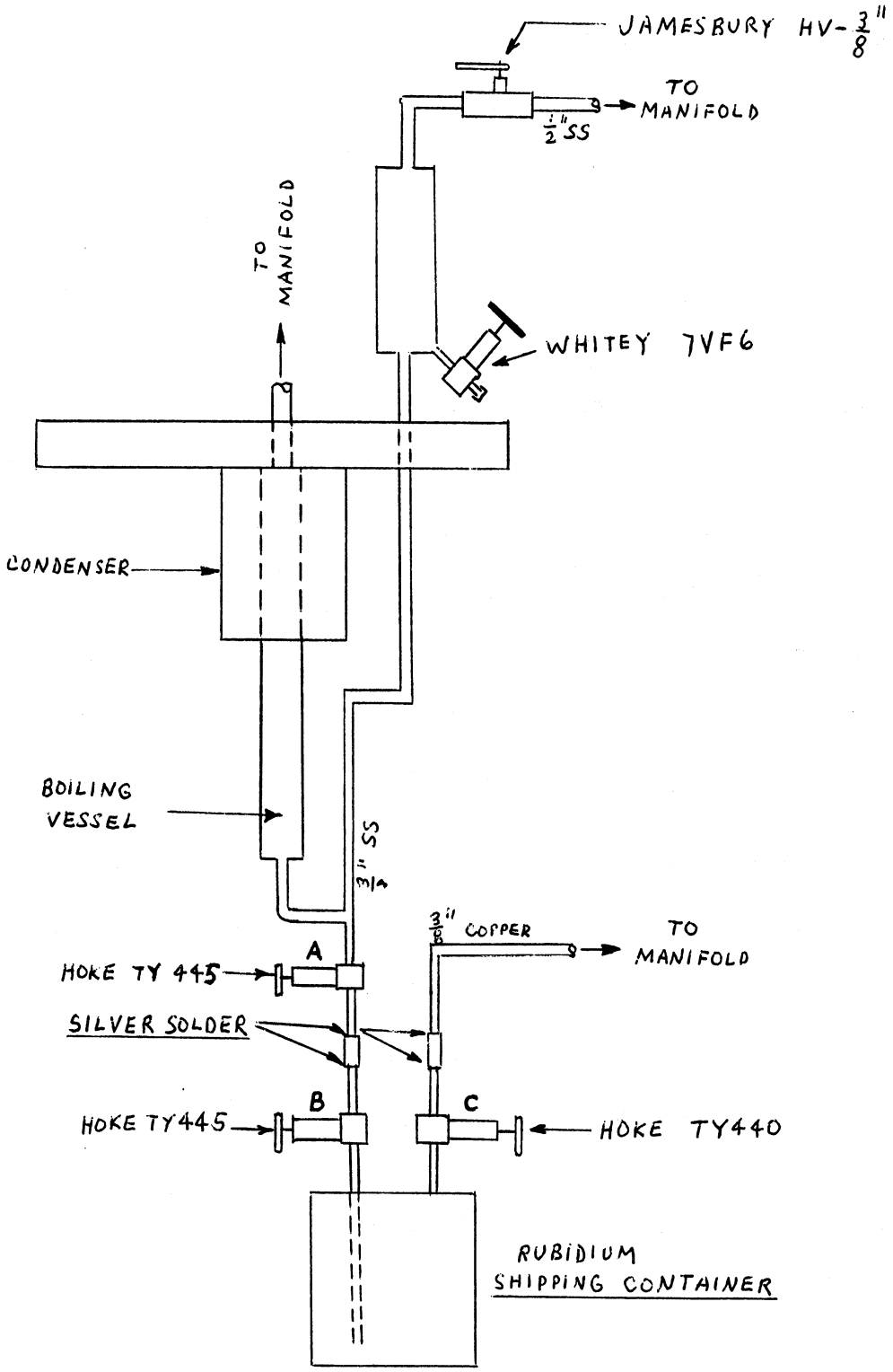

Figure 4. Rubidium Charging System

EXPERIMENTAL PROCEDURE

The procedure used for burnout determinations was similar to that described by Colver (13). The pool was brought up to the boiling point by the guard heaters only. These were adjusted individually so that the temperatures on the outer surface of the vessel were as close as possible to the bulk liquid temperature. In practice they were all maintained within 0-20°F above the bulk temperature to eliminate the possibility of heat being lost through the walls of the vessel which would result in subcooled boiling.

After the system had reached a thermal steady state the main heater power was set at a flux level corresponding to a somewhat lower pressure than the present system pressure. The system pressure was then slowly reduced until burnout occurred. At the burnout point the heater temperature increased by 300°F almost instantly until the alarm circuit shut off the power. This is discussed more thoroughly in the next sections.

BURNOUT RESULTS ON WATER

The burnout heat flux for water was measured at pressures from 15 to 135 psia. The heater used to boil was a 3/8-inch OD by 1 1/4-inch long bayonet tube made of Haynes-25. The design of this heater is described by Colver (13). The data are presented in Table I below.

TABLE I. BURNOUT DATA FOR WATER

Pressure, PSIA	$(q/A)_c$, Btu/(hr)(sq ft)(°F)
15	490,000
15	425,000
15	485,000
35	740,000
80	705,000
118	765,000
118	800,000
135	845,000

The above data follow the relation: $(q/A)_c = 1.70 \times 10^5 \, p^{0.25}$ with the same units as before. These data are plotted in Figure 5 along with the results of Kazakova (30), using a flat plate, Addoms (1), 0.024-inch platinum wire, Van Wijk (57), 0.02 x 6cm platinum wire, and Howell and Bell (26) on a 0.001-inch stainless steel strip. The predictions of Rohrenow-Griffith (49) and Zuber-Tribus (60) are shown as dotted lines on the graph. The data from this work agree well with the data of Addoms (1) and Kazakova (30), but are above the results of Howell and Bell (26) and Van Wijk (57). It is possible that the data of the latter two investigators, since it was taken on thin strips and wires, respectively, represents premature burnout of the heater to some extent. That is, since burnout occurs locally on a heater before general burnout occurs, the heating elements failed at the first point where locallized burnout occurred.

The pressure dependency of the burnout heat flux measured here is lower than that predicted by the Zuber-Tribus correlation but slightly higher than that of the Rohrenow-Griffith correlation as shown on Figure 5.

BURNOUT RESULTS ON SODIUM

Two burnout points for sodium were obtained. These data are tabulated in Table II and are plotted in Figure 6 along with the results of other investigators.

TABLE II

Run	Pressure	$T_{Saturated}$	$(q/A)_c$, Btu/(hr)(sq ft)
A-2	0.80 PSIA	1150 °F	530,000
A-3	2.15 PSIA	1300 °F	845,000

The burnout points were obtained by maintaining a constant heat flux while slowly decreasing the pressure until burnout occurred. In run A-2 the temperature of the heating surface was fluctuating 200 °F just before burnout occurred.

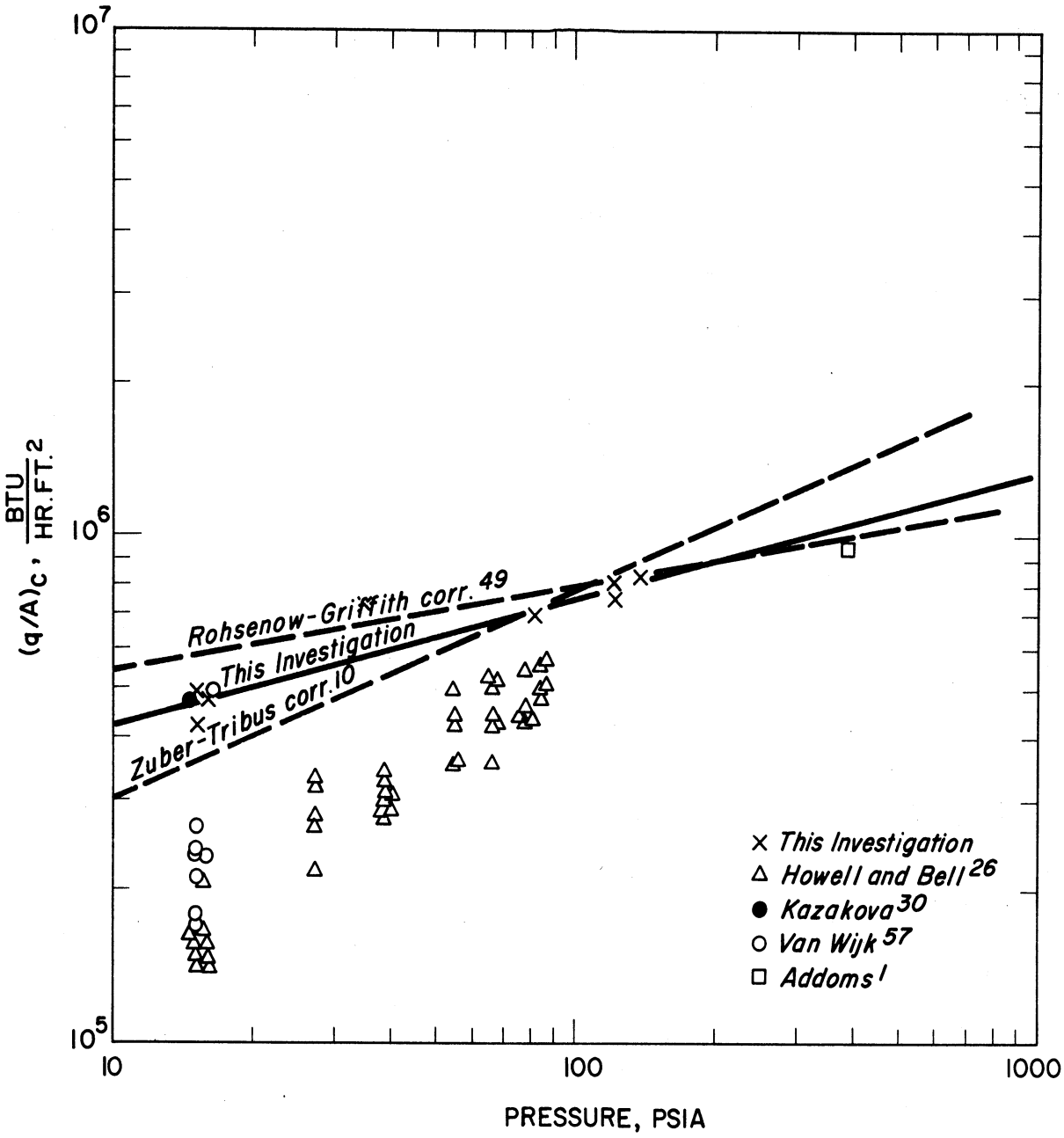

Figure 5. Burnout Data for Water

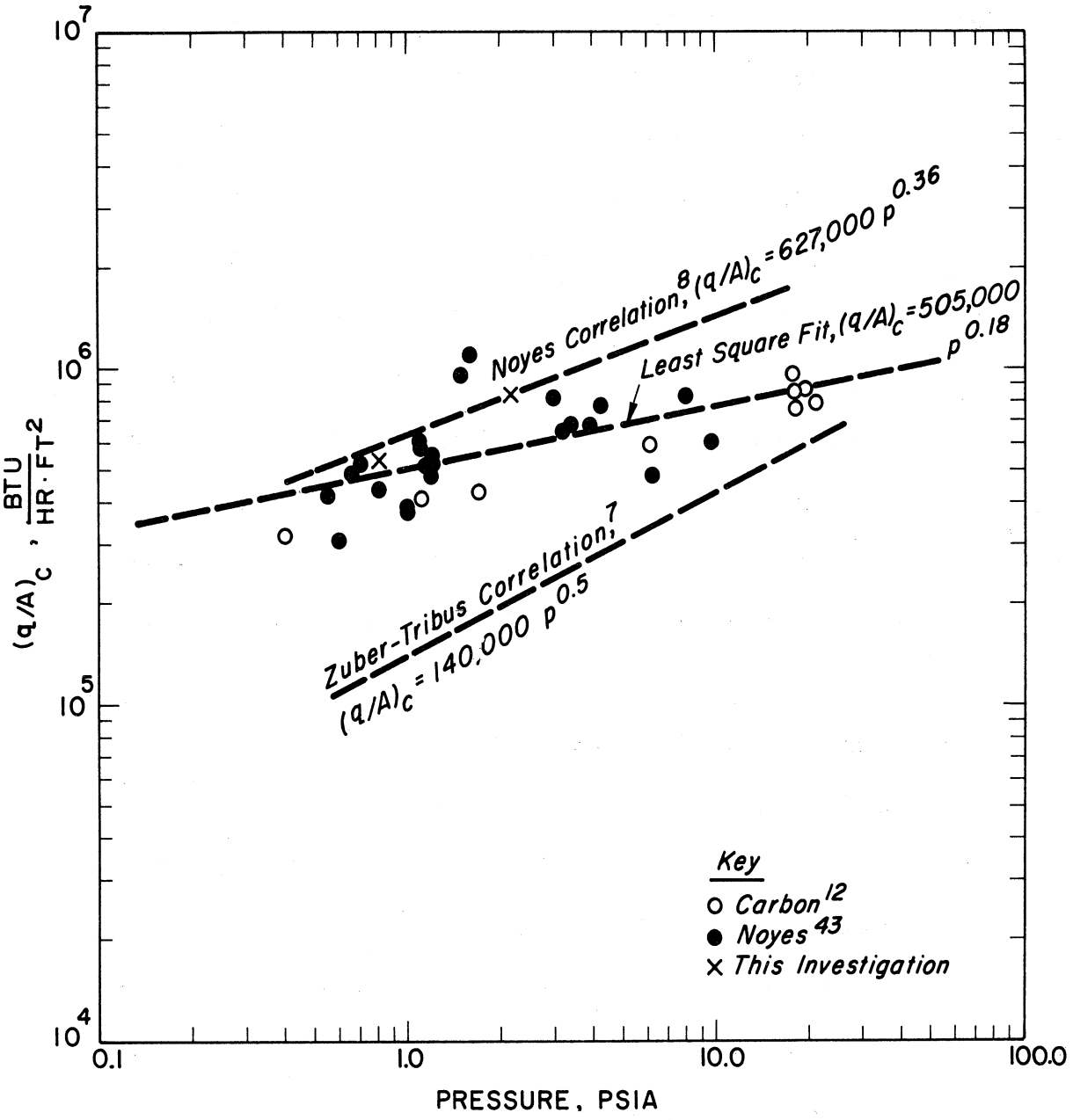

Figure 6. Burnout Data for Sodium

A sudden temperature excursion during which the surface temperature exceeded its normal peak fluctuating temperature by several hundred degrees was used as an indication of burnout. The power was immediately shut off and a second point obtained the following day at a higher pressure using the same boiling tube. No apparent damage had been done to the boiling tube in the first burnout excursion.

In run A-3 a hole was formed in the boiling tube during rapid temperature fluctuations and the run was stopped without being certain that burnout had occurred. The fluctuations were slightly less in magnitude and were accompanied by a gradually using surface temperature. In these respects, this burnout was unlike those observed in earlier runs. The absence of a sudden large temperature excursion introduces some doubt as to whether the actual burnout point had been reached.

Similar behavior was encountered in run A-1 when a gradual temperature excursion occurred which required about a minute to cause the surface temperature to rise close to its melting point. This could be due to a gradual lowering of the sodium level below the tube. Holdup in the condenser may increase at higher pressures resulting in a drop in the liquid level. The pressure level and flux at which it occurred were about the same as in run A-3. It resembled run A-3 except that it was made by increasing the heat flux at constant pressure.

Figure 6 is a plot of all the sodium burnout data known to this author. A linear regression using a least squares method was made of all the data and is shown on the curve. The equation of this line is:

$$(q/A)_c = 505{,}000\ p^{0.18}$$

The theoretical prediction of Zuber and Tribus (60) is also plotted as is the empirical correlation of Noyes (43). Both of these predict a pressure dependency greater than that observed experimentally although the data from this work fall very close to Noyes' correlation, as shown in Figure 6. Noyes'

data were taken on a 1/4-inch OD, horizontal, stainless steel heater. Carbon's (12) data were for a 0.443-inch OD stainless steel heater. The heater used in this work was a 3/8-inch OD by 1 1/4-inch long Haynes-25 horizontal bayonet heater.

BURNOUT RESULTS ON RUBIDIUM

Two burnout points were obtained for rubidium near 3 psia. These are tabulated in Table III.

TABLE III

Run	Pressure	$T_{Sat.}$	$(q/A)_c$, Btu/(hr)(sq ft)
12 A	2.8 psia	10°F	360,000
12 B	3.0 psia	10°F	345,000

Run 12A was made by slowly increasing the heat flux at constant pressure. Run 12B was made by decreasing the pressure while maintaining a constant heat flux.

The bottom and side boiling tube thermocouple records for both runs are shown in Figures 7-10. The bottom thermocouple record for run 12A (Figure 8) shows that the surface temperature fluctuations start to increase just before burnout occurs. On Figures 7 and 8 there are instances of the fluctuations suddenly changing in magnitude for no apparent reason other than "bumping" was heard at these times. On Figure 10 there is evidence of several temperature excursions of at least 20°F outside the normal oscillating pattern. These may indicate locallized temperature excursions from which the heater recovers due to heat conduction away from this location. If this is the case, then some investigators may get lower results due to the inability of their boiling tubes to survive local burnout conditions such as these. In any case, this phenomenon would result in a lower value than the actual critical heat flux of the fluid being studied.

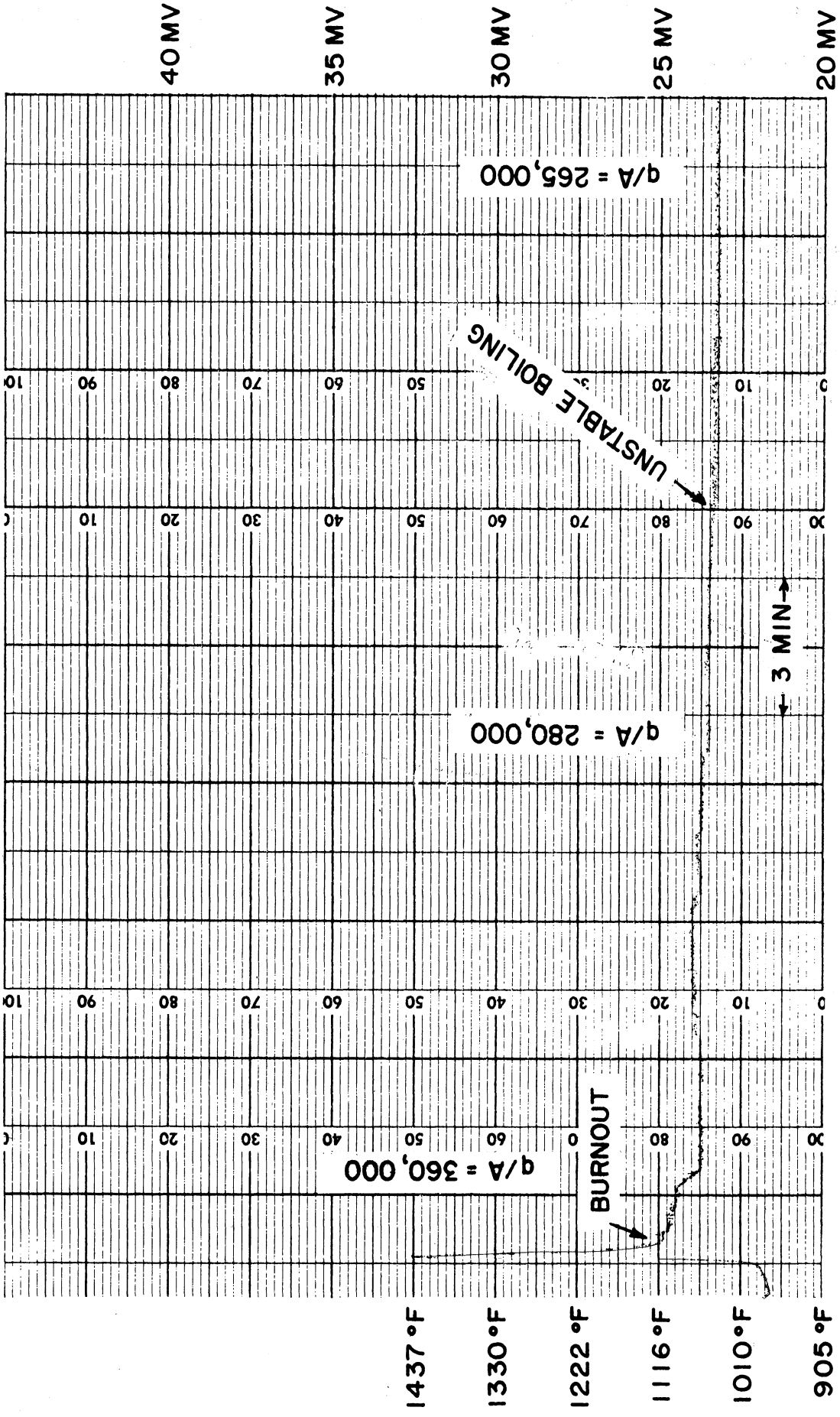

Figure 7. Boiling Tube (side) Temperature Record for Run 12A

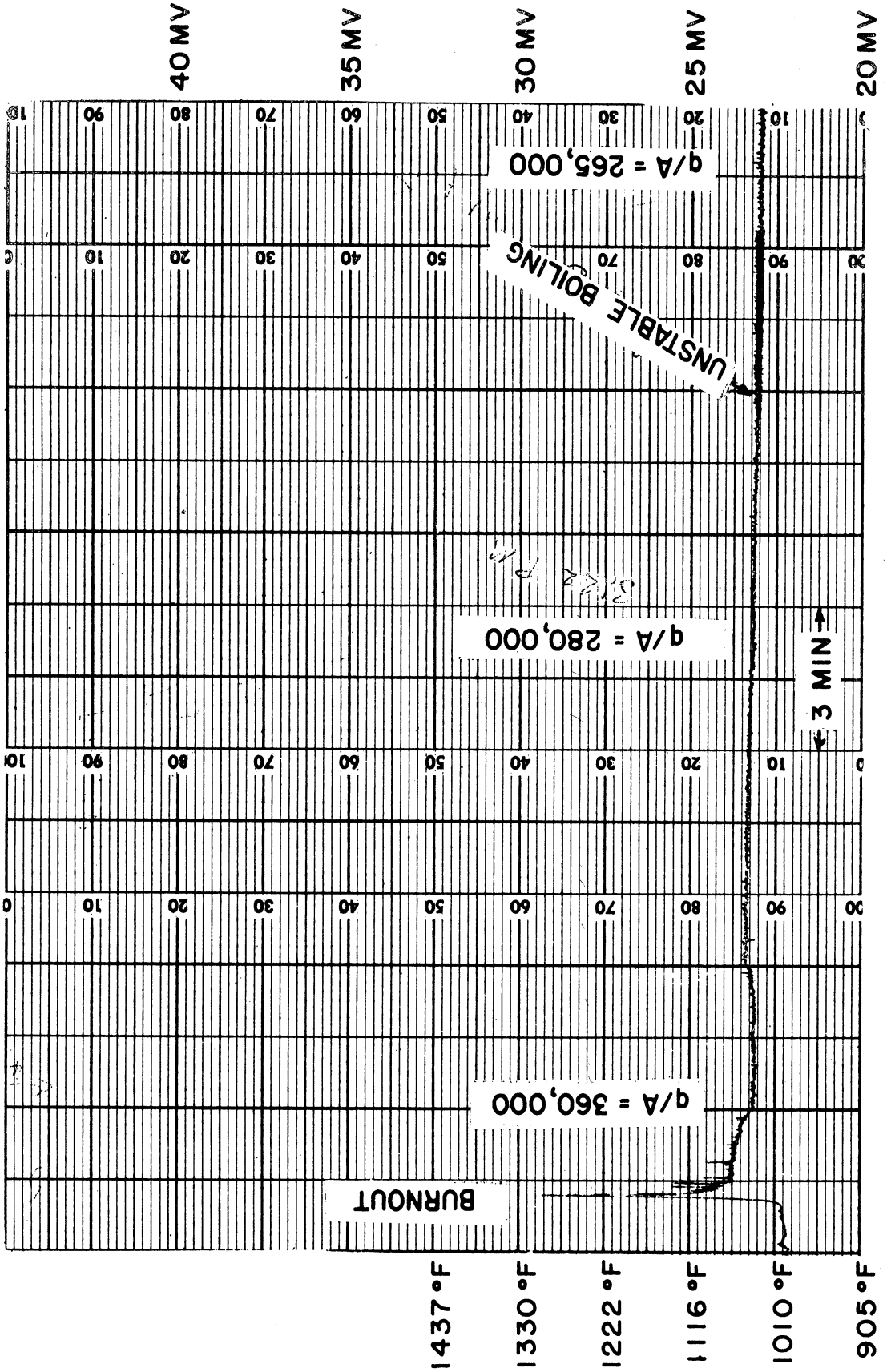

Figure 8. Boiling Tube (bottom) Temperature Record for Run 12A

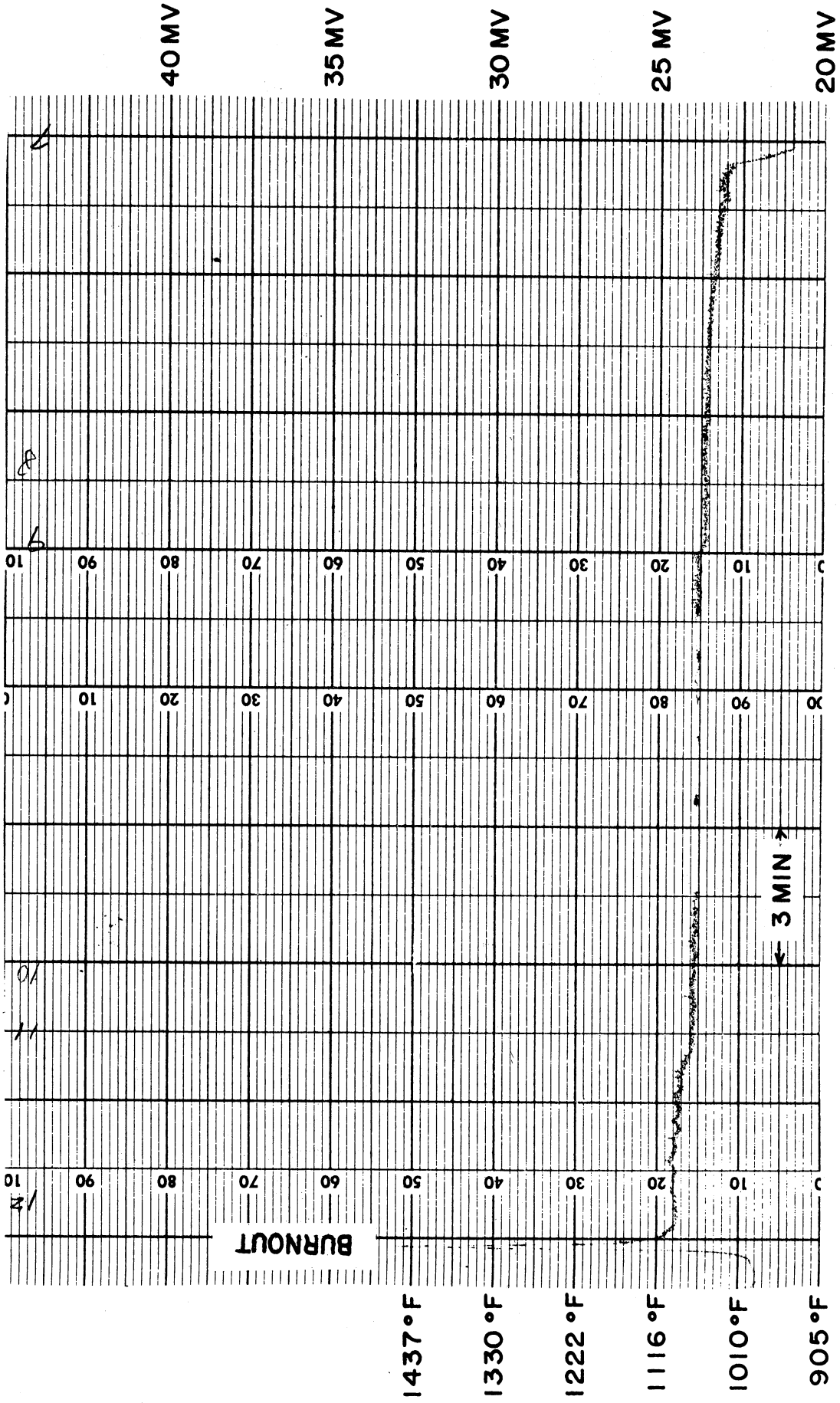

Figure 9. Boiling Tube (side) Temperature Record for Run 12B

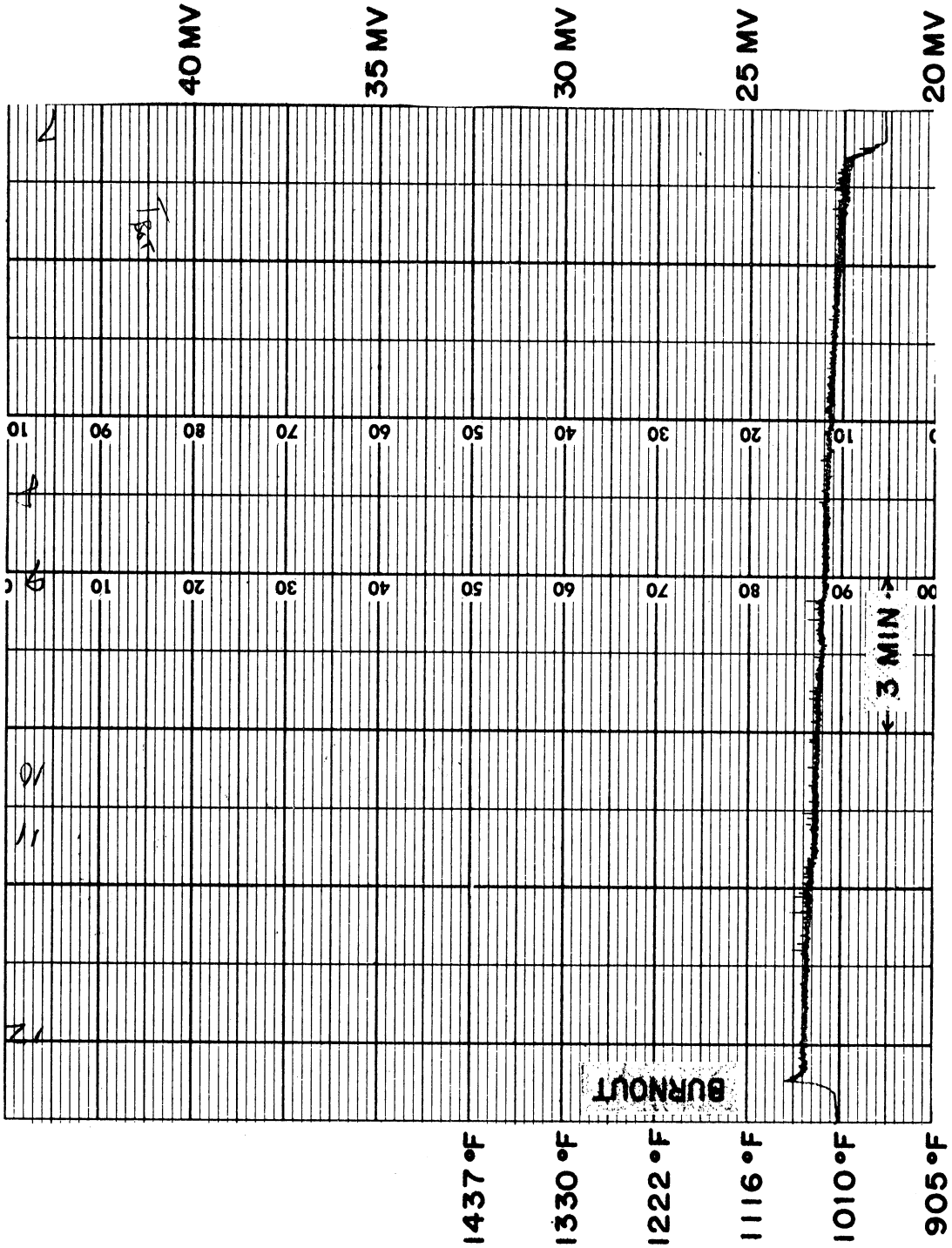

Figure 10. Boiling Tube (bottom) Temperature Record for Run 12B

Figure 11 shows the bulk liquid temperature measured by a thermocouple located one inch above the top of the heater for run 12A. This temperature was 1030°F just before burnout but dropped to 1015°F almost immediately after the power was cut off after burnout. This indicates 15°F of superheating 1 inch above the heater. Superheating in the pool was also measured on potassium by Colver (13). He reported about 10°F of superheat at this flux level for potassium at 13 psia. Because the system here was under vacuum, no other measurements were made of the variation of temperature with location in the pool because this would have necessitated loosening the tube gland on the thermocouple, a somewhat dangerous procedure with a hot system. However, this measurement will be made at different heat fluxes in future work with the system at a pressure above atmospheric. More measurements of the fine structure of the heater surface temperature vs time at different flux levels will also be made in future work.

.l available alkali metal burnout data is in Figure 13. The two points for rubidium were plotted and a dotted line was drawn through them parallel to the lines for K and Na. More data will be obtained for rubidium to check this pressure dependence. As shown, there now is good agreement on the pressure dependence between the sodium and the potassium data.

All of the alkali metal burnout data available, consisting of 54 points for sodium, potassium and rubidium have been correlated as shown in Figure 14. The following non-dimensional equation results:

$$\left[\frac{\frac{q}{A}_c \; C_p \; \sigma}{\lambda^2 \; \rho_v \; k}\right] = 1.18 \times 10^{-8} \left(\frac{\rho_l}{\rho_v}\right)^{0.71}$$

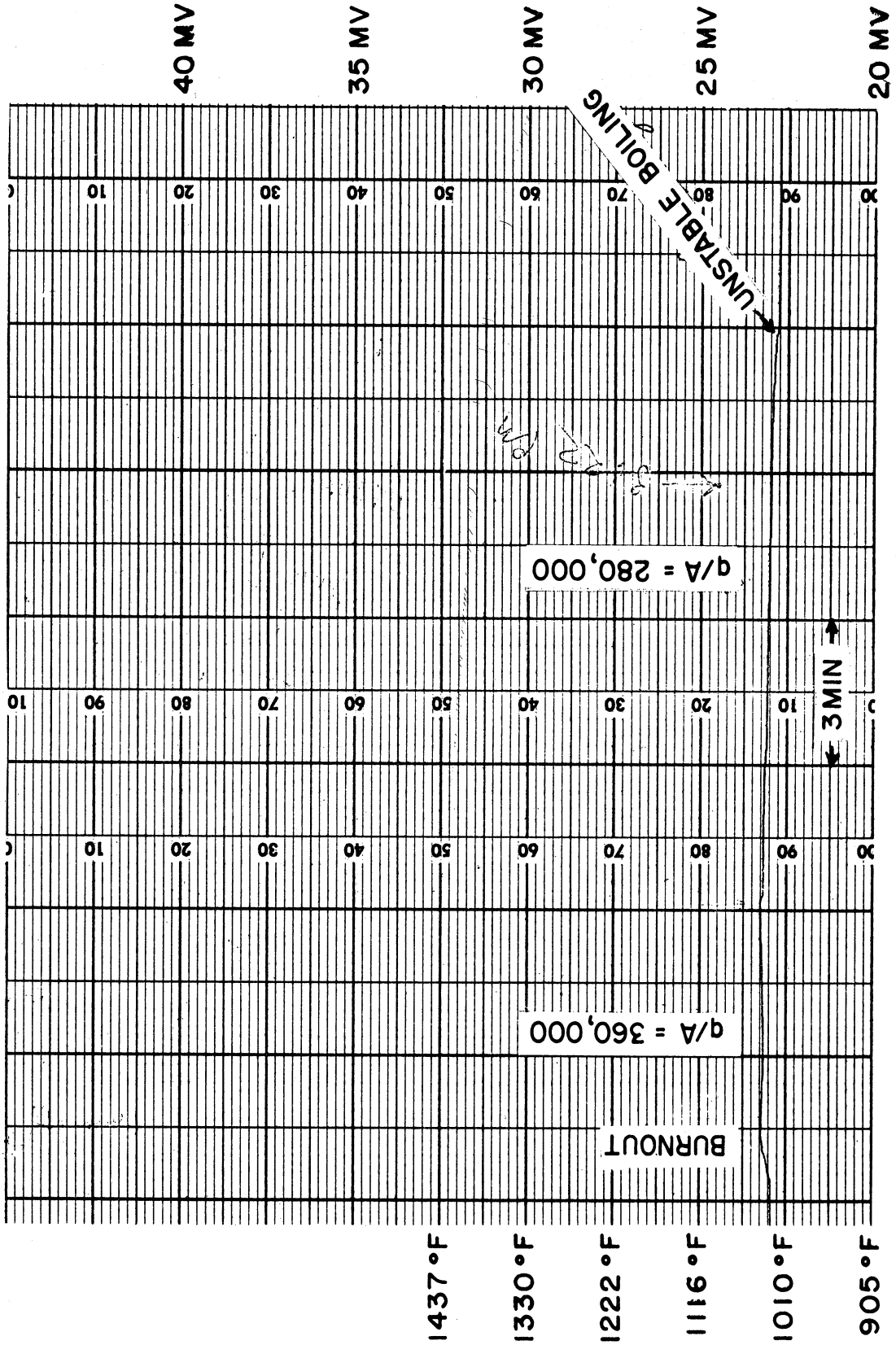

Figure 11. Bulk Liquid Temperature Record for Run 12A

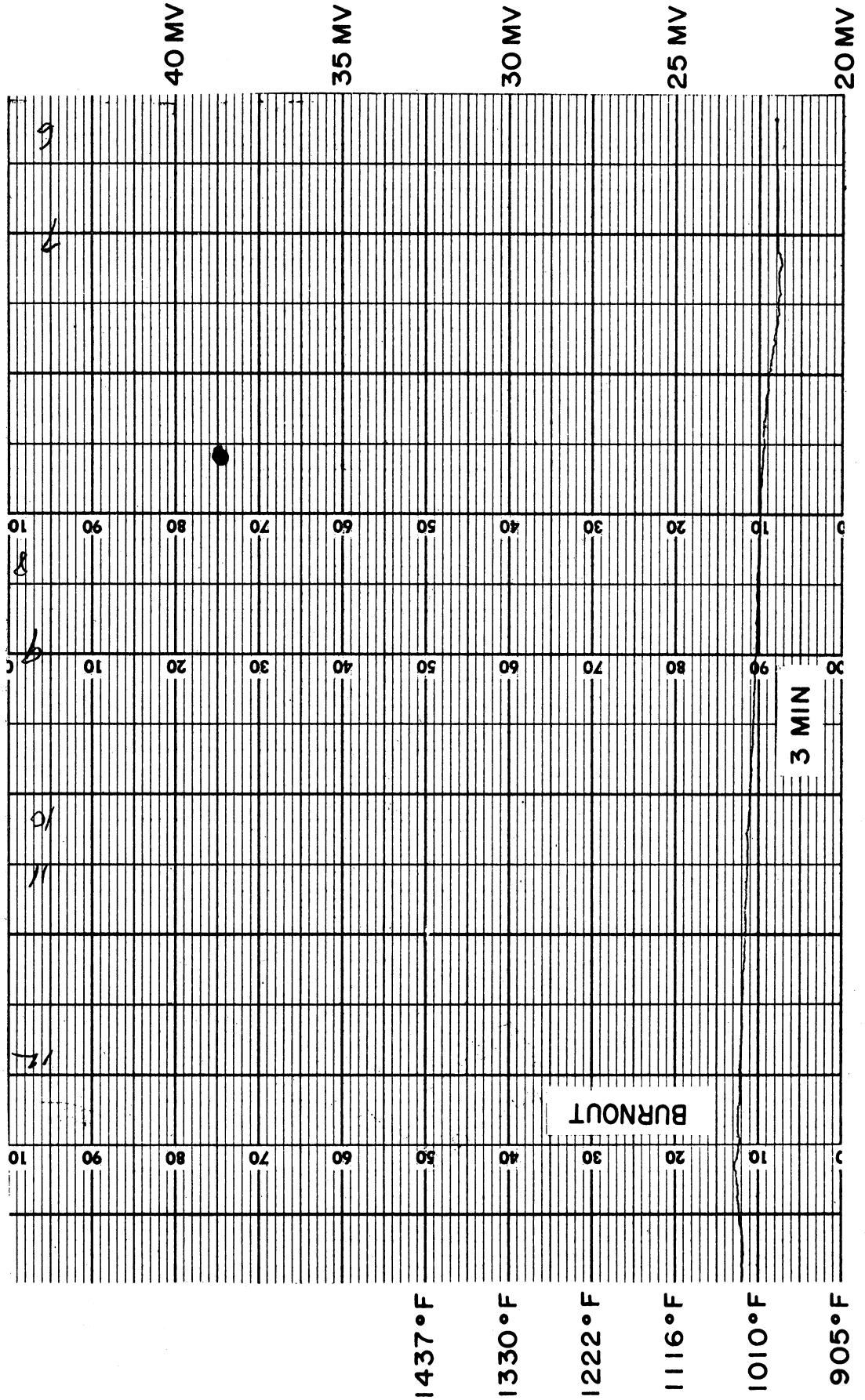

Figure 12. Bulk Liquid Temperature Record for Run 12B

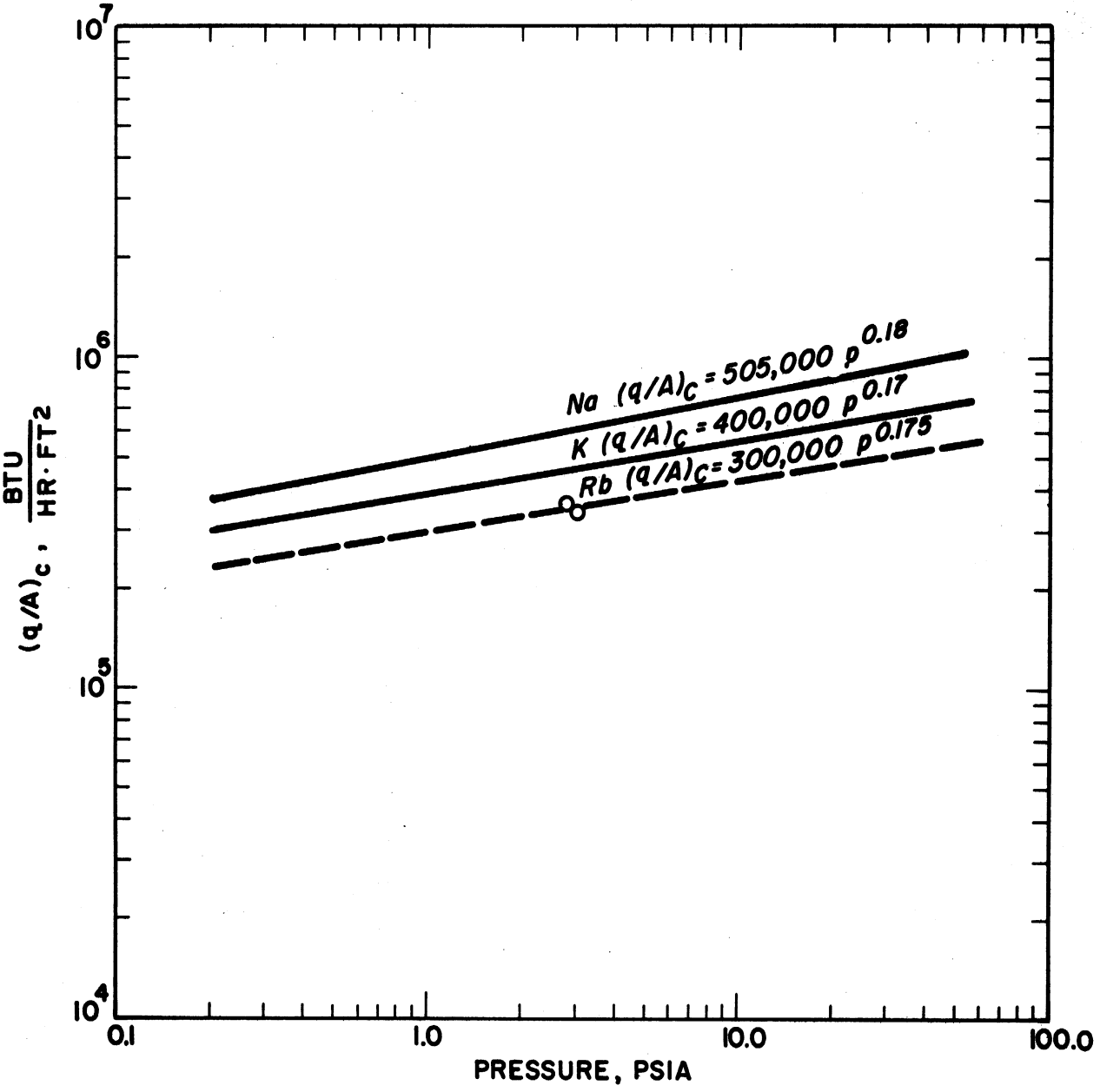

Figure 13. Summary of Alkali Metal Burnout Data

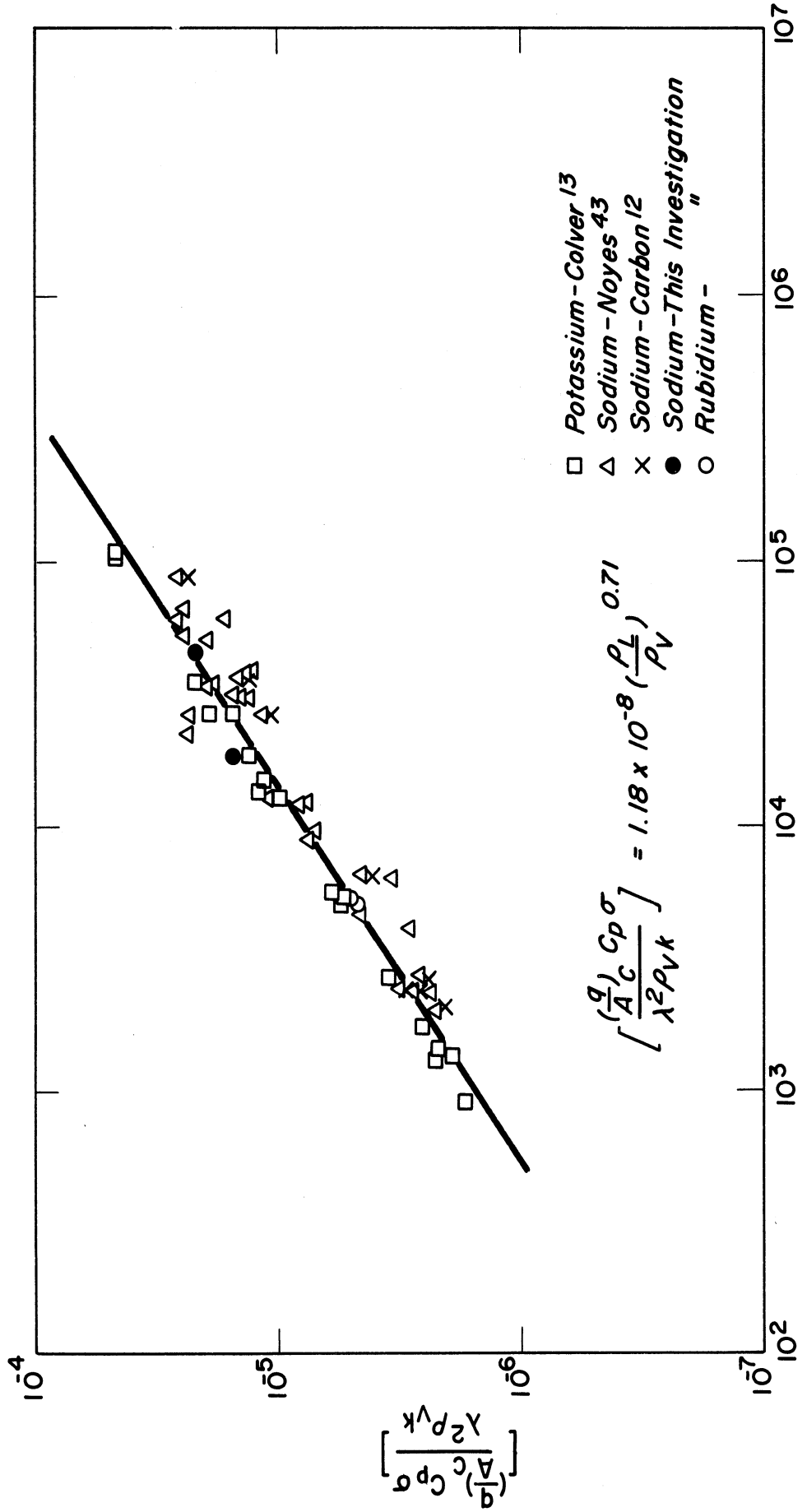

Figure 14. Correlation of Alkali Metal Burnout Data

where

$\frac{q}{A}_c$ = critical heat flux

C_p = heat capacity of the liquid

σ = surface tension

λ = latent heat of vaporization

ρ_l = density of the liquid

ρ_v = density of the vapor

k = thermal conductivity of the liquid

All properties are at saturation conditions.

FILM BOILING

Andrew Padilla, Jr.

INTRODUCTION

This phase of the program is intended to yield experimental results for potassium and sodium in the stable film boiling regime. Initial efforts were discussed in Report RTD-TDR-63-4130 submitted to the Aero Propulsion Laboratory in November 1963. This report discusses experimental and analytical studies conducted during the year 1964.

A computer simulation of the film boiling vessel revealed that for the anticipated film coefficients on both condensing and boiling sides of the plate, the magnitude of the heat transfer up the tube wall caused severe distortion of the isotherms in the boiling plate. The study showed that an accurate determination of the heat flux and the surface temperature would not be possible under these conditions, unless the condensing coefficient were known. Condensing behavior in liquid metal systems is currently being studied but an accurate prediction of the coefficient for this system is complicated by the difficulty in controlling non-condensibles in the vicinity of the plate. These difficulties have led to a redesign of the apparatus in which cartridge heaters replace condensing sodium in supplying heat to the potassium. The proposed design for a modified film boiler is presented.

EXPERIMENTAL WORK

A schematic diagram of the experimental system with details of the tube assembly and boiling plate are shown in Figures 15, 16, and 17, respectively. Sodium is boiled in the bottom chamber of the tube assembly by means of a

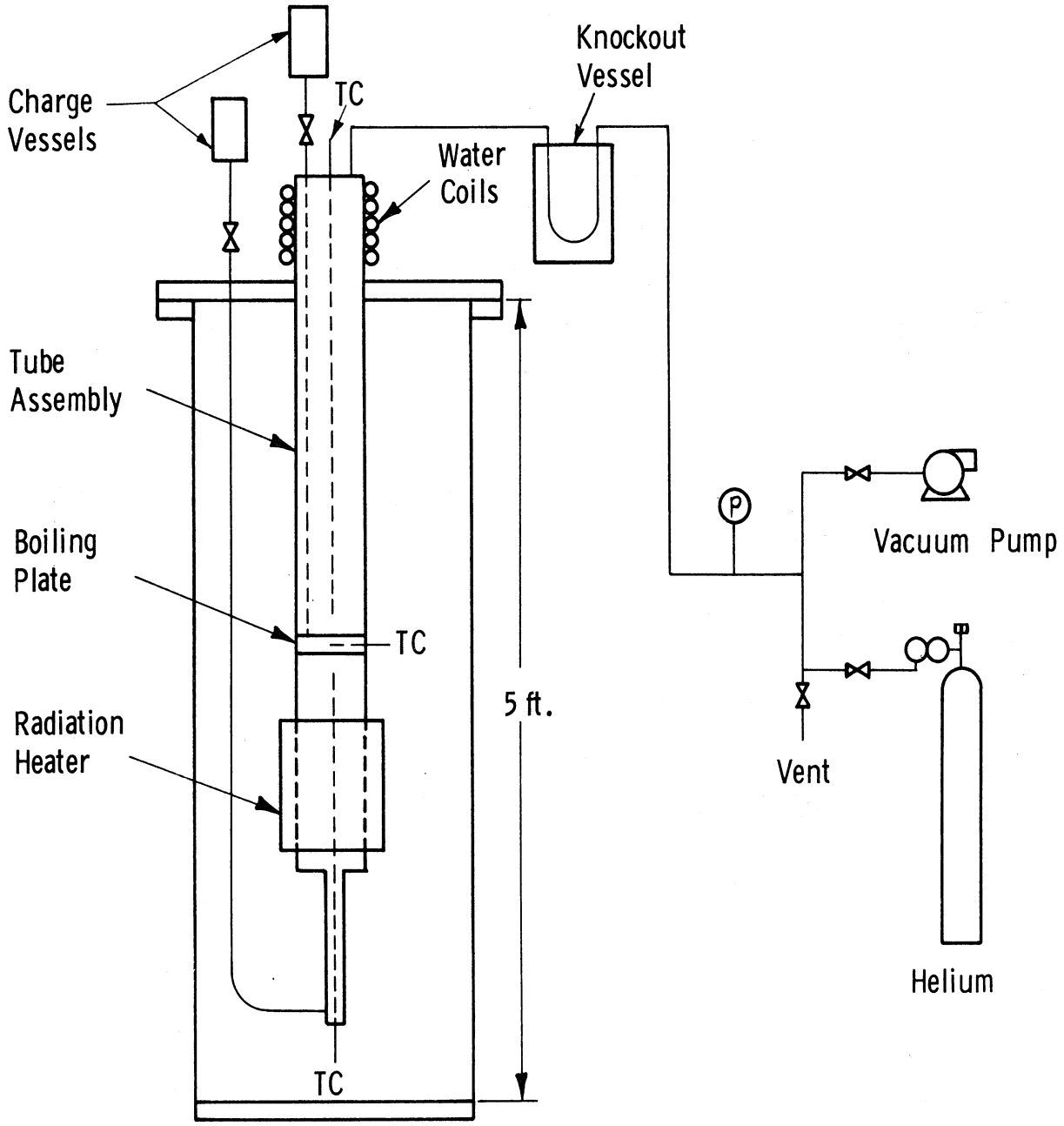

Figure 15. Schematic Diagram of Film Boiling Experimental System

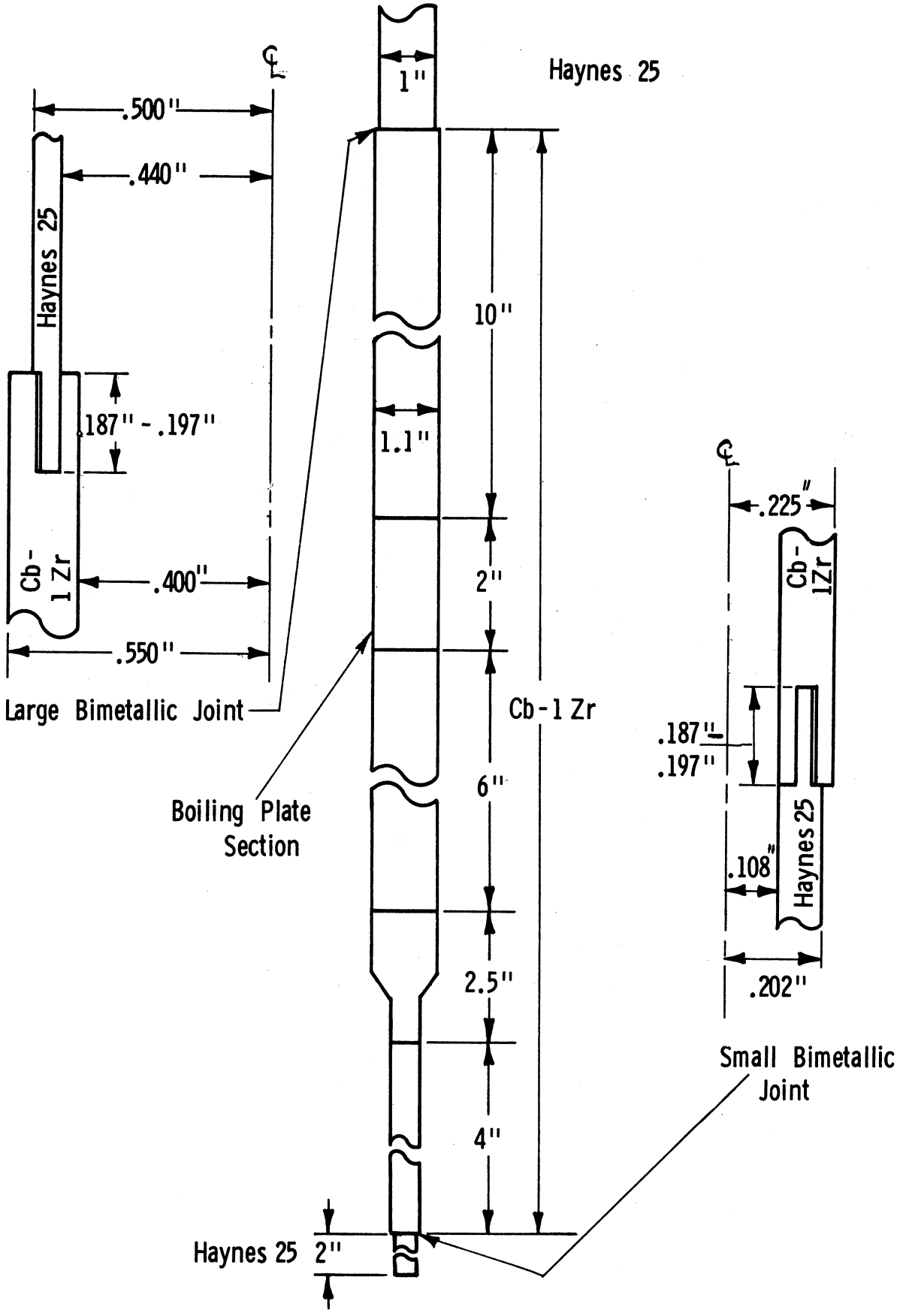

Figure 16. Tube Assembly

Thermocouple Hole Diameter 0.021"
Radial Depth of Thermocouple Holes

1	.250"
2	.450"
2A	.450"
3	.250"
4	.450"
5	.280"
5A	.250"
6	.450"

Inner Thermocouple Holes - 120° Apart
Outer Thermocouple Holes - 120° Apart
#2A Hole - 30° from #2
#5A Hole - 30° from #5

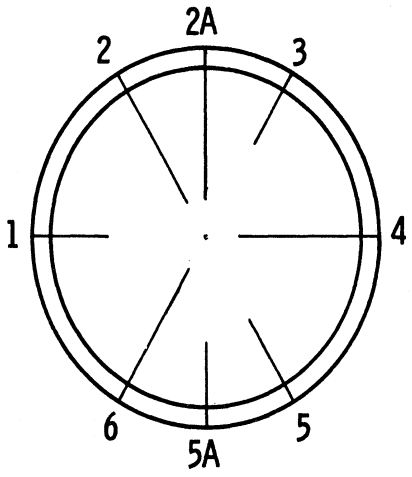

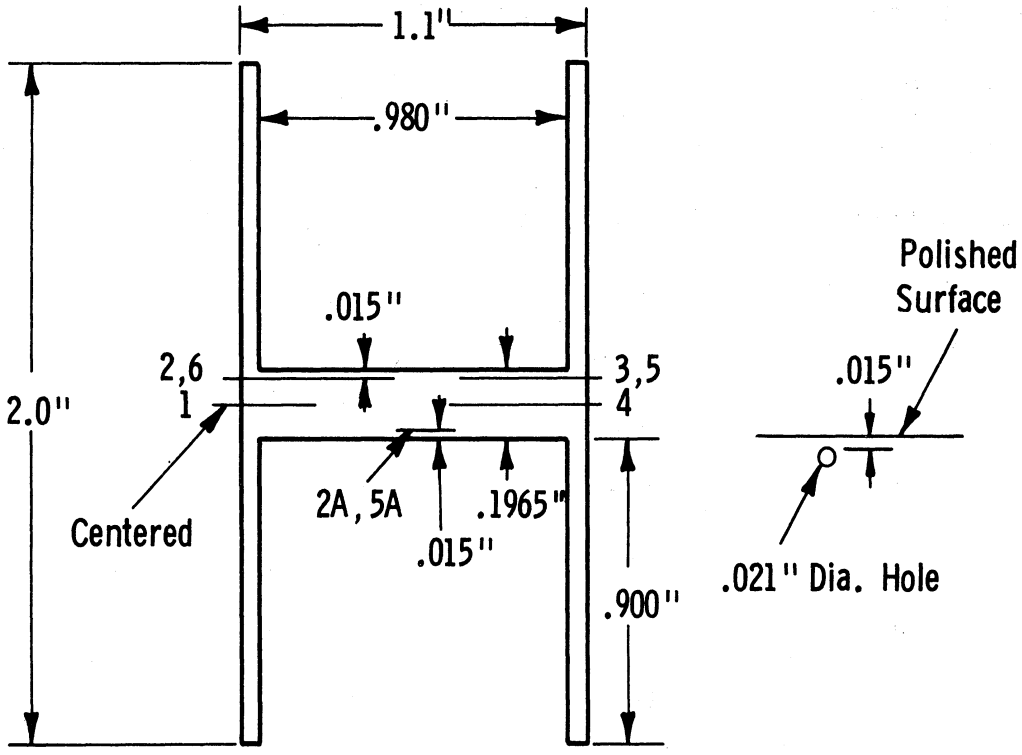

Figure 17. Boiling Plate Section

radiation heater and condenses on the bottom surface of a horizontal boiling plate. The potassium boils on the top surface of the plate and condenses in the upper part of the tube assembly by radiation to the walls of the containing vessel. The tube assembly is a composite Cb-1 Zr/Haynes-25 assembly 4 feet $2\frac{1}{2}$ inches long. The boiling plate was machined from a solid rod 1.10 inches in diameter and 2 inches long. The plate is 196.5 mils thick and contains eight 21-mil thermocouple holes at three different depths below the boiling surface and at two different radii.

Preliminary data on the film boiling of potassium at reduced pressures yielded fluxes which were apparently higher than those in nucleate boiling. Operational difficulties were encountered when surges in the sodium chamber occurred causing the boiling plate temperature to fluctuate 500°F. A failure of the thermocouple in the sodium chamber prevented close monitoring of the behavior in that system.

Later attempts to increase the pressure range of the data were curtailed by the occurrence of large temperature excursions in the boiling system. These fluctuations were also encountered while boiling potassium under reduced pressure. With the potassium at 1000°F and boiling plate temperatures of about 1500°F, an increase in the power to the heater for the sodium chamber resulted in oscillations of the boiling plate from 1500°F to 1000°F. The gradual drift to the lower temperature level was accompanied by the disappearance of the sound of boiling and the abrupt rise to the high level occurred after a loud knock. The cycle repeated itself about every 30 seconds. The first attempt to show that the instability was due to excessive superheating of the sodium by pressurizing the potassium to prevent its boiling produced stable boiling of sodium at 1400°F. However, further boiling of potassium under reduced pressure produced instabilities which persisted even after the potassium had been pressurized into the natural convection regime.

To ascertain what was actually happening during these temperature excursions, the boiling plate was instrumented with newly-calibrated thermocouples. Thermocouples were also attached to the outside of the boiling tube immediately above and below the boiling plate in order to evaluate edge effects. The potassium chamber was fully evacuated to insure boiling at relatively low temperatures and then valved off. Figure 18 is a diagram of the boiling plate drawn to scale, indicating typical temperatures at various locations when the sounds of stable nucleate boiling could be heard. Figure 19 is a trace of the output from the thermocouple in the boiling plate (at Location A in Figure 18), which is 0.025 inch above the bottom condensing surface and 0.100 inch from the center of the plate, at slightly higher temperature levels. The knocks occurred about once every minute. An apparent steady-state condition at the high temperature level was reached but later slowly decayed to the temperature levels before the onset of the instability.

From Figures 18 and 19, it appears that the boiling plate is receiving the bulk of its energy by axial conduction up the walls of the sodium chamber. The very large temperature drop from the saturation temperature of the sodium to the bottom of the boiling plate is probably due to the effect of non-condensibles. The loud knocks at the onset of an upward temperature excursion are apparently due to vapor bursts. After a few such bursts, the condensing coefficient becomes high enough to support the boiling plate at temperatures near the saturation temperature of the sodium. However, the buildup of non-condensibles again causes the condensing coefficient to slowly decrease resulting in a large temperature drop between the sodium and the boiling plate.

To check the possibility that the difficulty in boiling the sodium may have been aggravated by insufficient vapor space, the sodium level was reduced by one-third. However, no indications of improved operation were observed.

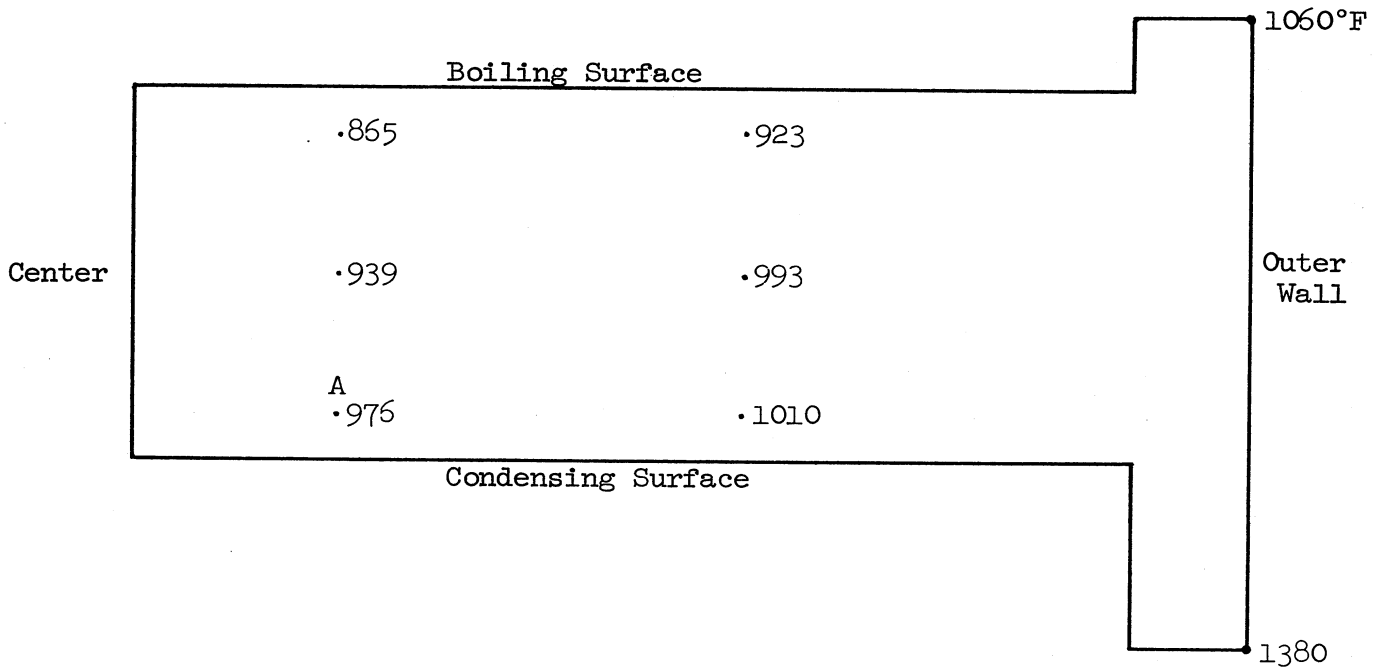

Figure 18. Temperatures in Boiling Plate During Nucleate Boiling of Potassium at Reduced Pressure

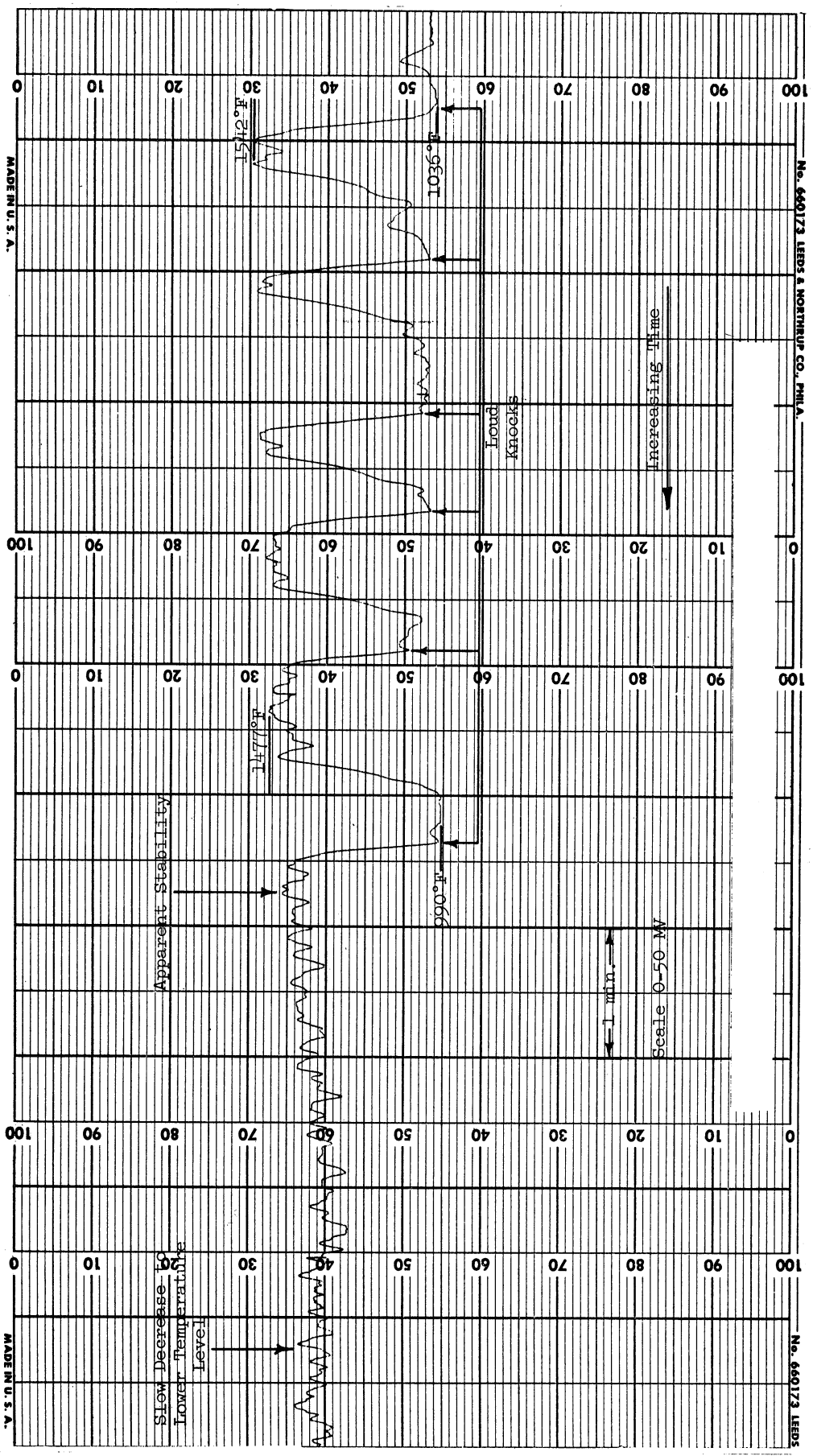

Figure 19. Boiling Plate Thermocouple Trace During Unstable Operation

MICRO-THERMOCOUPLE EVALUATION

The thermocouples inserted in the .021-inch diameter holes of the boiling plate are .020-inch OD, Inconel-sheathed, swaged thermocouples containing B. and S. 38-gauge Chromel-Alumel wires and MgO insulation. Since they are used to obtain temperature differences to calculate the heat flux by Fourier's heat conduction equation, considerable effort was devoted to calibrating them both in air and under vacuum. This inevitably led to an evaluation of their stability and accuracy at high temperatures. The results indicate that if thermocouples of such small size are to be used above 1200°F, they must be aged by cycling to a high temperature several times until no hysteresis in the calibration curve is detected. However, they rapidly burn out at 1800°F under oxidizing conditions.

The investigation into the stability of the micro-thermocouples was initiated unexpectedly while calibrating eight new ones to replace the old set in the boiling plate. The eight micro-thermocouples and a secondary standard Pt/Pt 10% Rh thermocouple were placed in a stainless steel thermowell and inserted into a Leeds and Northrop thermocouple checking furnace (catalog number 9004 with 1800°F maximum termperature) with care being taken to insure that all of the junctions were in contact with the bottom of the thermowell. While slowly heating the assembly to 1800°F, at least 30 minutes were allowed for temperatures inside the furnace to equalize after it had been raised to a certain level before making readings. Upon checking the calibration curve, while slowly decreasing the temperature of the furnace, five of the eight thermocouples exhibited significant deviations. A second calibration to 1800°F produced different curves for all eight thermocouples and marked hysteresis effects were again detected while decreasing the furnace temperature.

To determine the effect of temperature on this drift, the micro-thero-couples were held at 1200°F for 7 hours. Although the individual emf outputs varied widely and corresponded to temperatures as low as 120°F below the expected calibration, the readings were stable with time. The furnace was then cooled to 300°F and reheated to 1200°F for another 8 hours. The same stable readings were obtained. It, therefore, appeared that after the initial aging process, consisting of cycling the thermocouples to 1800°F twice, the micro-thermocouples were stable at 1200°F. To check their stability at a higher temperature, they were heated to 1800°F for 7 hours. Widely-varying, but stable readings were again obtained. However, upon cooling to 450°F and reheating to 1800°F, a drop in emf for all of the thermocouples was defected. After 8 hours at 1800°F, all thermocouples were drifting unpredictably. When the experiment was terminated 10 hours later, they were drifting widly and after cooling to room temperature, it was discovered that 7 of the 8 thermocouples had open circuits.

Although the thermocouples were to be used in a vacuum environment, all of the calibrating operations had thus been carried out in air. Accordingly, a 2-inch OD stainless steel vessel containing a 1 11/16-inch diameter x 2-inch long copper equilizing block with .032-inch diameter x 1/2-inch long holes was fabricated for calibrating the thermocouples under vacuum. Up to 1200°F, the new set of micro-thermocouples followed the expected temperature-emf relationship closely. However, a significant change in the slope of the calibration curve was detected from 1200°F to 1800°F. After cooling to room temperature and reheating to 1800°F three times, stabilization was apparently reached. The thermocouples were then calibrated during two additional cycles with measurements being taken while both increasing and decreasing temperature.

These experiments indicate that the .020-inch OD, Inconel-sheathed, Chromel-Alomel swaged thermocouples are unsuitable for high temperature use in an oxidizing atmosphere. They can probably be used up to 1800°F under a vacuum environment provided that they are stabilized by cycling between room temperature and 1800°F several times. Under these conditions, it is suggested that they be recalibrated at least every 50 hours when used above 1200°F.

ANALYTICAL STUDIES

Concurrently with the experimental work, an effort was made to predict quantitatively the accuracy of the heat-transfer data which could be expected under a variety of stable operating conditions. The mathematical analysis was first done in two dimensions and later extended to three dimensions and involves the solution of the finite-difference form of Laplace's equation using the IBM 7090 computer. Figure 20 shows the model used for the analysis in comparison with the actual boiling plate.

The computer program allows for a constant condensing and boiling coefficient along the bottom and top of the boiling plate respectively and for radiation from the outer wall to a shield at constant temperature. Since the inside tube wall immediately above the boiling plate must pass from film boiling through transition and nucleate boiling to natural convection whenever the top surface of the plate is in film boiling, a variable boiling coefficient along this wall is used.

In the present experimental system, the heat flux at the boiling surface must be calculated by measuring the temperature at several points in the boiling plate using micro-thermocouples. The temperature measurements are then used with the known distance between thermocouples and the thermal conductivity to establish the heat flux across the plate. This heat flux is equal to the flux at the boiling surface only if no radial gradients exist. The boiling plate contains thermocouples at three different depths to measure the temperature gradient across the plate and at two different radii to detect any radial flow.

The boiling plate is connected to a tube which serves as the containment vessel for the boiling liquid. The flux lines in the boiling plate depend on the relative resistances to heat flow across the boiling surface and up the tube wall by axial conduction. If the boiling coefficient is very low, as in film boiling, then the relatively low resistance to heat flow by axial conduction up the walls of the tube distorts the flux lines in the plate. This radial heat

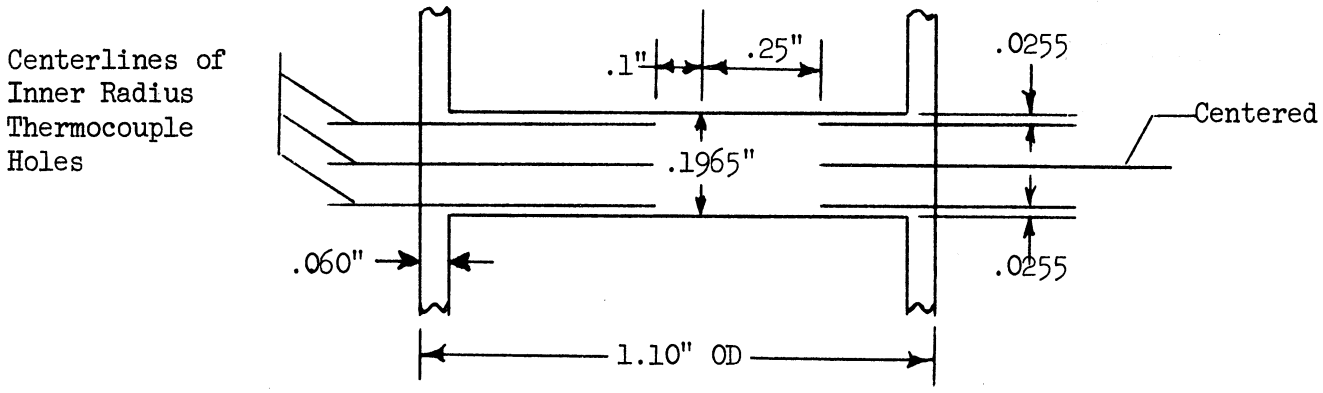

BOILING PLATE

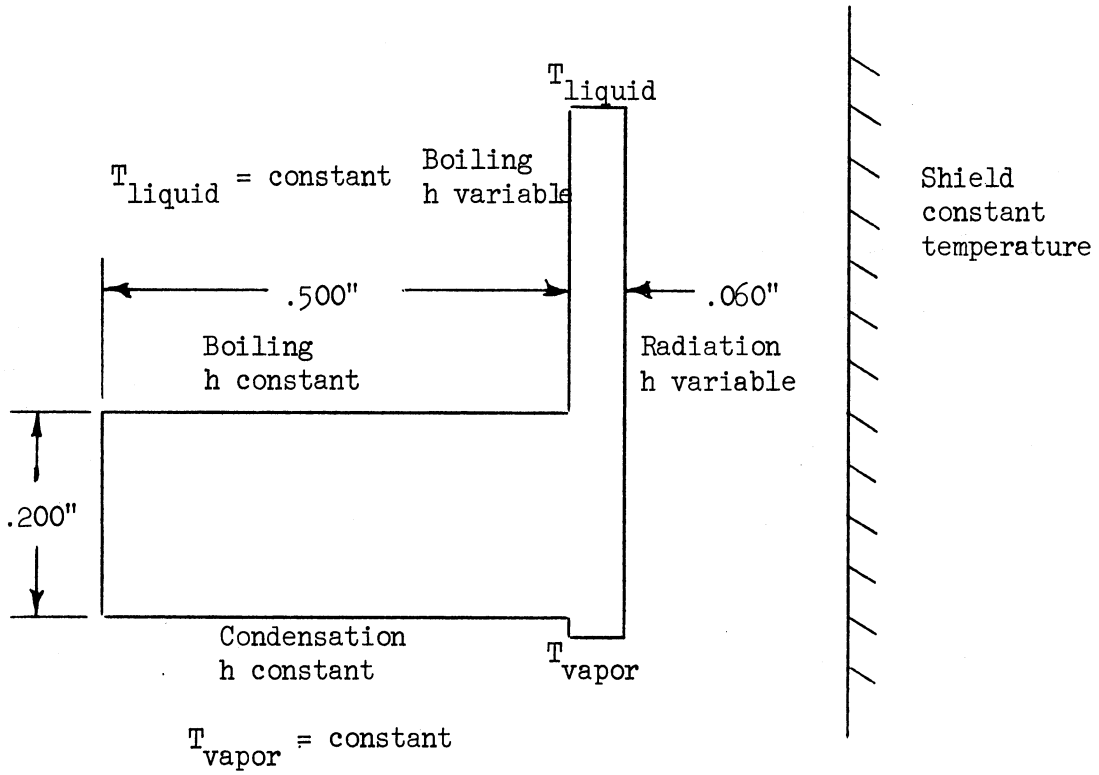

Figure 20. Model for Analysis of Boiling Plate

flow causes a radial temperature variation along the boiling surface. The axial temperature gradient in the boiling plate is then no longer an accurate indication of the flux occurring at the boiling surface. The relationship between the boiling surface flux and the flux calculated by measuring the axial temperature profile in the plate is quite complicated and requires the determination of the temperature field in the boiling plate for the desired set of operating conditions.

The computer program for the test section determines the temperature field in the boiling plate and the tube wall immediately above the boiling plate. The temperatures along the top surface of the plate can then be used with the assumed boiling coefficient to calculate the radial variation in the boiling surface flux. By taking the temperatures of two different depths below the boiling surface, the radial variation in the "measured flux" can also be calculated. For the cases which follow, this "measured flux" is based on calculated temperatures .020 inch below the boiling surface and .020 inch above the condensing surface (.160 inch apart) and on the thermal conductivity of columbium-1% zirconium.

Figure 21 shows the temperature field in the boiling plate for a film boiling coefficient of 100 Btu/(hr)(sq ft)(°F) and a condensing coefficient of 5000 Btu/(hr)(sq ft)(°F). The boiling coefficients along the inside-tube wall immediately above the boiling plate were assigned according to an independent calculation. It is noticed that the isotherms are severely distorted especially at the junction of the boiling plate and the tube wall where axial conduction up the tube wall affords a resistance to heat transfer in comparison with the low film-boiling coefficient. Figure 22, which summarizes the results that can be calculated from the temperature field in Figure 21, shows that the "measured flux" calculated by using one thermocouple .020 inch below the boiling surface and another thermocouple .020 inch above the condensing surface would be considerably higher than the flux actually occurring at the boiling surface.

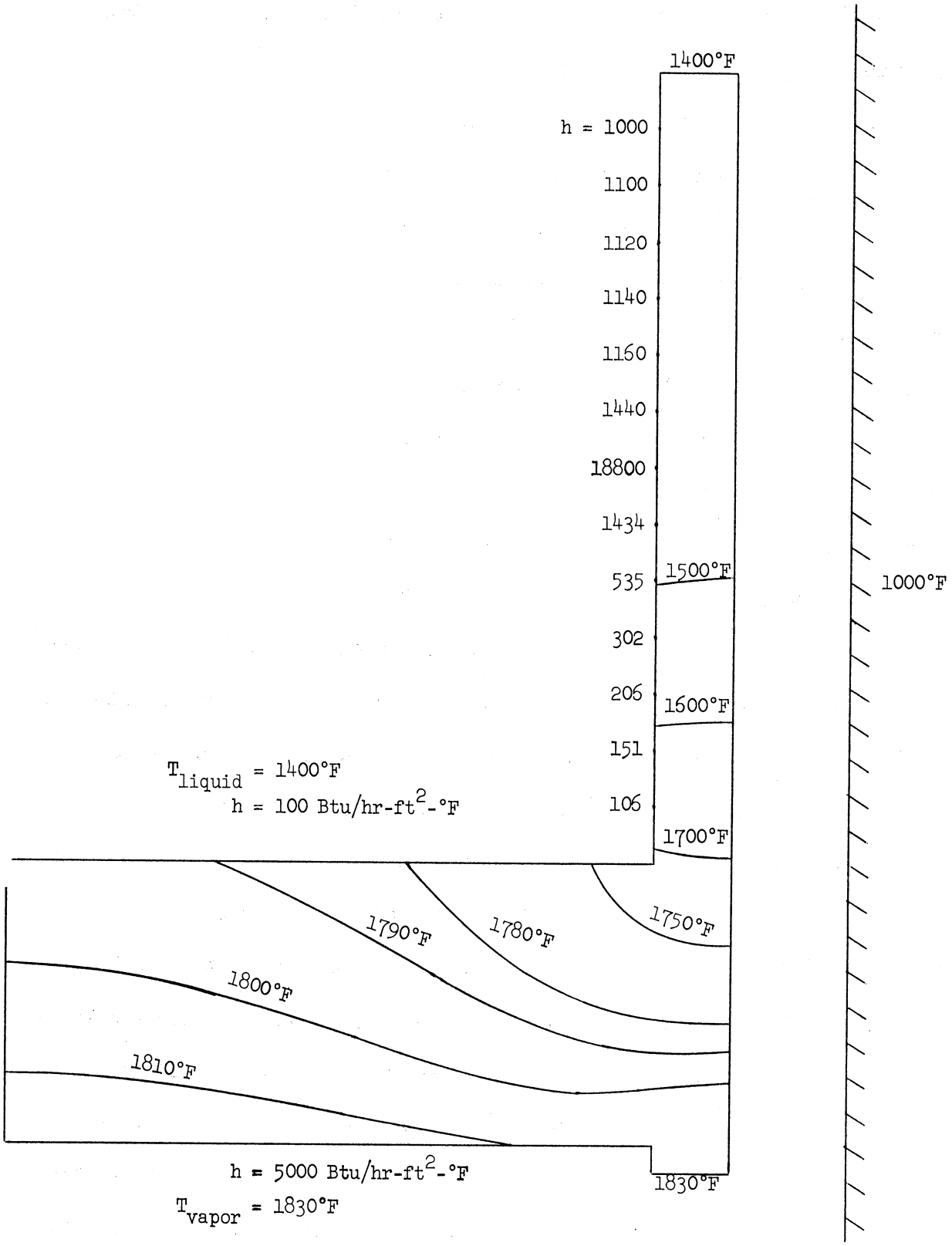

Figure 21. Calculated Temperature Field for Boiling Plate in Film Boiling Regime

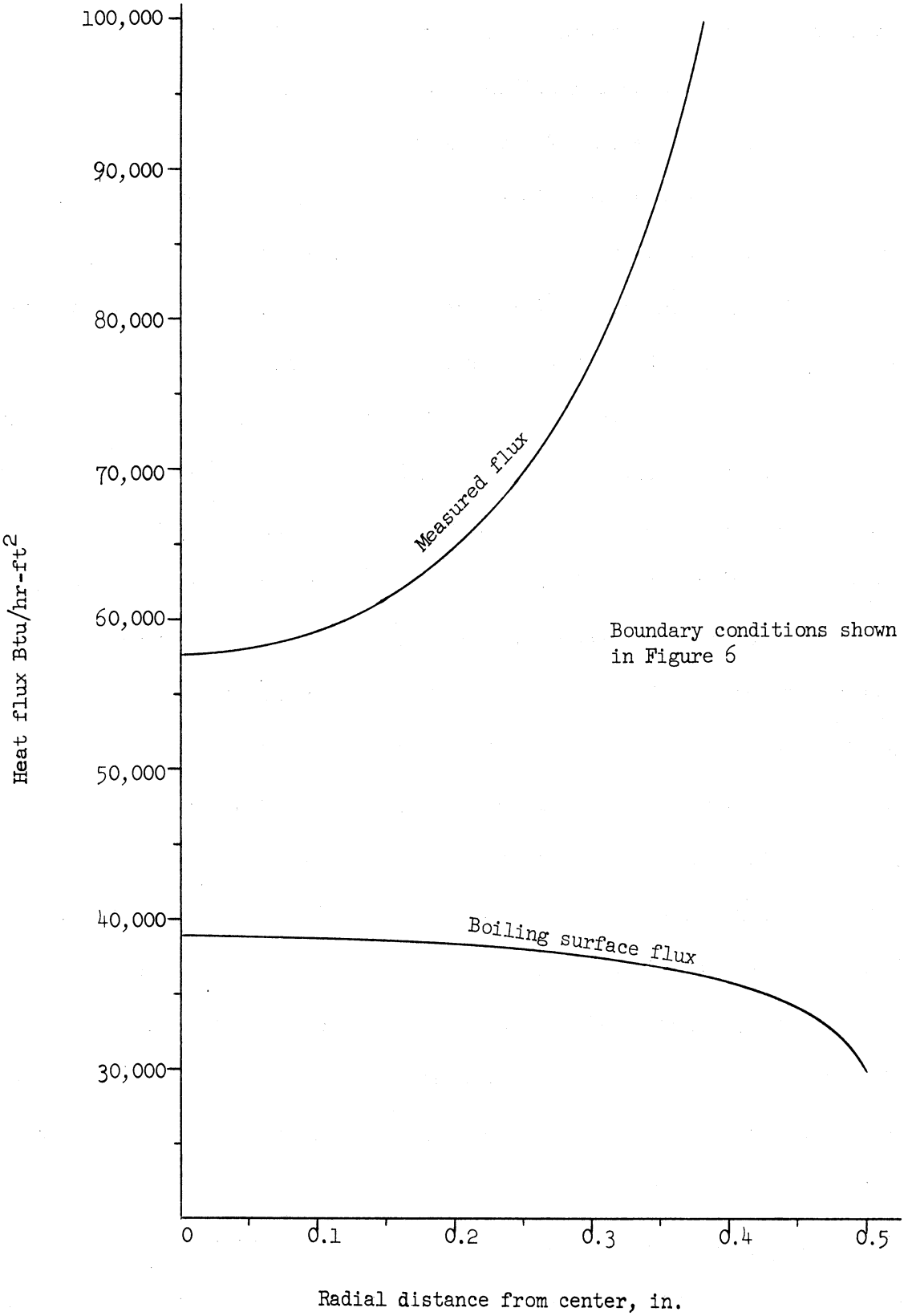

Figure 22. Hypothetical Comparison of Actual Boiling Surface Flux and Flux Calculated from Measured Data

This measured flux would be 37% higher at the center of the boiling plate and would increase to over six times the boiling surface flux at the tube wall. Since the thermocouples in the actual boiling plate are located at .10 inch and .25 inch from the centerline, the errors for these two radii are 41% and 66% respectively.

The distortion of the flux lines (which are perpendicular to the isotherms) as a result of axial conduction up the tube wall depends very strongly on the boiling coefficient. The ratio of the measured flux and the boiling surface flux can be plotted as a function of the radial distance from the center of the boiling plate. Figure 23 compares this ratio for the entire range of possible boiling regimes. The boiling coefficients of 50, 100, and 200 Btu/(hr)(sq ft)(°F) represent the probable range of film-boiling coefficients while 2,000 and 20,000 Btu/(hr)(sq ft)(°F) represent transition- and nucleate-boiling coefficients, respectively. The analysis shows that very small error can be expected in transition and nucleate boiling, especially if the measurements are made close to the center of the tube. In fact, the high value of the coefficient in the nucleate regime represents a lower resistance to heat transfer than axial conduction up the tube wall and the flux lines are slightly distorted towards the boiling plate rather than away from it. If a film-boiling coefficient as high as 200 Btu/(hr)(sq ft)(°F) is possible, then the error between the measured flux and boiling surface flux is 15% at the center and 28% at a distance of .25 inch from the center. However, a low coefficient of 50 Btu/(hr)(sq ft)(°F) introduces an error of 82% at the center which increases to 140% at .25 inch from the center of the boiling plate.

The results are also sensitive to the value of the condensing coefficient. Figure 24 shows the radial variation of measured flux to boiling surface flux for condensing coefficients of 500, 1,000 and 10,000 Btu/(hr)(sq ft)(°F) keeping the boiling coefficient constant at 100 Btu/(hr)(sq ft)(°F). At the center of the boiling plate, the respective errors are 5%, 24%, and 33%. This means that the

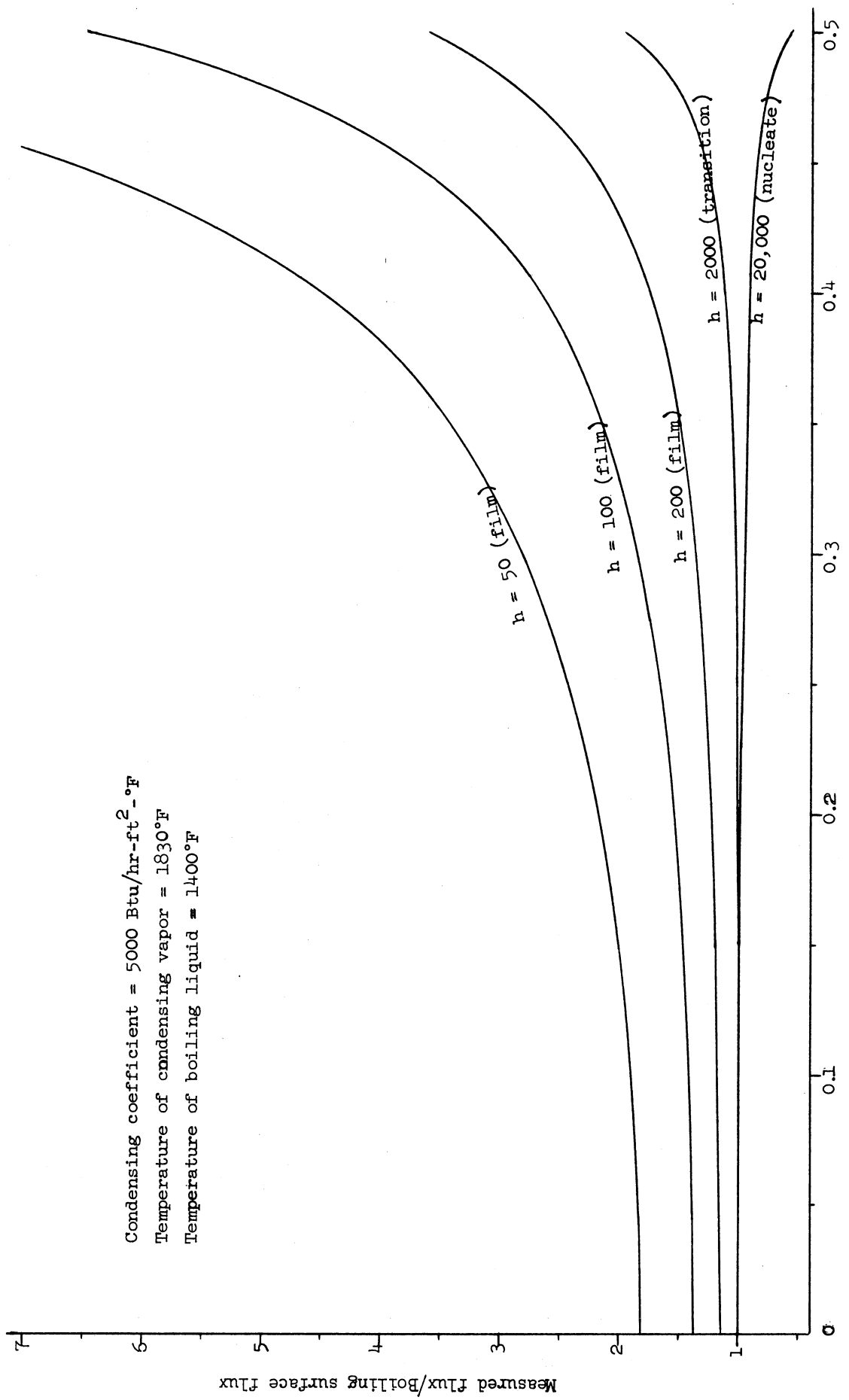

Figure 23. Effect of Boiling Coefficient

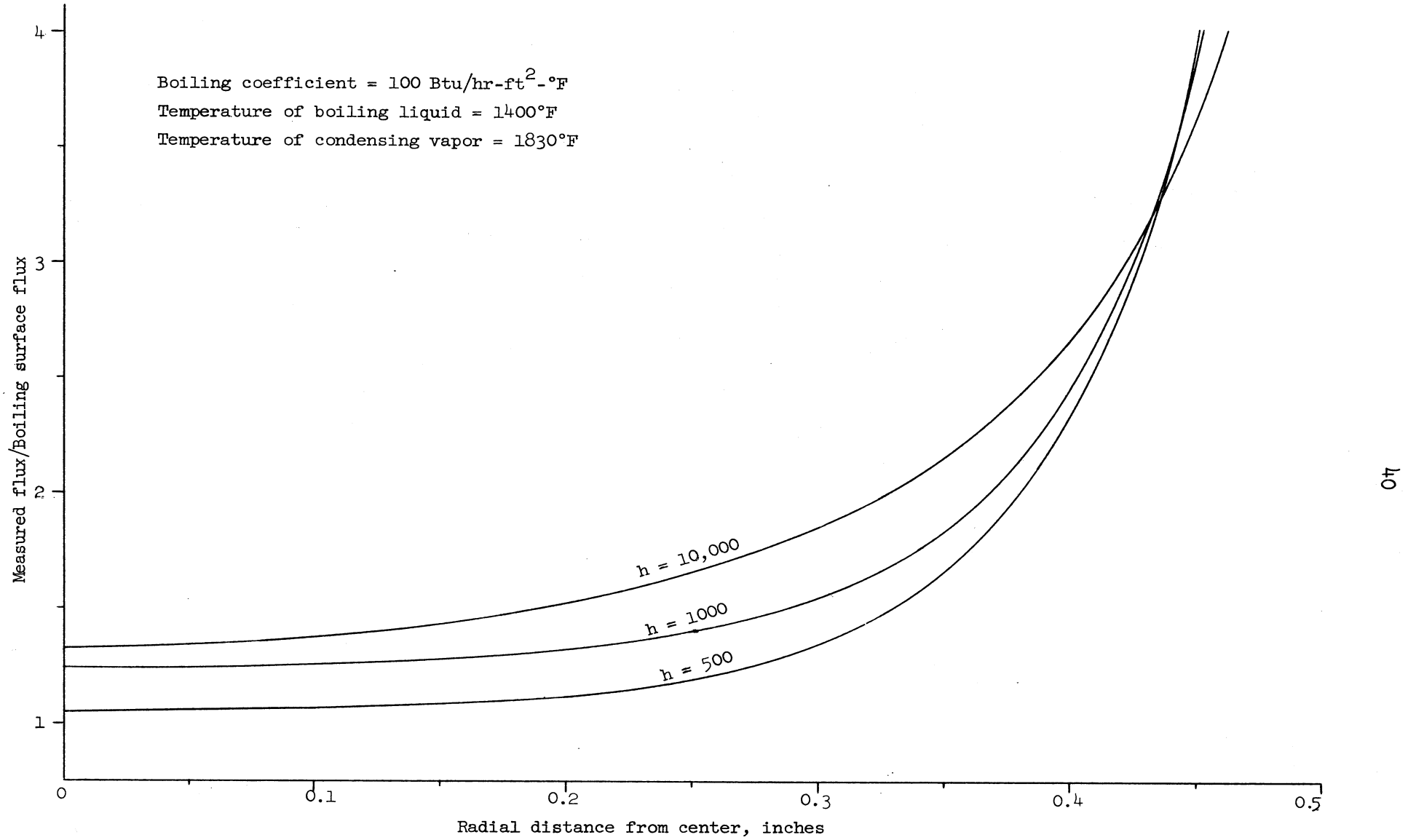

Figure 24. Effect of Condensing Coefficient

result of increasing the condensing coefficient during film boiling is that a larger fraction of energy is driven up the tube walls rather than across the boiling plate.

The temperature of the shield to which the boiling tube radiates was not found to be an important parameter. This also indicates that radiation-type guard heaters along the outside of the boiling tube would have little effect on the temperature distribution inside the boiling plate.

DESIGN OF 3-INCH DIAMETER BOILER

The original purpose in using a condensing media as the heat source was to obtain data in the stable film and transition regimes without experiencing burnout of the boiling surface. However, boiling instabilities were encountered in the condensing chamber during operation due to nucleation difficulties as evidenced by a loud knock and an abrupt rise of temperatures in the boiling plate as shown in Figure 19. This vapor burst seemed to remove noncondensibles and permit the anticipated heat transfer directly to the plate by condensing vapor. The deterioration of this stable condition has been attributed to a reaccumulation of non-condensible gases. Originally it had been hoped to eliminate non-condensibles from the system by charging the sodium under vacuum. It now appears that such an approach is unrealistic due to dissolved and entrained gases which eventually come out of the sodium. Although the nucleation problem could be alleviated by introducing a hot finger into the sodium chamber, the present design makes it very difficult to allow for a vent near the condensing surface to overcome non-condensible gas difficulties.

Since the analytical studies show that the film-boiling results would be sensitive to the value of the condensing coefficient, the uncertainty in determining the condensing coefficient is thereby added to the corrections which would have to be made on the data.

The experience with the present film-boiler indicates that a new type of test section would be better for obtaining film-boiling data. The work of Clark and Merte, in liquid metal boiling in agravic fields, indicates that a block heater using cartridge type heaters possesses sufficient thermal capacity to avoid failure of the boiling surface in passing from nucleate to film boiling. In addition, the experience with the high flux pool boiler has shown that boron-

nitride-insulated graphite cartridge elements can operate satisfactorily at very high temperatures and fluxes. These considerations have led to the design of the 3-inch diameter boiler which is shown in Figure 25. The 3 1/2-inch diameter block of Mo-0.5 Ti is to be joined to the containment vessel, consisting of 3-inch, Sch. 40, Haynes-25 pipe machined to a .060-inch wall thickness, in a tongue-in-groove configuration. The heater units will consist of a .160-inch diameter x 1-inch graphite rod inserted into a .180-inch OD x .160-inch ID boron nitride sleeve.

Analytical studies have also been carried out on the proposed design to investigate various configurations for the placement of the heater elements and to determine the length of calming section between the top level of the heaters and the boiling surface. Figure 26 is the model used to simulate operation of the system in the film-boiling regime. The program allows for the difference in the low thermal conductivity of the tube wall (14 Btu/ft-hr-°F for Haynes-25) and that of the block (60 Btu/ft-hr-°F for Mo-0.5 Ti). To avoid the difficulties involved in a true three-dimensional model which would have to include the polar direction, the heaters at the outer radius are simulated by an annular band. The results will be helpful in determining the placement of thermocouples in the block. It is planned to allow for eight thermocouples between the heaters and the boiling surface.

The distortion of the flux lines indicated in Figure 26 are due to the effect of axial conduction up the tube walls of the containment vessel. To compensate for this edge effect, a guard heater will be coiled around the tube wall immediately above the Mo-0.5 Ti block in order to deliver more flux to this critical area than would be possible with a radiation heater. A thermocouple will be located at the junction of the tube and the block and this

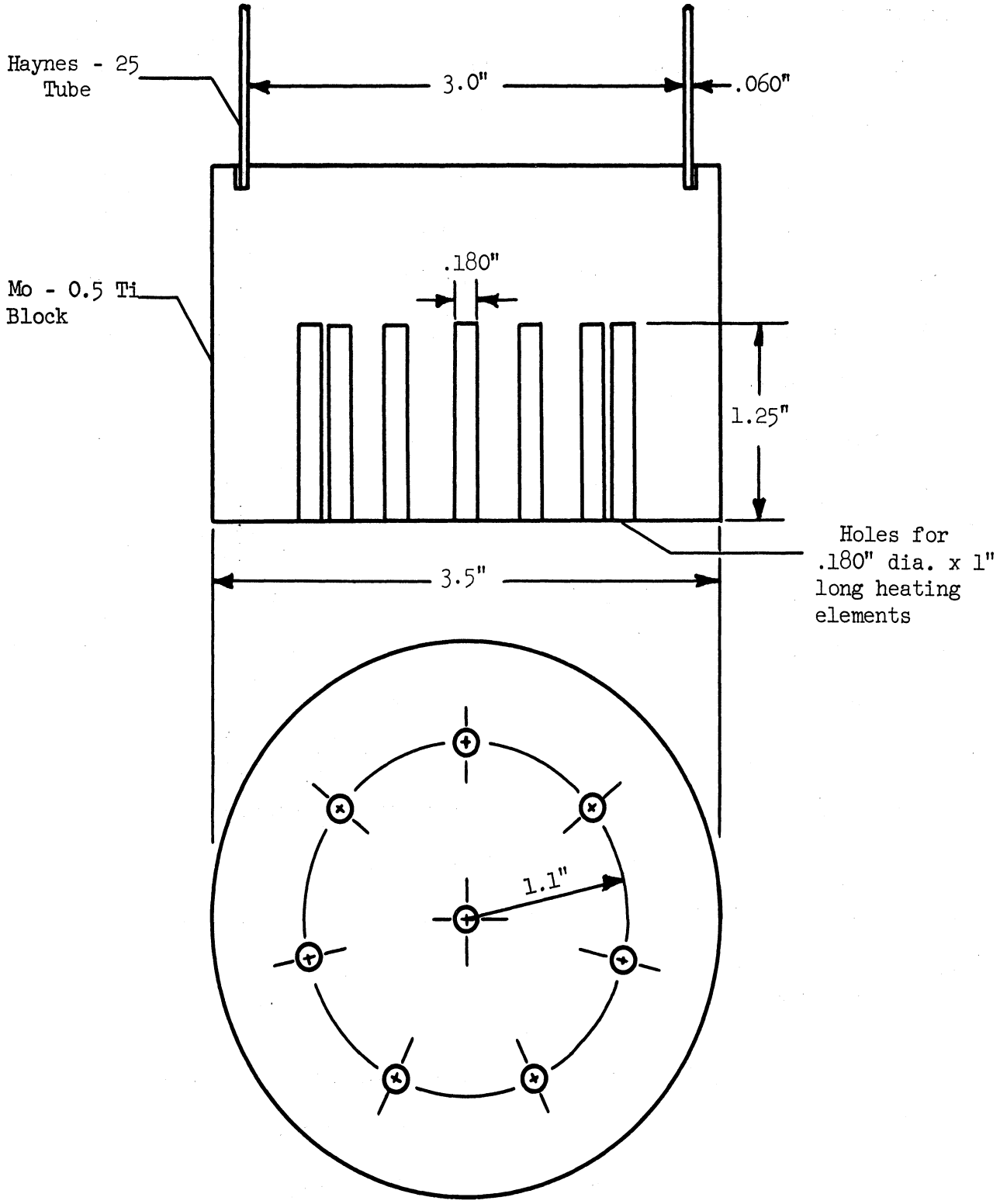

Figure 25. Test Section for Proposed 3-inch Diameter Boiler

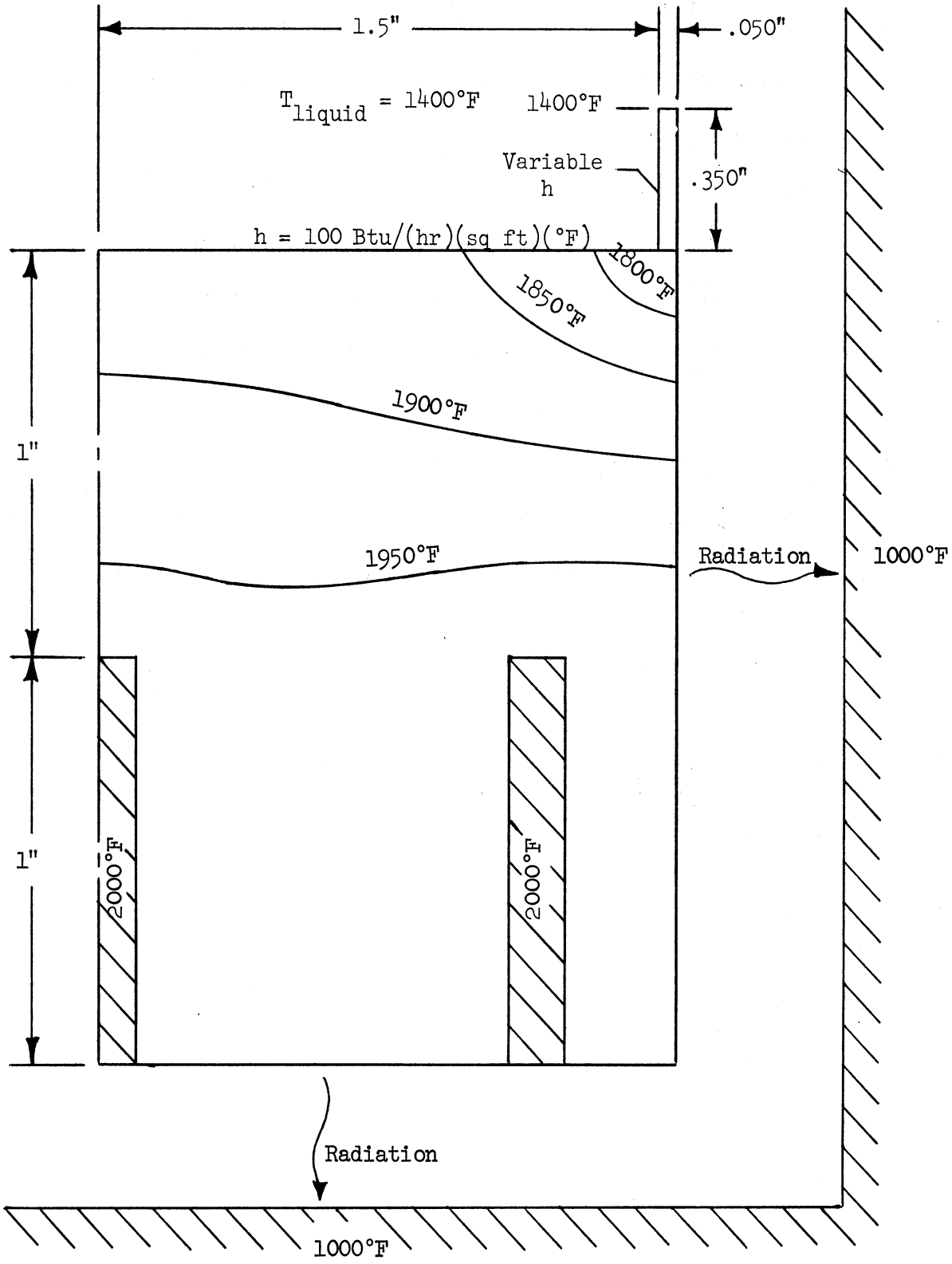

Figure 26. Model of Heater Block for Computer Simulation

measurement used in an analysis of the type above will serve to determine the effect of axial conduction up the tube wall on temperature measurements in the block. Measurement of the power to the heaters and determination of the heat losses by radiation and axial conduction affords another method of calculating the heat flux at the boiling surface which can then be used to check the heat flux calculated by temperature measurements in the block.

With this proposed design, the operating difficulties associated with a condensing media will be eliminated. Without the uncertainty in the results of the analytical studies caused by the effect of the condensing coefficient, it will now be possible to correct a calculated flux for the effect of axial heat losses with a higher degree of reliability.

FORCED CIRCULATION STUDIES

Robert E. Barry

INTRODUCTION

The objective of this program is to compare the two-phase heat transfer characteristics of liquid metals in swirl and straight-tube flow. The studies are being carried out in the forced circulation loop constructed under Contract AF 33 (616)-8277. The loop is described in detail in (4) and a schematic diagram of the main flow circuits is shown in Figure 27. The system utilizes two separate fluid circuits.

The primary circuit contains potassium or sodium as the working fluid and the secondary circuit utilizes condensing sodium as the heating fluid. The liquid metal in the primary circuit is pumped by an electromagnetic pump through a throttle valve and an electromagnetic flowmeter. The flow is then equally distributed into the three parallel heating sections of the preheater and exits into a common header at the test section inlet. The fluid then enters a 23-inch length of 1/2-inch tubing, the last 2 inches of which are heated by sodium condensing on the outside of the tube. The first 21 inches serve to provide a fully developed velocity profile at the entrance to the heated section and as shown in Figure 28, is enclosed by 1-inch pipe, a loose fitting cylinder containing thermocouples, the test section wall, guard heaters and insulation, all of which serve to provide essentially adiabatic flow during the development of the velocity profile. The fluid then passes through a horizontal section of pipe for measurement of pressure drop and void fraction. A condenser, hotwell, and subcooler complete the circuit. A bypass filter and a hot trap consisting of a bed of zirconium chips are connected in parallel with the main circuit to alleviate oxide contamination.

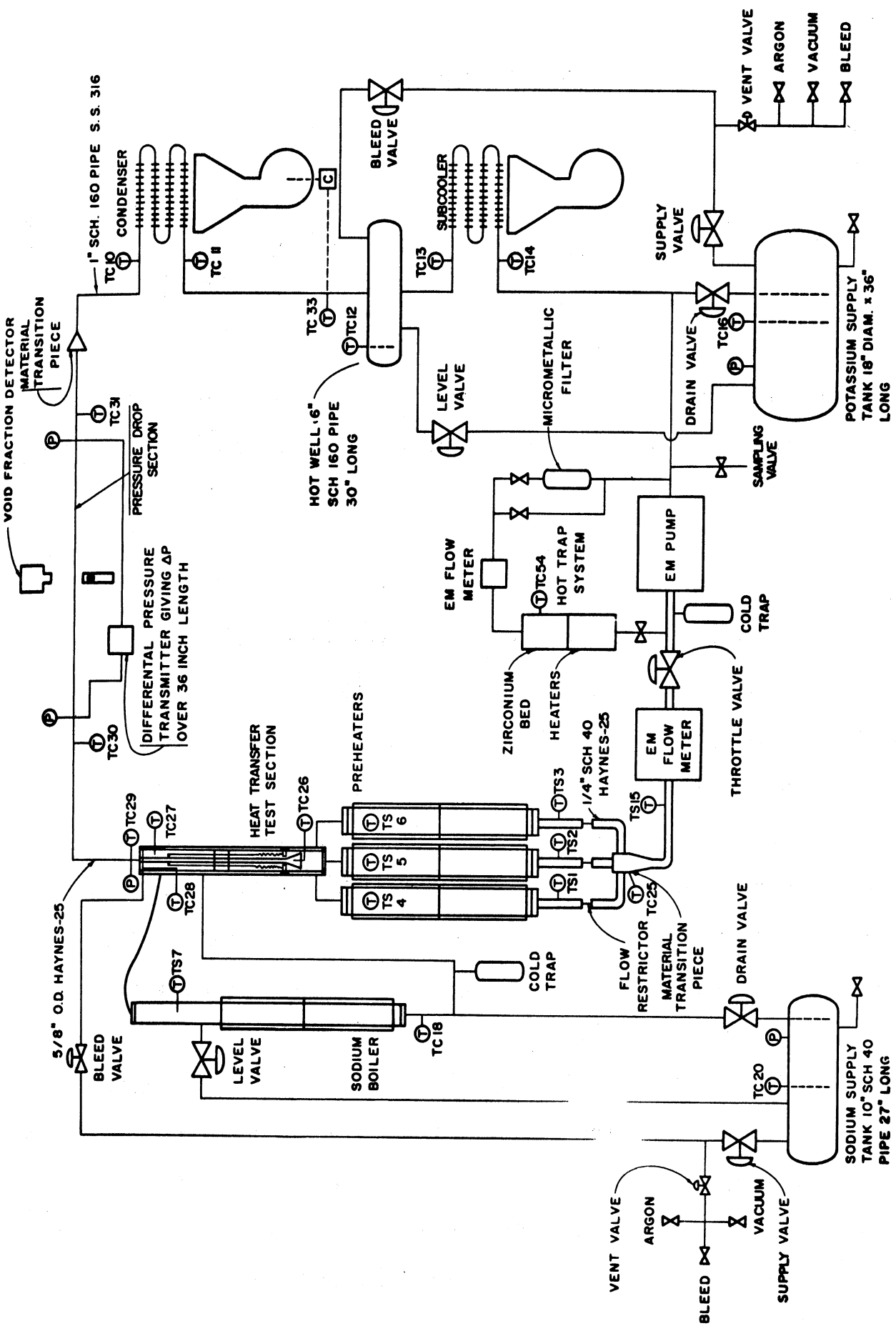

Figure 27. Flow Schematic-Boiling Liquid Metal System

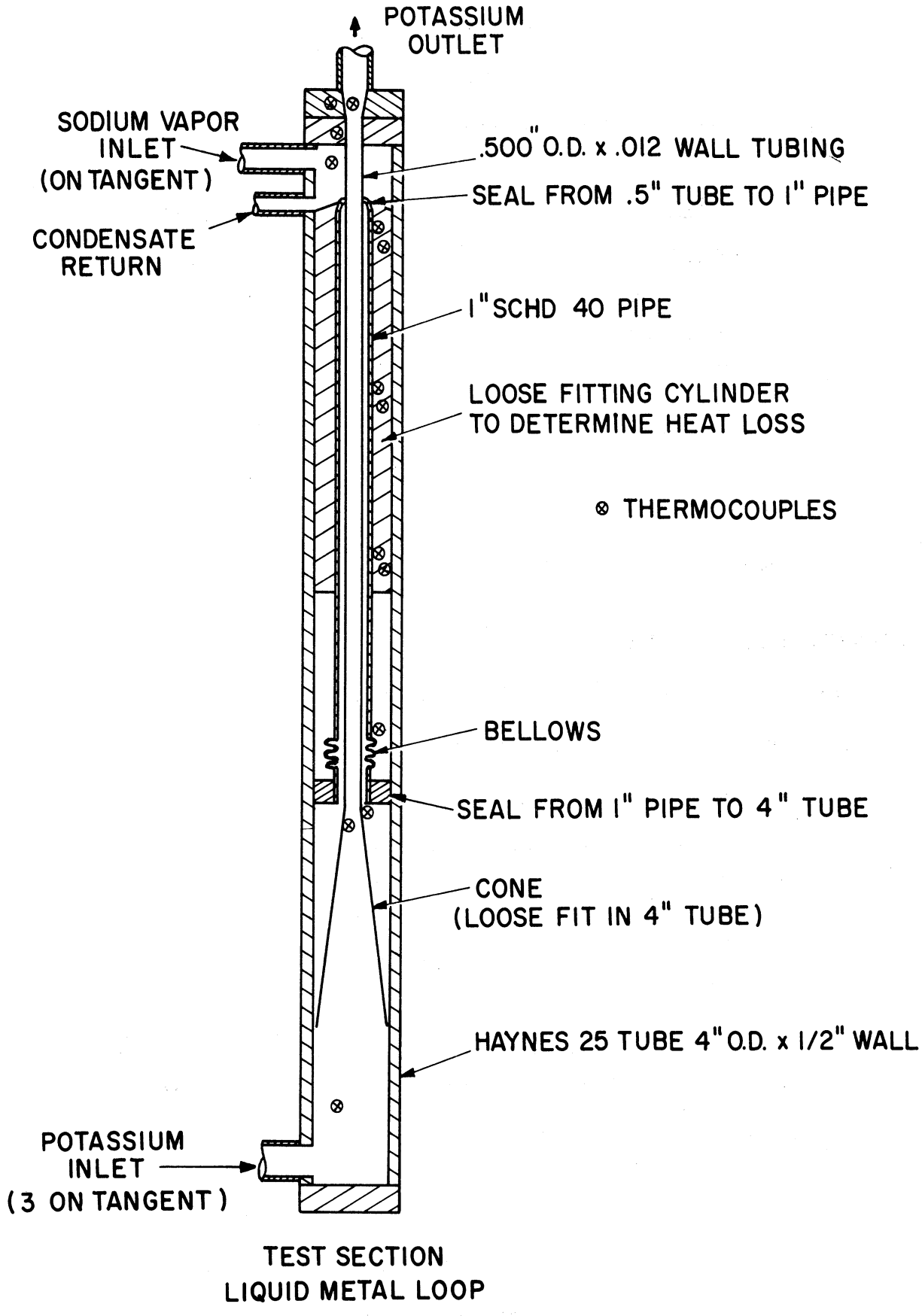

Figure 28. Test Section

In the secondary circuit, sodium is vaporized in the boiler, condensed in the shell side of the test section and returned by gravity to the boiler.

The operational specifications were the following:

Working Fluid	Potassium or Sodium
Fluid Temperature	1400 - 1800 °F
Design Pressure	200 psi
Flow Rate	0.2 to 2 GPM
Total power input	40 KW
Heat flux at the test section	1 million BTU/(hr)(sq ft)

After completion of the straight-tube studies, a swirl device is to be installed in the heated portion of the test section.

OPERATIONAL PROBLEMS AND DESIGN CHANGES, 1963

Operation of the loop during 1963 disclosed the following problems:

1. Cavitation in the electromagnetic pump.

   This occurred primarily at high flow rates and low temperatures and pressures. Apparently, at flow rates in excess of 0.4 GPM, a hotwell pressure of 5 psia is required to prevent cavitation. Therefore, at future startups under vacuum, a flow rate of 0.4 GPM will be maintained until the required pressure in the hotwell is achieved.

2. Excessive heat losses in the loop resulting in substantial subcooling at the preheaters.

   The major losses were in the condenser and subcooler. The length of finned tubing in both was reduced by one-half. The preheater insulation was increased and the test section was fitted with guard heaters and thermocouples both to reduce heat losses and to provide an accurate measure of the enthalpy changes of the fluid between the test section entrance and the heated portion of the tube.

3. Burnout of the heaters in the preheater and sodium boiler.

   These were clam shell radiant heaters consisting of 18 ga Kanthal wire coils imbedded in a heat conducting cement. The burnouts occurred primarily where the contact between the cement and the coil was poor and also at the point where the wire entered the heating unit. New heaters designed with heavier 13 ga coils and heavier connections at the wire entrance were installed. Special attention was given to maintaining good contact between the coils and the cement.

4. Mechanical failure of the test section bellows.

This bellows had cracked circumferentially allowing potassium to enter the sodium boiler. It was manufactured from Haynes-25 to allow operation at 1800 °F. The failure may have been due to embrittlement since the majority of loop operations had been carried out in the precipitation hardening range of this alloy. The bellows was replaced by one manufactured from Inconel-x. This choice reduces the maximum operating temperature in the primary loop to 1600 °F but affords more flexibility in loop operation in that greater temperature differentials between the potassium and the sodium can be maintained.

5. Boiling instabilities.

While not a serious problem in the preheaters, boiling instability of large magnitude was noted in the sodium boiler. The three preheaters were fitted with a 1/8-inch diameter rod, 40 inches long. 1/8-inch tube Swagelok nuts were welded to the rod at 1 1/2-inch intervals. These nuts, with the open end downward are to serve as vapor traps to provide vaporization nuclei. The sodium boiler was fitted with four such rods and, in addition, was provided with two 1/4-inch heated tubes to provide additional nucleation sites. These tubes project 2-inches outward from the boiler wall at heights corresponding to 1/3 and 2/3 of the liquid level.

OPERATIONS, 1964

By March, 1964, the primary supply tank had been cleaned and charged with high purity potassium; the test section condenser and subcooler had been reinstalled; and the installation of new heaters, insulation and wiring was completed. On March 24 potassium was charged to the loop, circulated at 800°F for 35 minutes and dumped. This procedure was followed in order to remove any oxides that had formed on the walls during alterations to the loop.

On March 25 circulation in the loop and hot trap began. The pump plugged immediately and was cut out and cleaned.

On April 2 circulation was maintained in the loop for one hour after which circulation was begun in the hot trap. Within 15 minutes after the hot trap reached 1200°F, the pump plugged and it was cut out and cleaned.

On April 16 the throttle valve plugged almost immediately upon start-up. Attempts to dislodge the plug by circulating hot potassium near it resulted in plugging of the preheater flow distributor and flowmeter. The lines from the

preheater to the pump were cut out and cleaned. It was suspected that the zirconium chips had become heavily laden with oxide and were spalling at high temperatures and therefore the hot trap circuit was cut out and cleaned and fresh chips were installed. At this time a bypass filter was installed upstream of the pump and a filter was installed on the charging line. Analysis of the residue in various parts of the loop indicated that zirconium was being transported from the hot trap to the various parts of the loop.

On July 10 start-up was attempted but the pump plugged during charging. By supplying power to the pump at no flow, the plug was dissolved at a temperature of about 1100 °F.

On August 8 circulation was begun through the hot trap alone. The pump plugged within 30 minutes. There appeared to be a good possibility that the previous rodding and flushing of the pump had resulted in only a small hole through the plug with the result that the already small (.065-inch) pumping section was reduced even further. Accordingly, the pump was cut out of the loop and the pumping section was removed, X-rayed and sectioned.

An X-ray photograph of the pumping section is shown in Figure 29. The dark areas consisted of a hard black material and a hard greenish white substance. Both types of material absorbed water, turned mushy and then apparantly took up water of crystallization to produce a hard green cystalline material. None of these materials were readily soluble in the weaky acidic solutions used to flush the pump. X-ray diffraction studies of this material have not as yet led to an identifiable compound but spectrographic analysis has indicated a high zirconium content (6-12%) along with some chromium (1%), nickel (0.15%), and molybdenum (0.10%).

It is evident that plugging problems have occurred in conjunction with circulation through the hot trap. The relatively high concentrations of zirconium in the plugs indicates that zirconium is being transferred from the hot trap into the primary loop.

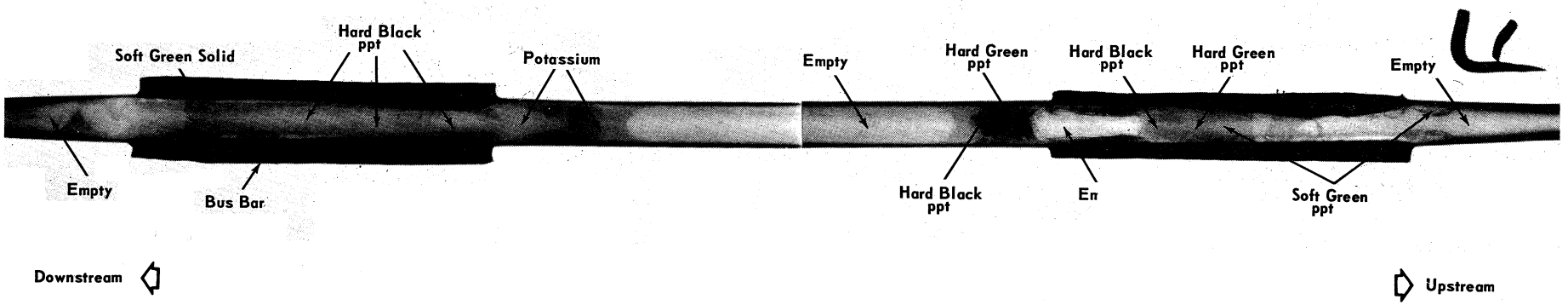

X-RAY OF PUMP

Figure 29. X-Ray of Pumping Section

One possible mechanism for this transport is as follows: zirconium reacts with the potassium oxide to produce a coating of zirconium oxide on the surface of the chips. Since the diffusion of the oxide into the body of the chip is slower than the formation of oxide on the surface, the higher oxide would tend to form. This oxide is not as adherent as the lower oxygen form and likely spalls off with the result that small particles of zirconium oxide are carried along with the potassium. These particles would then tend to collect in restricted portions of the loop such as the pump, throttle valve, flowmeter and preheater inlet.

A new pumping section has been procured and placed in the loop. The auxiliary lines from the loop to the argon pressurizing system and the vacuum system have been tested leak-tight by a helium leak detector. When circulation is again initiated, flow will bypass the hot trap but will pass through a stainless steel filter upstream of the pump. If the filter plugs up, it will be replaced with a clean one until sustained operation at high temperature is possible. By such a procedure, it is hoped that the loop can be returned to a condition such that the heat transfer experiments can proceed.

ANALYSIS OF THE EXPERIMENT

There are several methods of characterizing heat transfer to a boiling two-phase fluid in forced circulation. The method chosen in this experiment is to evaluate the overall coefficient of heat transfer from the sodium vapor, through the tube wall, to the two-phase fluid, defined as:

$$U_2 = \frac{q_w}{T_v - T_2}$$

where:

U_2 = overall coefficient to the two-phase fluid.

q_w = heat flux at the test section wall.

T_v = sodium vapor temperature.

T_2 = bulk temperature of potassium fluid at test section outlet.

The heat flux at the test section may be evaluated from knowledge of the total power input to the sodium boiler from which are subtracted previously calibrated losses from the sodium boiler and loop. At the high temperatures involved, these losses are a function of only the sodium vapor temperature. The outlet bulk temperature of the two-phase flow is a satisfactory measure of the temperature existing within the test section if the temperature and pressure are assumed to be in equilibrium since the pressure drop along the 2-inch length of the test section is negligible.

By varying the experimental conditions, the overall coefficient can be studied as a function of the inlet quality, mass flow rate and temperature of the fluid. (The latter being important because of its effect on the liquid-vapor density ratio.)

It is possible, however, to obtain a more meaningful characterization of the heat transfer by evaluating the individual film coefficient of heat transfer to the boiling two-phase mixture defined by:

$$h_2 = \frac{q}{T_{iw} - T_2}$$

where:

h_2 = flim coefficient of the two-phase fl

T_{iw} = temperature of internal surface of t

The overall coefficient and the film coefficient are related by:

$$\frac{1}{U_2} = \frac{1}{h_c} + \frac{t_w}{k_w} + \frac{1}{h_2}$$

where

h_c = condensing film coefficient on outside of tube.

t_w = tube wall thickness.

k_w = tube wall thermal conductivity.

Since V_2 is obtained from experiment and t_w and k_w are known, it would be possible to determine h_2 if h_c, the condensing film coefficient, was known. It is, in fact, possible to determine h_c as shown by the following considerations:

If a single phase fluid were flowing in the tube, one could define an overall heat transfer coefficient:

$$U_1 = \frac{q}{(T_v - T_1)_{mean}}$$

where

U_1 = overall coefficient to the single phase fluid.

$(T_v - T_1)_{mean}$ = mean temperature difference between the sodium vapor and the internal fluid.

For single phase flow U_1 and h_c are related by

$$\frac{1}{U_1} = \frac{1}{h_c} + \frac{t_w}{k_w} + \frac{1}{h_1}$$

where

h_1 = film coefficient of heat transfer of single-phase fluid.

Since V_1 can be determined experimentally and T_w and k_w are known, it would be possible to determine h_c, the condensing film coefficient, if h_1, the single phase film coefficient, were known. It is well to note here that $1/h_c$, $1/h_1$ and $1/h_2$ are expected to be roughly of the same order of magnitude and t/k is quite small in comparison. If this were not the case, unavoidable experimental scatter would render such calculations useless.

Since the 1/2-inch diameter test section is only 2 inches long, it is evident that the test section constitutes a thermal entrance region for the internal fluid and the heat transfer coefficient, h_1, can be expected to be higher (because of the thin developing thermal boundary layer) than it would be for long tubes (where the thermal boundary layer is fully developed). There is a good deal of experimental data for heat transfer to liquid metals in long tubes, but very little for heat transfer in tubes where the ratio of length to diameter is small. If a reasonable criterion could be found to evaluate h_1 by using the existing experimental data for long tubes, then h_c, the condensing coefficient, and h_2, the film coefficient for two-phase flow, could be evaluated. The establishment of such criterion is the subject of the next section.

HEAT TRANSFER TO POTASSIUM IN THE THERMAL ENTRANCE REGION

The heat transfer length of 2 inches in the liquid metal loop gives a length to diameter ratio of 4 and since this is within the usually accepted range for entrance region effects, a theoretical analysis has been conducted to determine what correction factor should be applied to the available data for heat transfer in long tubes.

The salient features of the theoretical analysis are given here and since the results are based on premises which have proven very successful in predicting fully developed heat transfer coefficients, it is felt that they may be applied with confidence to the prediction of entrance region data.

In the theoretical determination of temperature profiles and, hence, the heat transfer coefficient, the following equations are commonly used:

$$\frac{\tau}{\rho} = \left(\frac{\mu}{\rho} + \epsilon_m\right)\frac{du}{dy} \qquad (1)$$

$$\frac{q}{\rho C_p} = \left(\frac{k}{\rho C_p} + \epsilon_h\right)\frac{dT}{dy} \qquad (2)$$

In Equation (1) μ/ρ represents the contribution of molecular processes and ϵ_m represents the contribution of turbulent eddies to the total local shear stress. In Equation (2) k represents the contribution of molecular thermal conductivity and ϵ_h represents the contribution of turbulent eddies to the heat transfer.

Dividing Equation (2) by (1) gives for T

$$dT = -\frac{q}{\rho C_p} \cdot \frac{\rho}{\tau} \cdot \frac{\mu/\rho + \epsilon_m}{k/\rho C_p + \epsilon_h}\, du. \qquad (3)$$

This equation may be integrated if q, τ, ϵ_m and ϵ_h are known and thus a bulk temperature obtained from

$$T_b = \frac{\int_o^R u\,T\,dr}{\int_o^R u\,dr}$$

Then the heat transfer coefficient may be obtained by

$$h = \frac{q_w}{T_w - T_b}$$

and the Nusselt number by

$$Nu = \frac{h\,D}{k}$$

In Equation (3) q is obtained from a heat balance over an element of fluid. τ can be obtained from the friction factor by

$$\tau = \frac{f_i}{2}\rho u_b^2$$

and

$$\tau = \frac{r}{R} \tau_w$$

and ϵ_m can be obtained rom Equation (1) along with a generalized velocity distribution for flow in tubes (14).

Alternatively ϵ_m can be obtained (using a generalized velocity distribution) from:

$$\epsilon_m = n^2 u y$$

for flow close to the wall, and the von Karman relation:

$$\epsilon_m = K^2 \frac{(du/dy)^3}{(d^2u/dy^2)}$$

for flow at a distance from the wall, where n and K are experimentally determined constants. The alternate method has been experimentally verified for air in reference (14) and (15).

The crucial problem in theoretical analyses of liquid metal heat transfer has been the determination of ϵ_h. Reasonably successful results have been obtained by assuming there is a close relationship between the contribution of turbulent eddies to heat and momentum transfer which can be described by:

$$\Psi = \epsilon_m/\epsilon_h .$$

A knowledge of Ψ thus permits the integration of Equation (3). Martinelli (36) chose $\Psi = 1.0$ in his analysis which led to the Martinelli-Lyon equation:

$$Nu = 7.0 + 0.25\ Pe^{0.8}$$

This approach has, in general, given theoretical results higher than the experimental data and Deissler (16) and other workers have accounted for this by

taking into account the heat loss from an eddy while it traverses the tube. This has resulted in values of Ψ less than unity since the eddy transport of heat becomes less efficient than the eddy transport of momentum for the high conductivity liquid metals. Deissler's equations have been successful in predicting the Nusselt number for liquid metals in fully developed flow and therefore his subsequent analysis for the thermal entrance region (17) has been programmed on the IBM 7090 computer to obtain the correction factor for thermal entrance regions.

The correction factor is shown in Figure 30 as a function of Peclet number. Values of Ψ for the top curve range from .001 to .08 in accordance with Deissler's analysis whereas the bottom curve represents a value of $\Psi = 1.0$. Note that at a Peclet number of 100 (corresponding to a flow of about 1GPM in the loop). The curves predict a correction factor of 1.17 and 1.15. Therefore, since a large variation in the assumption for Ψ makes a very small difference at low Peclet numbers and further, since the correction itself is small, it is felt that a factor of 1.16 may be used with confidence.

The final question to be answered is the value of the Nusselt number for fully developed flow. Herrick (23) in a 1964 review of experimental results recommends

$$Nu = 5.0 + .025\ Pe^{0.8}$$

which corresponds quite closely with Deissler's analysis at Peclet numbers up to 500. There are some results however, notably Subbotin (54), which indicate that the Martinelli-Lyon equation is applicable to alkali metals (later work of Subbotin was included in (23)) and also indications (10) that at low Peclet numbers, the Nusselt number falls substantially under the above prediction.

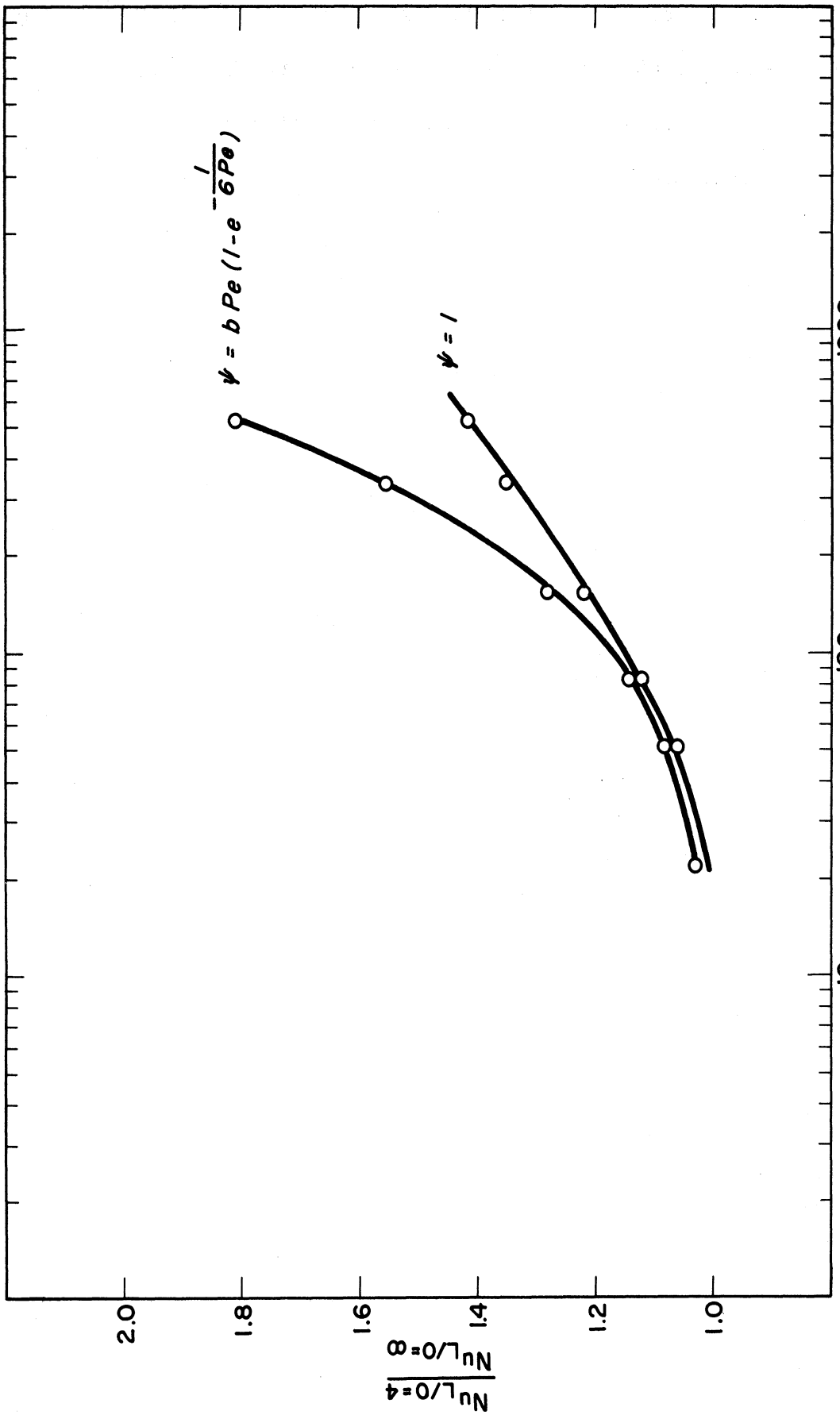

Figure 30. Correction Factor for Thermal Entrance Region

Considering all of the experimental data, however, it appears that the Nusselt number can be best predicted by the above equation. Applying the correction factor of 1.16 results in a predicted Nusselt number of 7.0 for the single phase flow at 1GPM in the loop.

TWO PHASE PRESSURE DROP AND VOID FRACTION STUDIES

INTRODUCTION

In recent years metallic fluids have received much attention as possible heat transfer media in space electrical power generation cycles. All proposed cycles include boiling and condensing of the carrier fluid and therefore involve the flow of vapor-liquid mixtures. The rigorous designs required in these applications necessitate the ability to predict two-phase flow phenomena to a high degree of accuracy. Although voluminous literature exists on the subject of two-phase fluid flow, few investigations have been reported on metallic two-phase flows, and the need for such experimental studies has thus been widely recognized.

For two-phase flow in a tube, the pressure drop between two points in general is the summation of losses due to friction, acceleration effects, and hydrostatic head. The complex interactions between vapor and liquid, when added to the drag of the fluid phases on the tube wall, usually lead to greater pressure losses than are experienced in single-phase flow. Such frictional losses occur for any orientation of the flow channel and for adiabatic or heated conditions. The acceleration losses occur primarily in forced-circulation boiling flows, where the continuous phase change causes the mixture density to vary along the tube. Hydrostatic head terms are present only for vertical or inclined flow systems.

Knowledge of the mean density of the two-phase mixture is necessary in predicting acceleration losses and hydrostatic head. In gas-liquid flow, the mean velocities of the two phases based on the cross sectional area of each generally are not equal. Because of this inequality of velocities, referred to as "slip,"

the true fraction of the pipe cross section occupied by either phase differs from that calculated on the basis of the volumes of gas and liquid entering the tube. As a result of this situation, the mean mixture density cannot be calculated on the basis of quality (vapor mass fraction) alone, and knowledge of the void fraction (fraction of the channel cross section occupied by vapor) is also necessary. The void fraction, then, is an important parameter in predicting the hydraulics of many two-phase flow systems, since without it the accelerative and hydrostatic contributions to the pressure drop cannot be obtained.

The scarcity of information concerning two-phase flows of metallic systems prompted this experimental study of two-phase flows of potassium. Pressure drop and void fraction data were obtained from a boiling heat transfer test loop. Two-phase mixtures were generated in a preheater section, and the pressure drops were measured over a horizontal three-foot length of 0.495-inch ID tube. The total flow rate and mixture qualities at the entrance and exit of this test section were measured. Void fractions were obtained at the middle of the pressure drop section using the gamma-ray attenuation technique.

The potassium heat transfer test loop also included a heat transfer test section in which sodium vapor from an auxiliary pool boiler was condensed in an annulus, thereby transferring heat to two-phase potassium flowing in the central tube. Prior to making these experimental runs a leak developed in the heat transfer test section which allowed sodium to enter the potassium system. Two-phase flow runs were not prevented but the data obtained are for flows of a potassium-sodium mixture containing eight per cent sodium by weight. This composition was constant over the period during which these data were obtained. This fluid is referred to as potassium in this report. A careful study of the data indicates that the results should closely approximate the two-phase flow behavior of pure potassium.

SUMMARY OF PREVIOUS WORK

The literature dealing with two-phase fluid flow is vast, encompassing many aspects of a complex phenomenon. A tremendous amount of data on gas-liquid pipe flows has been obtained. The most widely known generalized treatment of two-phase flow is that of Lockhart and Martinelli (35). This approach to isothermal flows was extended by Martinelli and Nelson (37) to predictions of forced circulation boiling pressure drops for water. The techniques put forth by Martinelli and co-workers did not call for positive knowledge of the flow regimes as have many of the theoretical approaches to two-phase flow.

Anderson and Mantzouranis (2), Calvert and Williams (11), and Dukler (18) treated the annular flow regime using concepts from classical fluid mechanics. Linning (34) analyzed the adiabatic flow of evaporating fluids in terms of three modes of flow: annular, separated, and froth. Pike (44) recently presented a slightly modified version of Linning's annular flow analysis and found that his void fraction predictions were quite accurate for low quality steam-water flows. Bankoff (5) proposed a variable density single fluid model in an analysis of vertical bubble type flows. The model's predictions of void fractions and frictional pressure drops compared favorably with data obtained from steam-water flows. Levy (33) treated the two-phase system as a continuous medium and applied to it the single-phase turbulent mixing length methods. Two-phase density and velocity distributions as well as pressure drops were thus derived analytically. Good agreement was found between the theory and available data. Several authors have approached two-phase flow through the friction factor concept. Bertuzzi, Tek, and Poettmann (8) treated the two-phase system as a single phase and correlated a two-phase friction factor in terms of a two-phase Reynolds number.

Of particular interest to this study are investigations of metallic two-phase flows, few of which have been reported. Kutateladze (32) summarizes the results of Gremilov and co-workers who studied vapor-liquid flows of mercury.

Kutateladze also presents Siryi's results for mercury vapor-liquid system as well as those of Korneev who worked with a magnesium amalgam-mercury vapor system. These workers obtained void fraction values and correlated them against the ratio of superficial vapor velocity to total liquid velocity, using an all-liquid Froude number as a parameter. The Froude numbers were between 1 and 20. Smith, Tang, and Walker (52) obtained void fractions in vapor-liquid mercury flows where the all-liquid Froude numbers were of the order of 10^{-4}. A correlation similar to Gremilov's was given. Tang, Smith, and Ross (55) extended the work of reference (52) to the potassium-mercury amalgam system. They found that the potassium amalgam data did not correlate with the mercury data when the original method of correlation was attempted. However, a satisfactory void fraction correlation of the Martinelli type (35) was obtained.

Neal and Bankoff (39, 40) developed an electrical resistivity probe which allows high-order resolution of local void fraction, bubble frequency, and bubble size distribution in two-phase flows in the bubble regime where the liquid phase is electrically conducting. Neal (39) also discussed development of an impact probe for measuring local liquid velocity. These instruments were used to measure local parameters in vertical cocurrent mercury-nitrogen flows. A concomitant photographic study showed that the structure of mercury-nitrogen flow is much different from air-water flow, indicating that correlations for the latter fluid system would be inapplicable for mercury-nitrogen flows.

Koestel (31) obtained pressure drop and liquid fraction data for horizontal, isothermal mercury-nitrogen flows in a 0.395-inch ID by 51.75-inches long Pyrex glass tube. Qualities ranged from 0.020 to 0.469.

Pappendiek, et al (45) reported some values of boiling pressure drop for mercury in a 0.305-inch ID tube, approximately 14.8 inches long. Some flows were vertical and some horizontal; inadequate information was given concerning system pressure level and fluid temperatures. A plot of pressure drop as a

function of quality for mass flows of 65 lb/hr is given, but it is not clear whether the data are for horizontal or vertical flows, or possibly both with suitable corrections made in the vertical data. Whether the qualities are average, inlet, or outlet is not stated.

Considering work with alkali metals, Hoffman (25, 46) reports the results of studies of vertical boiling pressure drops for potassium. The test section was 0.325-inch ID by approximately 80 inches long. However, in addition to the boiler tube, an inlet mixing chamber, an exit and expansion section, and exit thermocouple wells were located between the pressure taps. Thus, the pressure drop data include irrelevant undetermined losses. Berenson and Killackey (7) obtained pressure drop data for flows of potassium through a horizontal boiler. The boiler tube was about 12.8 inches long by 0.180-inch ID, but flow was really through a helical passage formed by insertion of a twisted ribbon into the boiler tube. Temperature profiles were estimated by application of the Lockhart-Martinelli correlation (35), and pressure drops were reported as ratios of experimental values to values predicted by the Martinelli correlation. Noyes (41) reported four void fraction values for two-phase adiabatic sodium flows at 8 lb/sq in absolute. Qualities ranged from 0.0034 to 0.028. Fisher (20) obtained pressure drop data for boiling rubidium in a 0.28-inch ID, horizontal tube about 47 inches long, using a Taylor volumetric differential pressure gauge. The data were not presented in a manner suitable for comparison with results of other studies.

Baroczy (6), using the mercury-nitrogen data of Koestel (31) and the water-air data of Hewitt, et al (24), developed a generalized void fraction correlation which he believed, because of the inclusion of Koestel's data, could be generally applied to single component metallic fluids. Goldmann (21) presented estimates of boiling pressure drops for sodium, based on the technique of Martinelli and Nelson (37). His estimates were purely computational, and, ad in the case of the Baroczy void fraction correlation, lacked experimental verification.

Research efforts in two-phase flow are being intensified, particularly as regards the behavior of metallic fluids which appear promising in space applications. The work in metallic fluids cited above indicates that useful and reliable experimental data are being sought. This study presents an extensive set of pressure drop data for two-phase flows of potassium together with a general void fraction correlation for two-phase flows of single-component metallic systems. It is believed that the results of this study may prove useful in such practical problems as design and performance prediction and also in verifying the utility of various theoretical treatments for two-phase metallic flows.

EXPERIMENTAL EQUIPMENT AND PROCEDURES

The Potassium Test Loop

The basic experimental facilitywas a boiling metal heat transfer test loop constructed of Haynes-25 alloy* and 316 stainless steel. Two-phase flow data were obtained from a horizontal tubular test section. Void fraction measuring equipment was located at the mid-point of the test section.

A flow diagram of the boiling metal system is shown in Figure 27. Liquid potassium was pumped by the electromagnetic pump through a throttle valve and a magnetic flowmeter. Flow was then equally distributed into the three parallel heating sections of the preheater where vapor was generated. The two-phase mixture generated in the preheater passed through the heat transfer section and then the horizontal pressure drop test section. The flow continued through a condenser section and into a hot well from which liquid was returned to the pump via a subcooler. The circuit was equipped with a supply tank from which the system could be charged and into which liquid metal could be dumped. The loop included valves and auxiliary lines for bleeding, pressurizing, venting, levelling, and draining.

* A cobalt base alloy produced by Haynes-Stellite Division of Union Carbide Corporation.

Certain features of the equipment in Figure 27 are worthy of mention. The pump was a Mine Safety Research Style II electromagnetic conduction pump. Its developed pressure was rated at 100 lb/sq in at no flow and 80 lb/ sq in at 2 gal/min. Flow rate was controlled by varying the applied voltage up to 270 volts or by regulating the throttle valve. This valve was a stainless steel bellows sealed valve, the ball position of which was set by an air signal. The flowmeter was a Mine Safety Research Style FM-2 magnetic flowmeter. Maximum possible errors in mass flow rates determined from this meter were shown to be 2.8 per cent (53). Since this is the statistical maximum error, the accuracies of flow rates were actually much better than 2.9 per cent.

The preheater consisted of three sections of 4-inch OD by 3-inch ID by 45-inches long Haynes-25 pipe mounted in parallel. Approximately 3 feet of each section were heated by four electrical radiant heaters. The power supplied to the preheater was read within 0.1 KW on a General Electric AC Kilowatt meter. Total rated preheater power was 30 KW.

The heat transfer section was a double-pipe heat exchanger constructed of Haynes-25 alloy, for condensation of sodium vapor in the annulus, thereby transferring heat at high fluxes to two-phase potassium flowing in the central tube. The mechanical design of this section is quite complicated, the details of which are furnished by Balzhiser, et al (4). As mentioned in the Introduction, the thin inner wall of this section developed a leak causing the two-phase flow runs to be made with a mixture containing 8 per cent sodium. During the two-phase runs the heat transfer section was not operated and merely acted as piping.

The condenser and subcooler were each fabricated from 10 feet of 1-inch, schedule 160, stainless steel finned tube over which air was passed at rates up to 800 std cu ft/min. The subcooler's specific function was to assure that the liquid entering the pump was subcooled, thus helping to prevent pump cavitation. The hotwell was a horizontal section of 6-inch schedule 160 stainless steel pipe

54-inches long. Its functions were to assure a liquid level above the pump intake even in the event of large flow rate instabilities, to act as an accumulating chamber for system cover gas (argon), and to act as an expansion tank for liquid, the total volume of which varied with temperature and vapor fraction changes in the loop.

Figure 27 indicates four thermocouples (TC 25, TC 26, TC 30, and TC 31) which were vital to the establishment of a loop heat balance. These thermocouples were platinum/platinum plus 10 per cent rhodium and were calibrated against a National Bureau of Standards secondary thermocouple. Standardized thermocouple lead wire connected all thermocouples to the potentiometer selector switch. The thermocouples were electrically insulated from the loop. Temperatures indicated by these Pt/PtRh thermocouples were accurate to within 1°F.

The loop included about forty other chromel-alumel thermocouples which were used to monitor loop operation. The potassium circuit included five air operated valves in addition to the throttle valve. All piping was traced with electrical warm-up heaters which were used on start-up and shut-down to keep temperatures above 145°F melting point. The system also included a zirconium hot trap for maintaining very low oxygen concentrations. The loop was remotely operated from a control panel, which contained several automatic safety features in addition to operating controls. Smith (53) furnishes a detailed description of the potassium loop.

Two-Phase Pressure Drop Measurement

The horizontal pressure drop section was fabricated of 5/8-inch OD by 0.495-inch ID Haynes-25 alloy seamless tubing. Pressure drops were obtained over a 36-inch length. Two-phase flows entered this section from a 10-inch horizontal calming section which was an upstream extension of the pressure drop section. The differential pressure taps were 1/4-inch schedule 40, 4-inch long, Haynes-25 pipe nipples welded vertically to the bottom of the tube.

Pressure drop was measured with a Taylor Transaire Volumetric D-P Transmitter. Stainless steel pressure transmitting diaphragms were welded to the Haynes-25 pressure taps. The volumes on top of these 5-ply diaphragms were filled with liquid potassium. The lower sides of the diaphragm assemblies were connected by stainless steel capillary hose to opposite faces of a single diaphragm which was a component of the pneumatic differential pressure transmitter. The capillary hoses and lower portions of transmitting diaphragm housings were filled with sodium-potassium eutectic alloy, a liquid at room temperature.

Differential pressures across the 36-inch test section were recorded on a Taylor Transcope Recorder. Values were read as per cent of either 100 or 300 inches of water. The scale ranges were set at the pneumatic transmitter, and pressure drop values were accurate to 1 per cent of full scale.

Fluid temperatures 10 inches upstream of the first pressure tap (calming section entrance) and 13 inches downstream of the second pressure tap were measured by thermocouples TC 30 and TC 31 (Figure 27). These well type thermocouples were located away from the ends of the pressure drop section to minimize their effect on flow patterns in the test section. Temperatures at the pressure taps were estimated from the thermocouple readings by means of the experimental pressure gradient, assuming thermodynamic equilibrium existed. Accuracy of the estimated pressure tap temperatures was shown to be better than 0.3 per cent for values above 1000°F (53).

Void Fraction Measurement

The theoretical basis of the gamma-ray attenuation technique for measuring void fractions has been thoroughly reviewed by Smith (53). Basically, the method measures the mean density of the two-phase fluid in the region covered by the gamma-ray beam. Because appropriate gamma-ray absorption coefficients are usually lacking, density values are not directly obtained. The usual procedure

is to obtain indirectly the void fraction by interpolation between detector signals read for all-liquid and all-vapor flows. It can be shown from Beer's Law that, for the probable flow regimes encountered, the void fraction is given by (53)

$$\alpha = \frac{\ell n\ (N/N_\ell)}{\ell n\ (N_g/N_\ell)} \qquad (4)$$

Correct application of Equation (4) requires that all the N's be observed at the same flow temperature. Smith (53) shows that single values of N_g and N_ℓ at one temperature may be corrected for use with all two-phase flow temperatures encountered.

A schematic diagram of the void fraction measuring system is given in Figure 31. The gamma-ray source was a nominal 5-curies of encapsulated metallic Tm-170. This nuclide decays by beta particle emission to Yb-170 which gives off two soft rays--a 0.053 Mev K X-ray and a 0.084 Mev unconverted gamma ray (19). Equation (4) was developed on the assumption of a monoenergetic radiation beam, but since the low energy photons are almost completely absorbed by the pipe wall the detector saw primarily the 0.084 Mev radiation. The 127-day half life of Tm-170 was sufficiently long to insure essentially constant source strength during short experimental runs.

Gamma-rays were detected by the scintillation method, as indicated in Figure 31. The detector unit was a Harshaw Integral Line Assembly consisting of a $1\frac{1}{2}$-inch diameter by 1-inch thick, thallium activated, sodium iodide crystal coupled optically to a 2-inch photomultiplier tube. The assembly included an external magnetic shield.

Radiation count rates were obtained using a Tracerlab SC-18 Superscaler, which included the high voltage supply for driving the photomultiplier tube. The scaler had a resolving time of 5 microseconds, implying less than 1 per cent coincidence loss for count rates up to 120,000 counts/min. The preamplifier was

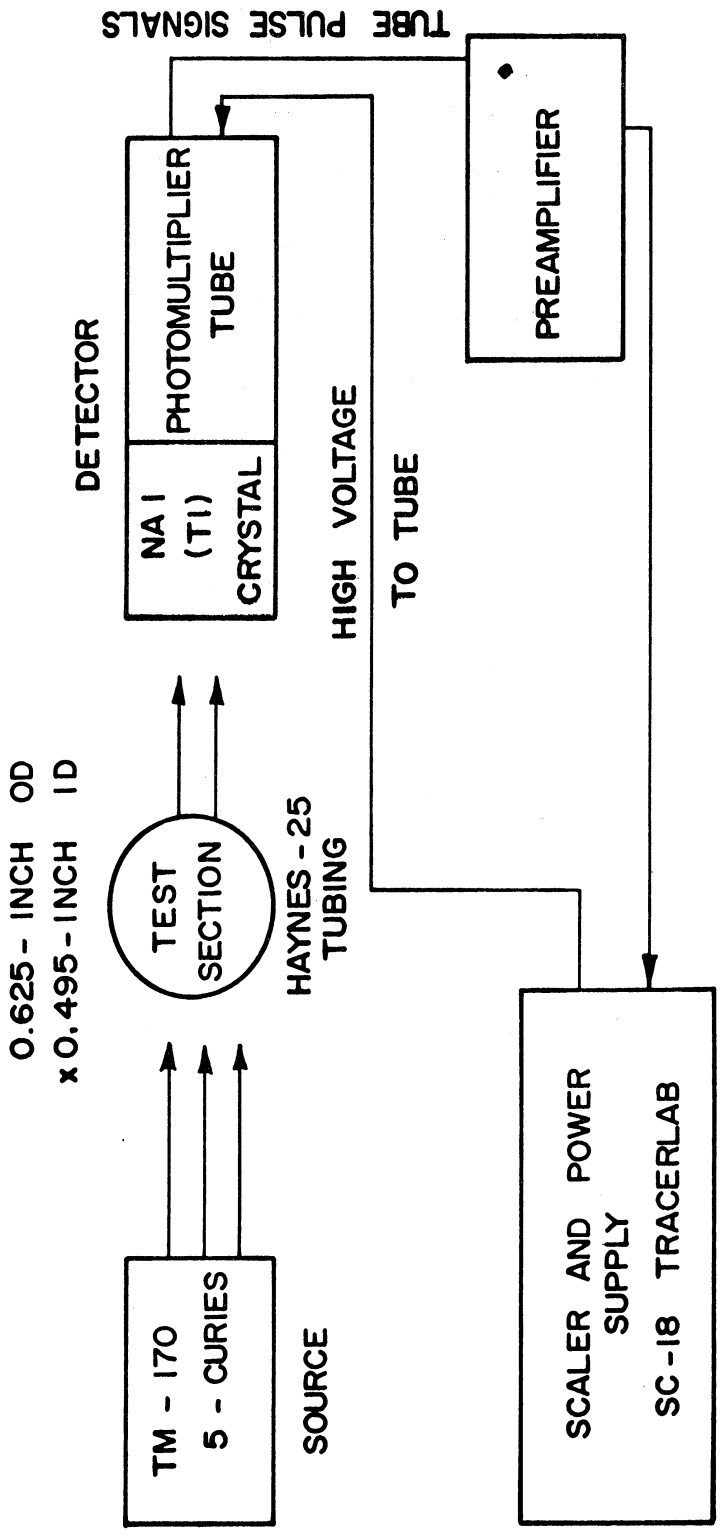

Figure 31. Schematic Diagram of Void Fraction Measuring System

The orientation of the source and detector with respect to the flow channel is of particular interest. The source was mounted on the end of a positioning rod, which was held in an 18-inch long steel tubular shield, having 11/16-inch thick walls. The source shield was vertically mounted under the flow tube, so that the gamma-rays passed upward through the pipe and fluid. The detector was mounted on top of the pipe, inside a steel shield having 1-inch thick walls. The shields for source and detector were accurately aligned on a common frame, the position of which was adjusted to align the gamma-ray beam with the center line of the flow channel (53). A beam collimator was positioned at the output end of the source tube. The diameter of the working beam was about 1/32-inch. The detector face was covered by a 3/4-inch thick steel plate. A 3/4-inch diameter hole was located in the center of this face shield, through which the transmitted radiation beam was detected.

Procedures

Pressure drop data were obtained for flow rates ranging from 108-752 lb/hr and for preheater power inputs from 6.0 to 19.0 KW.

It was necessary to check periodically the zero of the differential pressure transmitter, as it exhibited a slight drift. The procedure consisted of shutting down the flow, in which condition no pressure drop would exist, and decreasing the preheater power to prevent unstable pool boiling in the preheaters. It was found that two to three hours were necessary to restore the loop to steady operation following a transmitter zero check.

Prior to running two-phase flow experiments, a series of all-liquid flow data were taken to determine heat losses from the preheater, heat transfer section, and two-phase flow test section. These losses were found to be essentially independent of flow rate and were correlated as functions of appropriate temperatures (53). Knowledge of the heat losses was essential for calculating

the mixture qualities at the ends of the test section. The quality calculations were made from a heat balance (First Law) between the preheater entrance and the point of interest (53). The data for each pressure drop point included, in addition to the pressure drop, the total flow rate and thermal data necessary for calculating qualities.

Void fraction data were obtained over about the same range of total flow rates as were the pressure drop data--131 to 749 lb/hr. Gamma-ray count rates were obtained from scaler counts recorded for three-minute intervals. This counting time was chosen from consideration of statistical errors and coincidence loss. Over most of the experimental count rate range the standard deviation in counts was about 0.1 per cent, while coincidence losses were about 2.8 per cent. Corrections were made for the coincidence loss (53). An 18.25-inch source-to-detector was used, based on preliminary experimental measurements. To obtain a void fraction value, the procedure involved obtaining the corrected count rate from the collimated gamma-ray beam. The collimator was replaced by a steel shut-off plug, and the background rate was obtained. Background was deducted from the beam count rate, giving the N value for Equation (4). Each void fraction point also included flow rate and thermal data as for the pressure drop data.

RESULTS AND CORRELATION OF DATA

Two-Phase Pressure Drop

For nearly all the data the pressure drop fluctuated regularly about a mean value, which was taken as the pressure drop value. The pressure drop fluctuations were accompanied by oscillations in the flow rate. Both quantities were continuously recorded. The potassium loop thus exhibited instabilities, a situation commonly found in two-phase test loops. The data reported in this study were obtained for the steadiest possible flow conditions.

The differential pressure fluctuations were greatest at high preheater levels and low pumping rates. Qualitatively, liquid superheating in the preheaters is believed to be the cause of the oscillatory behavior. At low flow rates liquid moved into the preheater with little disturbance and the high heat input caused it to superheat, perhaps in the region near the wall, as it proceeded slowly upward. More or less periodically a sudden nucleation occurred, producing a large volume of vapor which pushed a liquid slug up through the heat transfer and two-phase flow test sections. Such a surge was evidenced by fluctuation in the pressure drop and flow meter traces, the latter being due to the momentary flow reversal caused by the sudden generation of vapor. At lower power settings and/or higher flow rates vaporization likely occurred nearer the top of the preheater producing less of a disturbance.

In processing the data to yield qualities and other correlating parameters, the physical and thermal properties were predicted for the binary metallic mixture containing 8 per cent sodium (53). Properties for the pure components were those reported by Weatherford, et al (59). A total of 226 pressure drop values were obtained, with the ranges of experimental quantities as follows:

Pressure Drop, lb/sq in	0.054-3.10
Total Mass Flow Rate, lb/hr	108-752
Inlet Pressure, lb/sq in abs	0.54-15.8
Inlet Temperature, °F	923-1428
Outlet Temperature, °F	862-1419
Inlet Quality	0.0004-0.3788
Average Quality	0.0065-0.3784
Quality change across section	-0.0051-+0.0312

Inlet and outlet qualities to the pressure drop section were calculated by heat balance, assuming equilibrium existed in the two-phase regions. Pressures in the test section were taken as equilibrium vapor pressures. Smith (53) considered

in detail the accuracy of calculated qualities and showed that for 81 per cent of the data quality values were known to within 10 per cent or better.

In operation of the potassium test loop, pressure drop data were obtained over a wide range of preheater power settings while keeping the flow rate essentially constant. In this way, two-phase pressure drop was obtained as a function of average quality in the test section, with total flow rate maintained as a parameter. This manner of processing data at first led to plots of pressure drops as a function of average quality in the test section, with curves for parametric values of total flow rate. Careful examination of the data, however, revealed that the pressure drop was also influenced by the absolute pressure level in the test section. At given flow rate and quality values, the pressure drop varied inversely with system pressure as would be expected. It was thus evident that the primary variables influencing the experimental two-phase potassium pressure drops were total mass flow rate, average quality, and absolute pressure.

Preliminary treatment of the data suggested that they might best be correlated using the two-phase friction factor concept. The specific correlation methods of Huntington (27) and Bertuzzi, Tek, and Poettmann (8) proved unsatisfactory. It was decided to derive suitable correlating parameters by dimensional analysis, taking the following as influencing variables:

Dependent variable:

Two-phase pressure gradient	$\Delta P/\Delta L$ lbf/sq in/ft

Independent variables:

Total mass velocity	G lbm/hr/sq ft
Average quality	x (mass fraction vapor)
Pipe inside diameter	D ft
Vapor density	ρ_g lbm/cu ft

The effect of system pressure level is accounted for by the vapor density, since this quantity is most heavily influenced by pressure. The pipe inside diameter,

while not a variable in this study, is included since it would be expected to influence the results. Any generalized dimensional analysis of vapor-liquid flow in pipes, such as that performed by Ros (50), would also include liquid density, viscosity of both phases, and perhaps surface tension and contact angle. These quantities did not vary widely over the range of temperatures encountered in this study and thus were not included in the dimensional analysis. Application of the Pi-theorem (51) to the above variables yielded a two-phase friction factor as a function of quality.

$$f = \varphi(x) \tag{5}$$

where

$$f = \frac{\rho_g D (\Delta P/\Delta L) g_c}{G^2} \tag{6}$$

(The factor g_c is necessary in conversion of units.) This friction factor has the same basic form as used by several other investigators (8 & 27), differing primarily in the density term.

Figure 3 presents a plot of the two-phase pressure drop data according to the relationship suggested by Equation (5). The least-squares line through the data is given by

$$f = 0.0138\, x^{1.54} \tag{7}$$

Statistical treatment of this correlation (53) showed that this is a highly significant correlation--i.e., there is less than a 0.1 per cent chance of being wrong (statistically) in correlating the data in the form of Equation (7). Figure 32 also indicates the 95 per cent confidence range for average f values predicted by the correlation (58).

It should be emphasized that the correlation of Figure 32 is valid only for potassium flows where acceleration contributions to the pressure gradient are negligible compared to frictional losses. This matter will be considered subsequently.

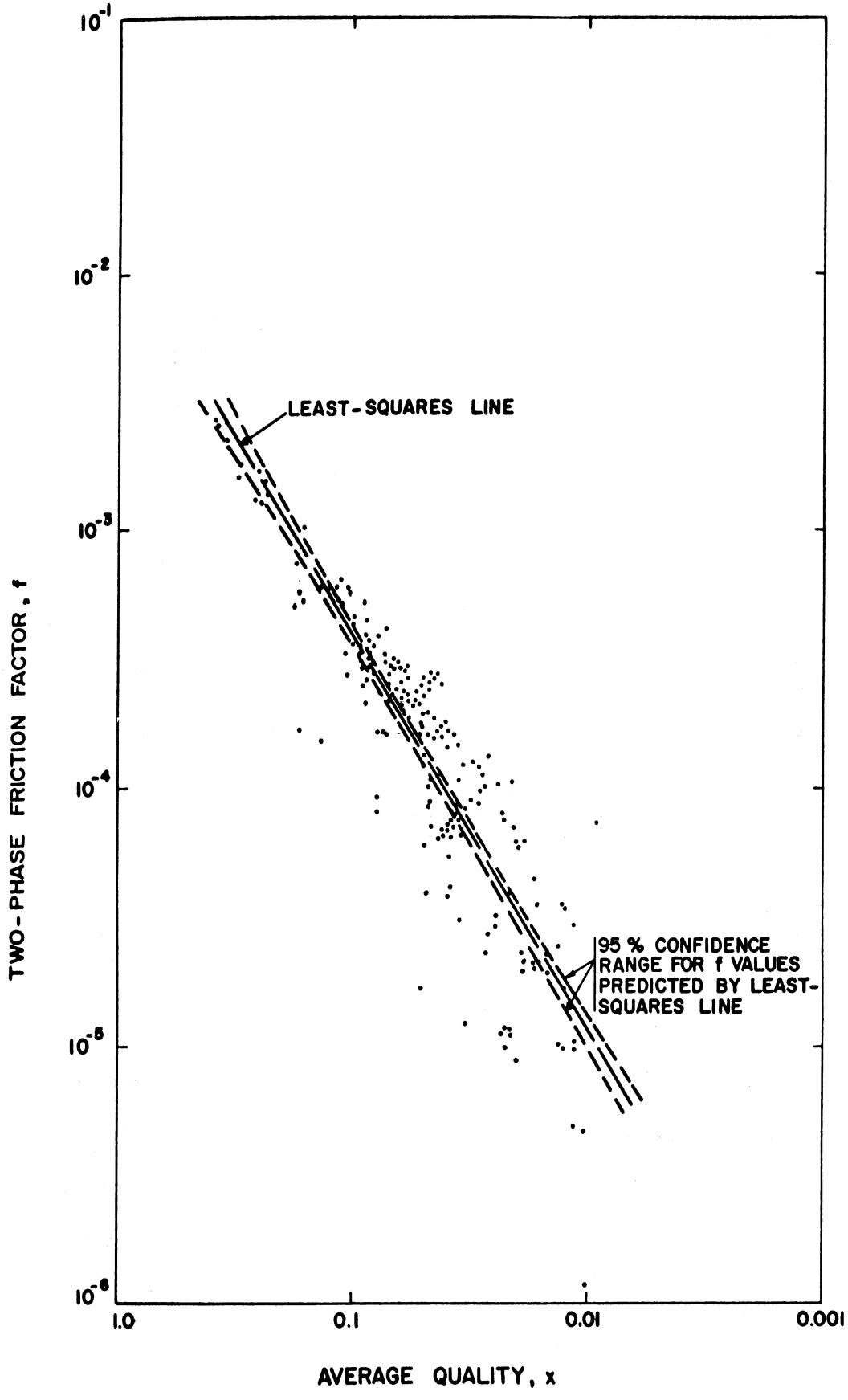

Figure 32. Two-Phase Frictional Pressure Gradient Correlation for Potassium

Metallic Void Fractions

Void fraction values for potassium were obtained by measuring the attenuation of 0.084 Mev gamma-rays from Tm-170, as discussed previously. Seventeen values were obtained, with the ranges of experimental quantities as follows:

Void Fraction	0.153-0.860
Total Mass Flow Rate, lb/hr	131-749
Temperature, °F	879-1320
Average Quality	0.0172-0.1647
Velocity Slip Ratio	53-1150

It was mentioned in the Introduction that the mean velocities of the two phases in vapor-liquid flow, based on the cross sectional area occupied by each phase, are usually not equal. The ratio of mean vapor velocity to mean liquid velocity is therefore greater than unity in many two-phase flows. From a consideration of mass balance this velocity slip ratio is given by

$$S = \frac{V_g}{V_\ell} = \left(\frac{x}{1 - x}\right)\left(\frac{1 - \alpha}{\alpha}\right)\left(\frac{\rho_\ell}{\rho_g}\right) \qquad (8)$$

which is the quantity mentioned above.

The list of experimental ranges indicates that the void fractions were obtained over the same flow rate range as were the pressure drop data. Actually, the distribution of flow rates is narrow, nine values occurring for flows between 200 and 300 lb/hr, and four values occurring for flows between 300 and 400 lb/hr. Smith (53) considered the accuracy of void fraction data and showed that sixteen of the values have standard deviations ranging from 4 to 19 per cent of the void fraction value. One point has a standard deviation amounting to 73 per cent of the void fraction value.

In the first examination of the void fraction data from this study, it was found that ten points occurred for all-liquid Froude numbers between 1.05 and 1.15; small groups of points also represented other Froude number ranges.

This situation prompted an attempt at correlating the data by the method summarized by Kutateladze in which the ratio of superficial vapor velocity to total liquid velocity and the all-liquid Froude number are regarded as independent variables. The resulting plot showed widely scattered points with no discernible parametric effect of Froude number. Tang, Smith, and Ross (55) also experienced failure with this correlation technique.

The potassium data were next plotted in the manner of Lockhart and Martinelli (35), where void fraction (or liquid fraction) is plotted as a function of the variable X, defined as

$$X = \left[\frac{(\Delta P/\Delta L)_\ell}{(\Delta P/\Delta L)_g}\right]^{1/2} \qquad (9)$$

where $(\Delta P/\Delta L)_{\ell(\text{or } g)}$ = pressure gradient that would occur if the liquid (or vapor) were passed through the tube at its own flow rate. For flows in which the liquid and vapor each exhibit Reynolds numbers in the turbulent range (Re 2000)--i.e., for the turbulent-turbulent (tt) flow type--X may be approximated as (1)

$$X_{tt} = \left(\frac{1 - x}{x}\right)^{0.9} \left(\frac{\rho_g}{\rho_\ell}\right)^{0.5} \left(\frac{\mu_\ell}{\mu_g}\right)^{0.1} \qquad (10)$$

For flows in which the liquid flow is laminar (Re$<$1000) and the vapor flow turbulent--i.e., for the viscous-turbulent (vt) flow type--X may be approximated as (1)

$$X_{vt} = \left[\frac{C_\ell}{C_g} \frac{\rho_g}{\rho_\ell} \frac{\mu_\ell}{\mu_g} \left(\frac{1 - x}{x}\right)\right]^{0.5} Re_g^{-0.4} \qquad (11)$$

Ssnce the potassium data were all of the tt flow type, void fraction was plotted against X_{tt}. The resulting graph, while showing a substantial amount of scatter, indicated that a definite correlation existed.

Even though the potassium void fraction data are few in number, the resulting Lockhart-Martinelli plot showed considerable difference compared with data from air-water flows and also with the original correlation curve of Lockhart and Martinelli (35). However, the potassium data did appear to lie on about the same curve as the mercury and potassium-mercury amalgam data of Tang, et al (55). In addition, Noyes' four reported points for sodium (41) also fell in the same region. The favorable comparison of the potassium data with these of other metallic data led to a general liquid fraction correlation for single-component metallic systems--Figure 33.

Almost all the mercury and potassium-mercury data of reference (55) occurred for vt type flows. The four sodium points of reference (41) were listed as occurring for tt type flows. The correlation of Figure 33, as in the original Lockhart-Martinelli correlation, makes no distinction for differing flow types; the scatter in the data precluded making such a distinction.

From the least squares line through all the metallic data, the void fraction is given by

$$\alpha = 1 - 0.574\, x^{0.342} \qquad (12)$$

Statistical treatment of this correlation (53) showed that the form of the correlation is significant at the 0.1 per cent level. Figure 4 also indicates the 90 per cent confidence range for average liquid fraction values predicted by the correlation (58).

DISCUSSION OF RESULTS

Fluid Properties

Since the experimental data were obtained for flows of a sodium-potassium mixture containing 8 weight per cent sodium, one might ask how closely the results approcimate the behavior exhibited by two-phase flows of pure potassium.

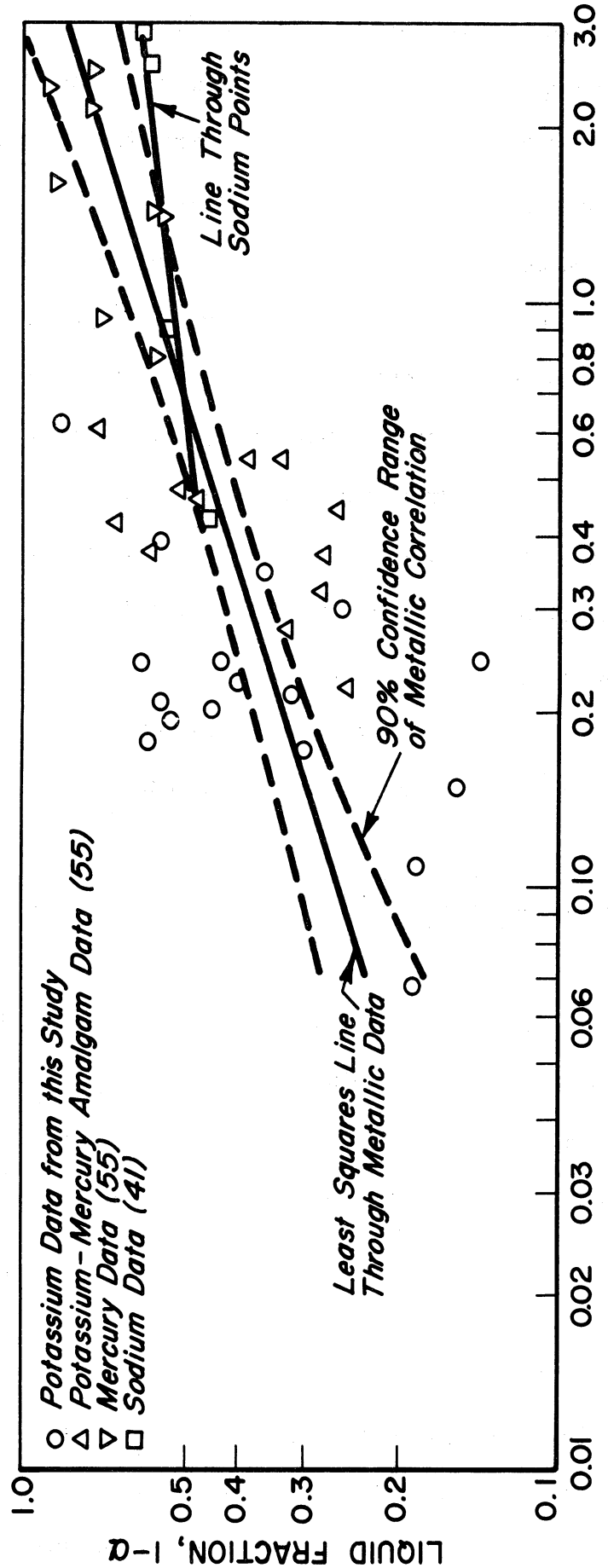

Figure 33. General Correlation of Liquid Fraction Data for Single-Component Metallic Systems

As mentioned previously, accurate estimates of the properties of the binary mixture were made, allowing comparison with pure-potassium properties. In the temperature range 900-1400°F only the vapor density deviates considerably from values for the pure metal, due principally to lowering of the vapor pressure. Since the liquid fraction correlation is derived from several metallic systems, no significant degree of generality is lost by presenting data for the binary mixture. Most of the data used in development of the correlation display more scatter than can be attributed to uncertainty in physical properties.

With regard to the pressure drop results, examination of the effect of property changes on the friction factor is possible. Considering Equation (6), the effect of property deviations on the total mass velocity, G, is negligible; the effect on the pressure gradient, $\Delta P/\Delta L$, cannot be stated and is assumed negligible since viscosity and liquid density changes are small. The effect of vapor density deviation on f can be easily determined from

$$\Delta f = \frac{\partial f}{\partial \rho_g} \Delta \rho_g = \frac{D(\Delta P/\Delta L) g_c}{G^2} \Delta \rho_g = \frac{f}{\rho_g} \Delta \rho_g \qquad (13)$$

where $\Delta \rho_g$ denotes the deviation in vapor density between the mixture and pure potassium. Between 900 and 1400°F the binary mixture vapor density on the average is 4 per cent lower than that of pure potassium--i.e., $\Delta \rho_g = +0.04 \rho_g$, where the positive sign indicates that values for the pure metal are higher. Then

$$\Delta f = +0.04 f \qquad (14)$$

Equation (14) indicates that two-phase fraction factors for pure potassium are about 1.04 of those determined experimentally for the 8 per cent sodium mixture. When the correlation line of Figure 32 is displaced upward by a factor of 1.04, the resulting line remains within the 95 per cent confidence band of the experimental correlation. Therefore, the addition of 8 per cent sodium to the potassium

appears to have nagligible effect on calculated f values, and it is concluded that the experimental results are good approximations to the two-phase flow behavior of pure potassium.

Two-Phase Pressure Drop

About 60 per cent of the pressure drop data occurred under conditions where the temperature drop across the test section was greater than 15°F. In runs where such significant temperature drops occurred, the quality usually increased, such increase resulting because the sensible heat change of the fluid was greater than the heat loss from the test section. In a few instances the sensible heat change was less than the heat loss, causing the quality to decrease. In all cases where the pressure drop was accompanied by a quality decrease, the decrease was slight (0.005 maximum). But in many cases where an increase occurred, it was between 0.01 and 0.02, representing a significant percentage of the test section average quality. Such quality increases would be expected to contribute acceleration components to the pressure gradient.

It was previously emphasized that the potassium two-phase pressure gradient correlation is for frictional pressure losses. This statement needs justification in view of the possible acceleration effects. For any general flow system in which a change of phase is occurring, the differential pressure drop can be written as

$$-dP_{total} = -dP_{friction} - dP_{acceleration} - dP_{hydrostatic}$$

which may be expressed quantitatively as

$$-dP = -dP_f + \bar{\rho}\frac{VdV}{g_c} + \left(\bar{\rho}\frac{g}{g_c}\sin\theta\right)dL \qquad (15)$$

For a two-phase mixture flowing with slip, the local mixture density is given in terms of the local void fraction and individual phase densities as (53)

$$\bar{\rho} = \alpha\rho_g + (1 - \alpha)\rho_\ell \qquad (16)$$

The potassium flows were horizontal, eliminating the hydrostatic term from Equation (15). The question that must now be answered is this: What fraction of the total pressure drop is represented by the acceleration component? The mean mixture velocity may be written in terms of the total mass velocity, G, and mean density as

$$V = \frac{G}{\bar{\rho}} \qquad (17)$$

Then the acceleration component of the total pressure drop becomes

$$-dP_a = \frac{\bar{\rho}\, V dV}{g_c} = -\frac{G^2}{g_c}\frac{d\bar{\rho}}{\bar{\rho}^2} \qquad (18)$$

In order to establish the $-dP_f$ term in Equation (15), all the essentially isothermal potassium data (88 points in which the temperature drop was less than 15°F) were used to formulate a correlation for the two-phase friction factor. These data, because of the small temperature drops, displayed only very slight quality increases and hence were certain to represent almost purely frictional flows. Use of these "isothermal" two-phase friction factors, together with Equation (18), reduces Equation (15) for horizontal flow to

$$-dP = f_I\left(\frac{G^2}{g_c P_g D}\right) dL - \frac{G^2}{g_c}\frac{d\bar{\rho}}{\bar{\rho}^2} \qquad (19)$$

where f_I denotes the isothermal two-phase friction factor, defined by Equation (6). Integration of Equation (19) between entrance and exit of the test section gives the overall pressure drop. The unknown axial variation of f_I and $\bar{\rho}$, due to changes in temperature and quality, prevents analytical integration of Equation (19). However, the integrations were performed numerically, under the following assumptions:

(a) Thermodynamic equilibrium existed at all points along the tube.

(b) Flows were steady-state and fully developed.

(c) The heat loss from the test section was distributed such that the quality varied linearly from entrance to exit.

Experimentally know values of total flow rate, inlet and outlet quality, and inlet temperature were the only necessary input information for the computer program. Use of the metallic void fraction correlation, Equation (12), was the key to successful integration of Equation (19), since mixture densities could be readily evaluated. The numerical procedure consisted in dividing the tube into a number of equal length segments and stepwise calculating the pressure drop along the tube. The pressure at the end of each segment was iterated to a given tolerance before stepping ahead. At the end of the tube the total pressure drop was also tested against a set tolerance, and if it was not satisfied the procedure was repeated using smaller length increments.

This procedure was used for many experimental flow conditions where the temperature drop was greater than 15°F. The calculated overall pressure drops agreed well with experimental values. The important result of these calculations, however, was that clear comparisons between the friction and acceleration pressure gradient components could be made for a wide range of flow conditions. The acceleration component never exceeded 3 per cent of the overall pressure gradient, and for most cases it was less than 1.5 per cent of the overall value. While the frictional pressure gradients ranged from 0.016 to 1.03 lb/sq in/ft, the acceleration components ranged from 0 to 0.014 lb/sq in/ft. These results made it clear dhat the experimental potassium two-phase pressure drops were essentially frictional.

In Figures 34 and 35 the potassium pressure gradient correlation is compared with the values predicted by the frictional pressure drop correlations of Lockhart and Martinelli (35) and Bertuzzi, Tek, and Poettmann (8), as well as

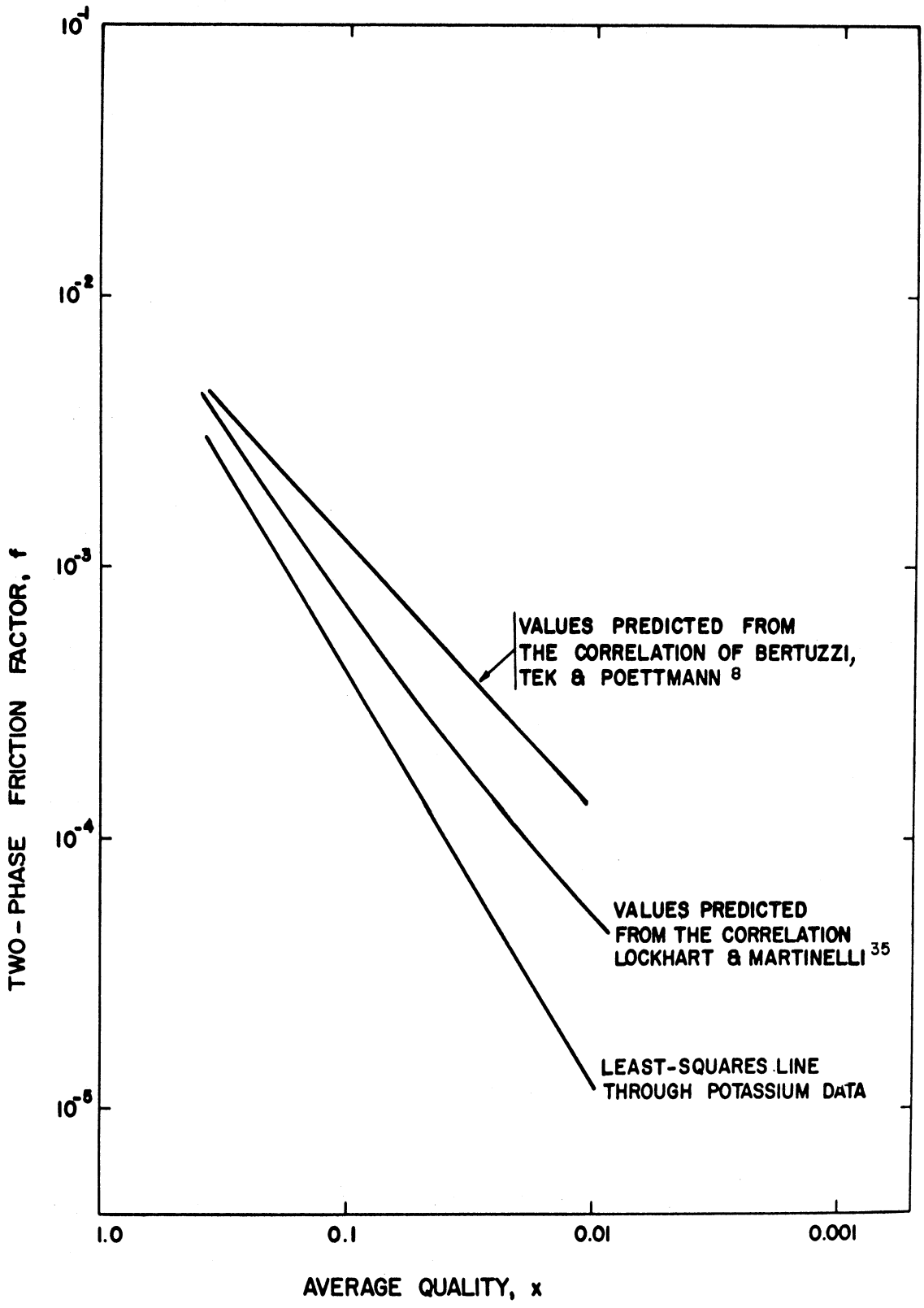

Figure 34. Comparison of Potassium Results with Values Predicted by Correlations of Lockhart and Martinelli (35) and Bertuzzi, Tek and Poettmann (8)

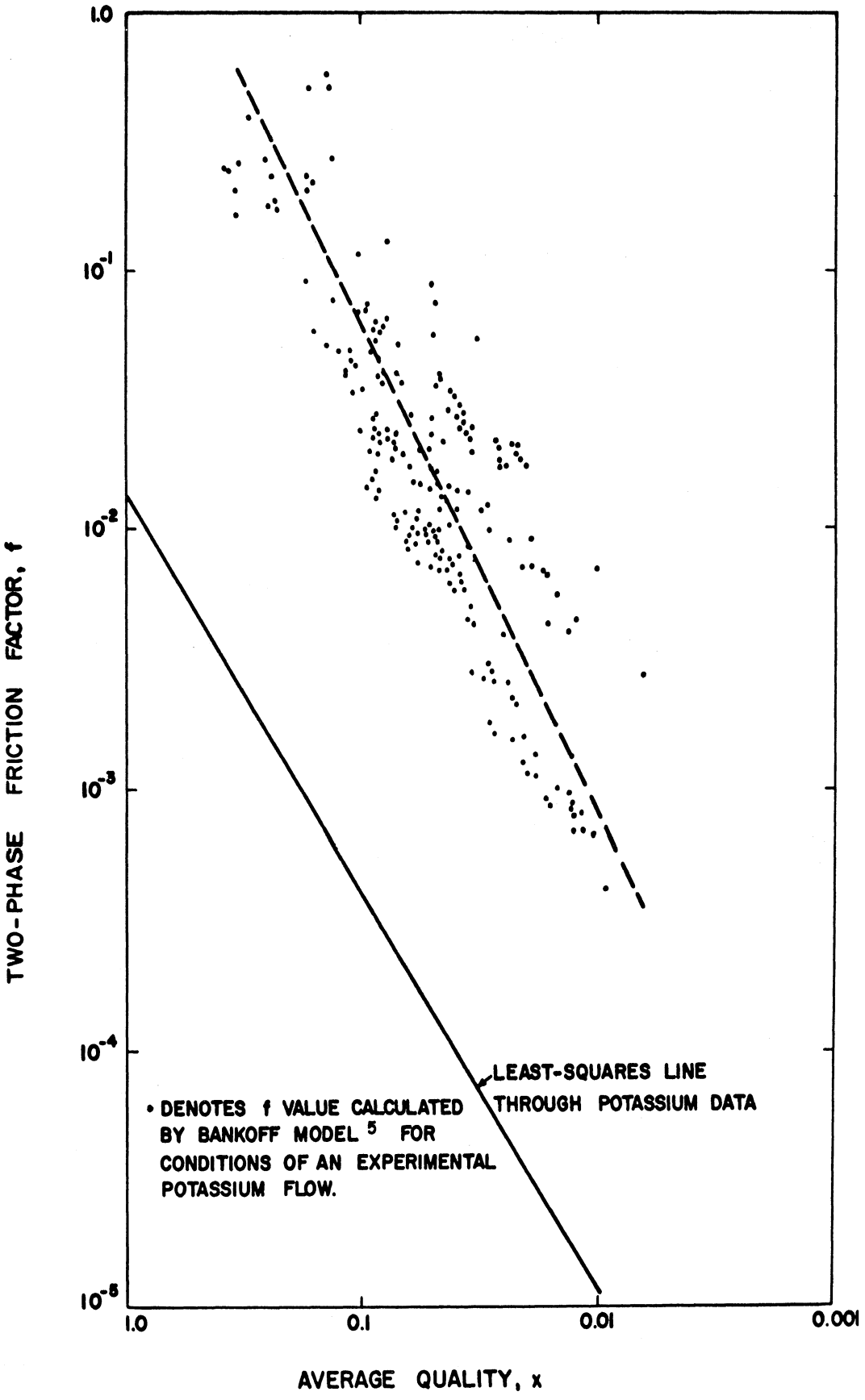

Figure 35. Comparison of Potassium Two-Phase Pressure Gradient Correlation with Values Predicted using Bankoff's (5) Model

with values calculated by the Bankoff variable density single fluid model (5). The correlations of references (35) and (8) were developed from air-liquid and natural-gas liquid data. The predicted values for potassium are appreciably high, lying above the 95 per cent confidence range of the potassium correlation and even outside the total scatter range of the data. The Bankoff model (5) predicts f values even higher than do the other methods. Generally, the Bankoff predictions are a factor of 10^2 higher than the potassium data. In contrast with values predicted by the correlations of references (35) and (8) which lay essentially on curves, the Bankoff predictions show a great deal of scatter as indicated in Figure 35.

These is evidently some deficiency in these methods for making satisfactory pressure drop estimates for potassium, and probably also for other metallic fluids. In the case of the Bankoff model, inaccuracy may arise from the assumption that the ratio of mean two-phase viscosity to liquid viscosity is unity. The potassium void fraction data indicate high slip ratios, violating another primary assumption of the theory which is derived for bubble type flows where slip ratios are low.

In Figure 36 the potassium correlation is compared with data obtained from other fluid systems. The steam-water data of Isbin, Sher, and Eddy (28), obtained from flows in a vertical tube, were corrected for hydrostatic head before plotting in Figure 35. Pike's steam-water data (44) were obtained from nearly-adiabatic flows in a long horizontal tube. The data reported by Johnson and Abou-Sabe (29), Govier and Omer (22) and Reid, et al (47) were all for horizontal air-water flows in pipes of various lengths and diameters. Johnson and Abou-Sabe reported data in isothermal and heated runs; both types are included in Figure 36. The data of Govier and Omer are for isothermal flows. Reid, et al, obtained isothermal data in 4-inch and 6-inch commercial steel pipes, each measuring 56 feet between pressure taps. The data furnished by

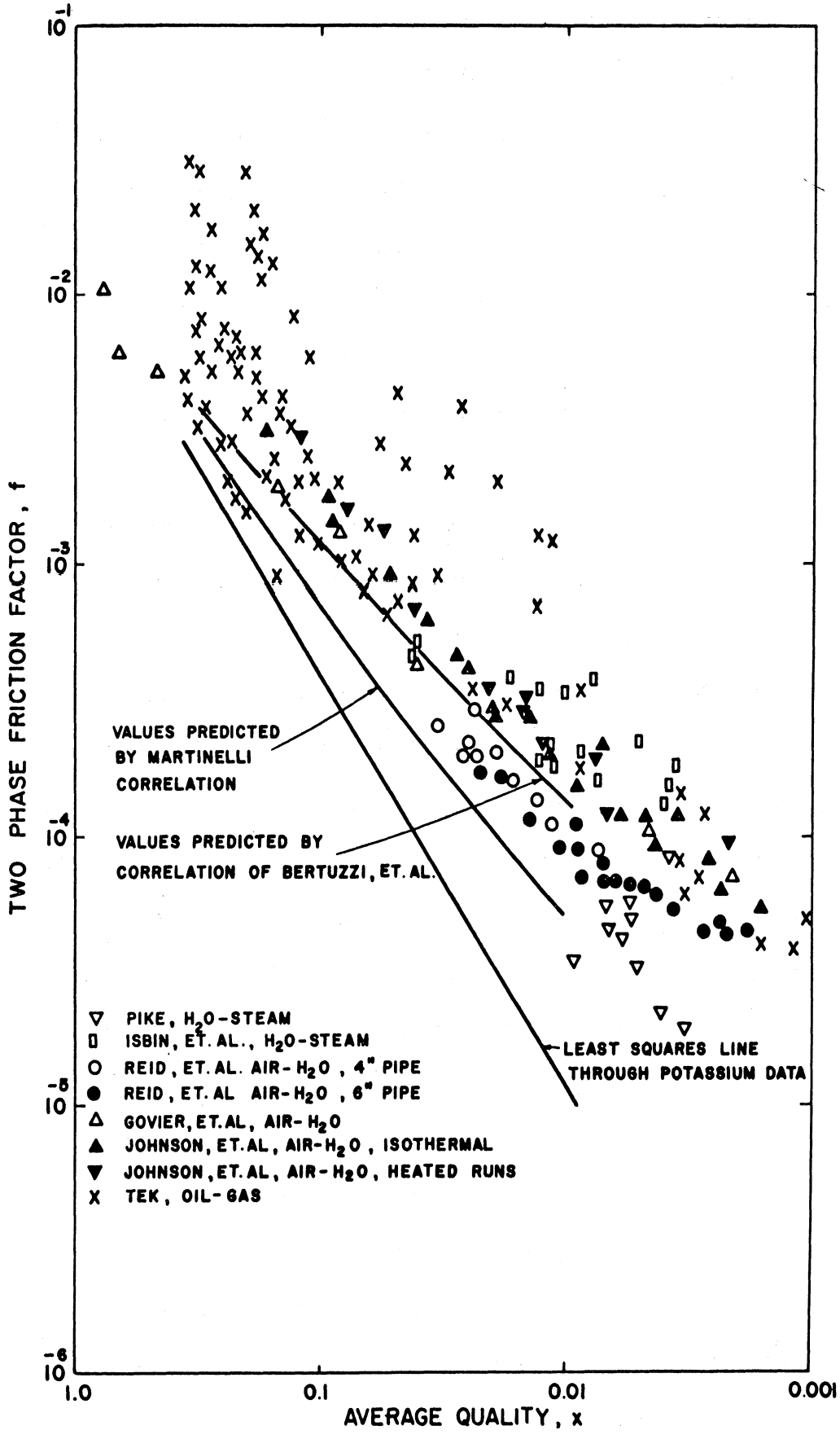

Figure 36. Comparison of Potassium Two-Phase Pressure Gradient Correlation with Data of Other Investigations

Tek (56) are from horizontal isothermal flows of oils and air or natural gas in various sized pipes. Figure 36 also includes the curves through values predicted by the correlations of Lockhart and Martinelli (35) and Bertuzzi, Tek, and Poettmann (8). The data shown in Figure 36 all fall substantially higher than the potassium results, as would be anticipated from Figure 34, since the correlations of references (35) and (8) are based on data of the type plotted in Figure 36.

It is desirable to compare the potassium results with data from other metallic experiments. As cited earlier, metallic pressure drop data have been obtained by a few investigators. Except for one case, however, either the flow characteristics involved, the system geometries, or the method of data presentation precludes comparison with the results of this study. The only metallic data for which a valid comparison could be made are the horizontal isothermal mercury-nitrogen results of Koestel (31). Pressure gradient and liquid fraction data were obtained. The pressure gradient data are compared with the potassium correlation in Figure 37. It is evident that the results from the two flow systems agree very favorably. This finding, when reviewed with regard to the differences shown in Figures 34, 35 and 36, suggests that some fundamental difference exists between the pressure drop behavior for metallic flows and that for nonmetallic flows.

An effort was made to determine a parameter which distinguishes the metallic data of Figures 32 and 37 from the data of other systems shown in Figure 36. Neither the vapor-to-liquid viscosity ratio nor density ratio provided a suitable parametric effect (53). Of several other possible parameters examined, the liquid viscosity influence number of Ros (50) showed the most promise. This dimensionless number is defined as

$$N_{\mu} = \mu_{\ell} \sqrt[4]{\frac{g}{\rho_g \sigma^3}} \qquad (20)$$

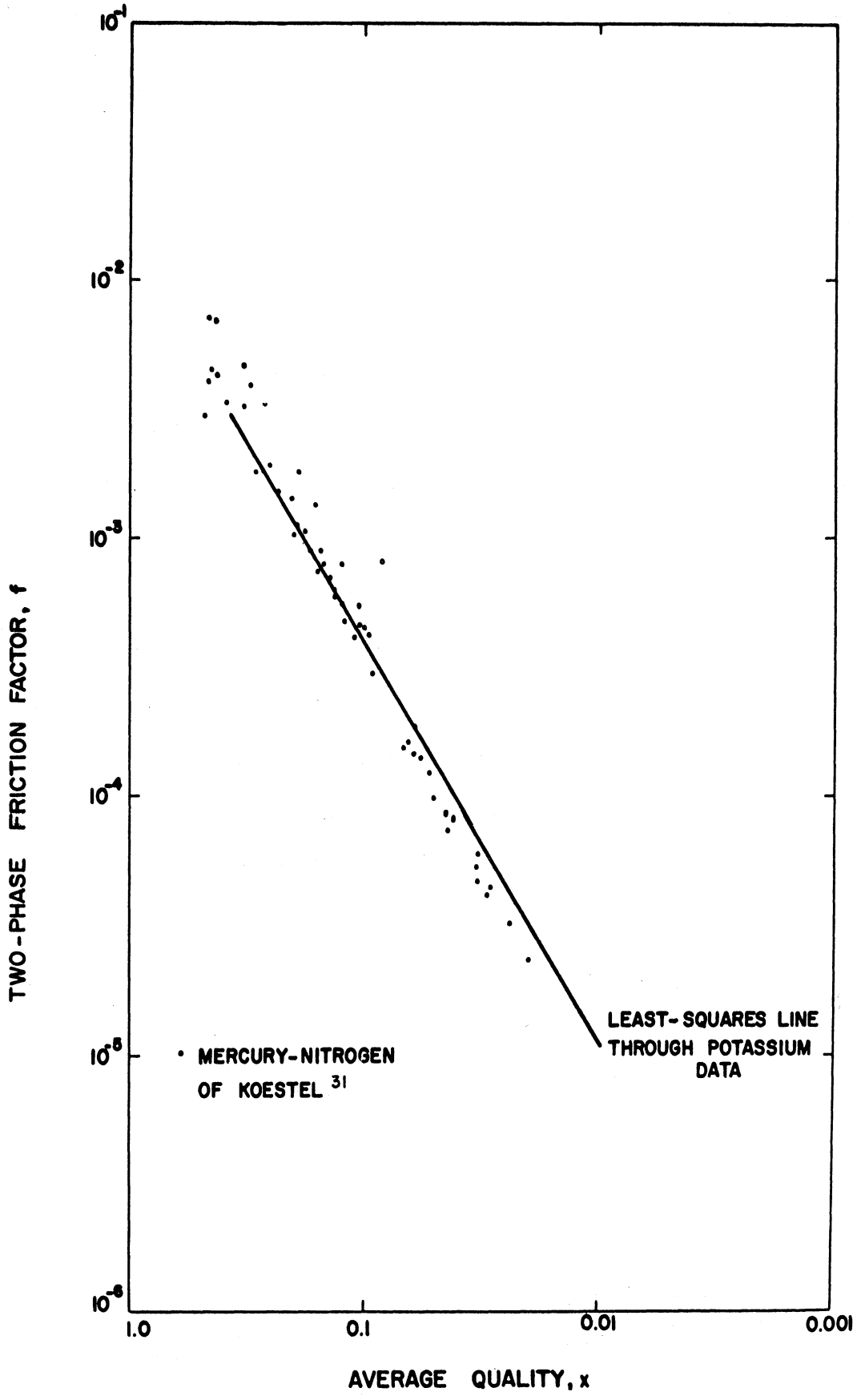

Figure 37. Comparison of Potassium Two-Phase Pressure Gradient Correlation with Mercury-Nitrogen Data of Koestel (31)

Ranges of values of this quantity are given below for various fluid systems.

Fluid System	$N_\mu \times 10^4$	Temperature, °F
Potassium containing 8 per cent sodium	3.52 to 3.12	879 to 1320
Mercury-nitrogen	3.7	60
Water-air	21.5 to 6.8	60 to 200
Water-steam	6.0 to 4.9	225 to 295

The metallic results for N_μ show very favorable agreement, but some inconsistencies exist between the other fluid systems. The inclusion of surface tension in such a parameter seems particularly sound, since indications are that interfacial characteristics and wettability may be principal factors which differentiate two-phase flow behavior among various fluid systems.

It is desirable to ascertain whether an empirical correlation, such as developed in Figure 32, has physical significance. Since the two-phase friction factor defined by Equation (6) is based on vapor density, it was decided to determine if the results would extrapolate to proper values in the all-vapor limit. The two-phase friction factors were all normalized against single-phase Moody friction factors corresponding to all-vapor flows at the same total flow rate and temperature. A plot of normalized two-phase friction factor as a function of quality is given in Figure 38. It appears that as quality approaches unity (all-vapor flow), the f/f_g values extrapolate to unity. This result is interesting and is believed to establish a firmer physical basis for the method of correlation used.

Metallic Void Fractions

The metallic liquid fraction correlation is compared with other correlations and data from other fluid systems in Figure 39 which shows that all the comparative data and predicted values fall substantially lower than the metallic data.

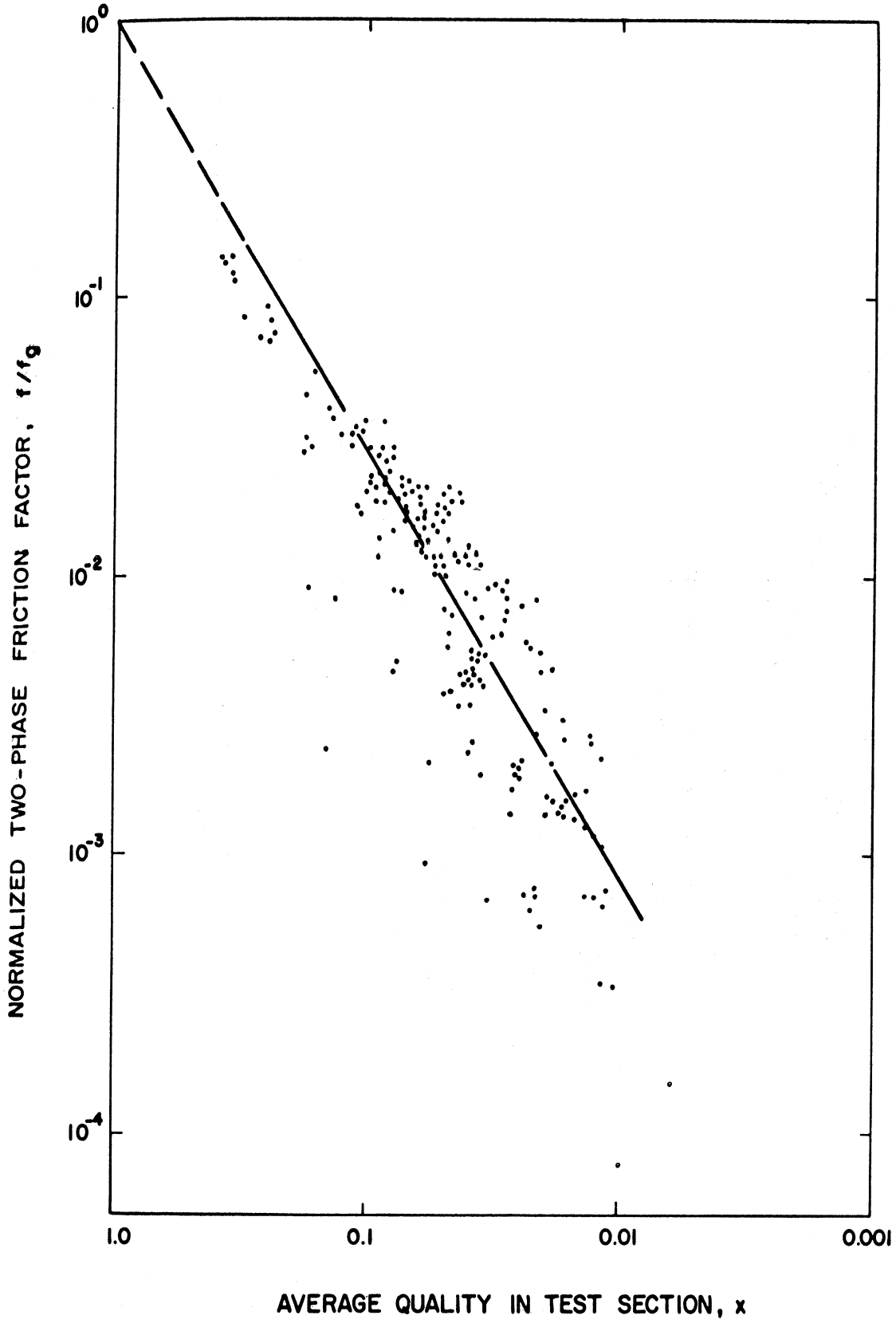

Figure 38. Normalized Two-Phase Friction Factor as a Function of Quality

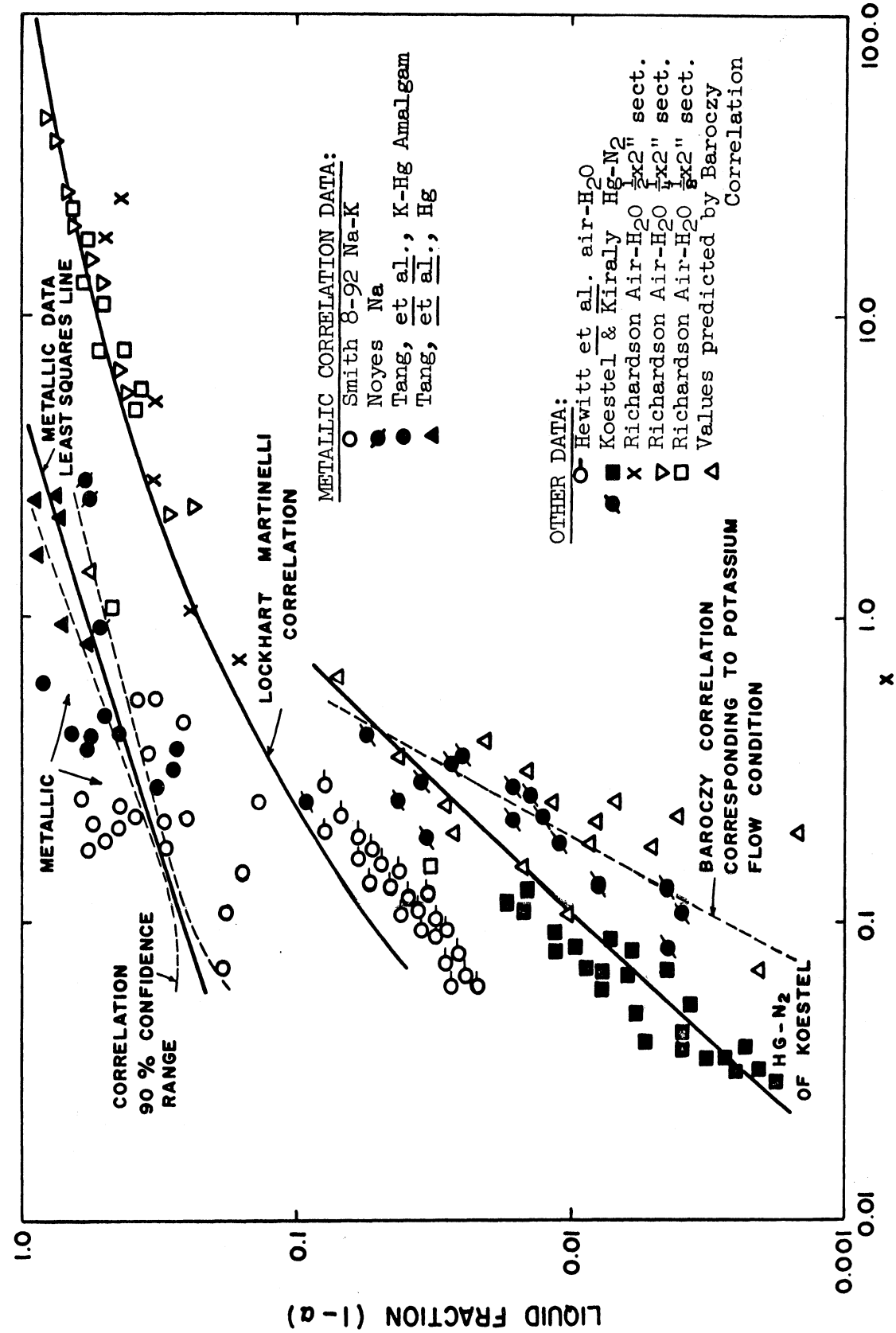

Figure 39. Metallic Liquid Fraction Correlation Compared with Other Data and Correlations

The correlation curve of Lockhart and Martinelli (35) developed from water-air and oil-air data, shows about the same trend as the metallic correlation line. The turbulent-turbulent water-air data of Richardson (48) for flows in horizontal rectangular channels are shown. Richardson's data agree with the Lockhart-Martinelli curve, but the air-water turbulent-turbulent flow data of Hewitt, King, and Lovegrove (24) fall somewhat lower than the correlation.

The two most interesting comparisons are located in the lower part of Figure 39, which shows potassium liquid fraction values calculated using the Baroczy correlation (6) for the actual potassium flow conditions. The calculated points show a substantial degree of scatter, but a mean curve is indicated. It is evident that the Baroczy correlation is even more deficient than the Lockhart-Martinelli correlation in predicting potassium liquid fractions. Koestel's mercury-nitrogen data (31) lie near the Baroczy predictions, as would be anticipated since Koestel's data were used in the development of the correlation. Concerning Koestel's data, the dark squares are for vt type flows, and the remaining are for tt type flows.

The fact that Koestel's mercury-nitrogen data compare unfavorably with the metallic correlation is most interesting, since it was found that the two-phase pressure gradient data compared favorably with the potassium correlation (Figure 36). One clear distinction may be drawn between Koestel's flows and the potassium flows. This is the liquid wettability with respect to the pipe wall. Koestel's data were obtained from a glass test section which the mercury certainly would not wet. Liquid potassium, however, does wet Haynes-25 alloy. These facts, together with the comparisons offered in Figures 37 and 39, suggest that wettability may be a decisive factor in void fraction behavior but of only minor significance in two-phase frictional pressure gradient behavior. Another, but less decisive, factor in the wide divergence of Koestel's liquid fraction data is that his vapor phase was a noncondensable second component.

As in the case of the two-phase pressure gradient correlation, it is interesting to consider whether the metallic liquid fraction correlation tends to proper values in the all-vapor limit. According to its definition, Equation (9), the Martinelli parameter X must vanish as flows become all vapor. Therefore, the all-vapor criterion is that as X approaches zero, the liquid fraction, $(1-\alpha)$, must also approach zero. The form of the correlation, Equation (12), fulfills this criteriorn.

As mentioned previously the experimental velocity slip ratios calculated by Equation (8) for potassium ranged from 53 to 1150. This wide range is a result of the scatter in the void fraction data. The arithmetic average slip ratio is 350. Although the scatter in the void fraction data precludes precise knowledge of potassium slip ratios, the results suggest that values are of the order of 10^2. This is about a factor of 10^2 higher than the air-water slip ratios observed by Richardson (48) for flows in horizontal rectangular channels at atmospheric pressure. The appreciably higher metallic slip ratios would be expected upon consideration of Figure 39 and Equation (8), arising from two effects. First, Values of (ρ_ℓ/ρ_g) are generally higher in metallic systems. Second, since metallic void fraction values tend to be appreciably lower, higher values of the factor $(1-\alpha)/\alpha$ are obtained.

Before concluding discussion of void fractions, it is pertinent to consider possible flow patterns occurring in the potassium two-phase flows. Since flow regimes were not experimentally available, Smith (53) surveyed the flow patterns predicted by the correlations of Ros (50) and Baker (3). Both correlations attempted to include effects of varying fluid properties. The Baker correlation predicted annular flow, dispersed flow, and annular-dispersed transition flow, with an essentially even distribution of points between the three regimes. The Ros method indicated that flows would be prediminantly dispersed. The dispersed-flow predictions are not physically realistic in view of the void fraction and

slip ratio results. The seventeen liquid fraction values for potassium ranged from 0.140 to 0.847, with only two values less than 0.2. Bankoff (5) points out that, in vertical flows, bubble flow is usually observed when liquid fractions are greater than 0.2. It is not at all likely that dispersed flows could exist at the high liquid fractions observed in this study. From the occurrence of high velocity slip ratios, it seems probable that flows were stratified or wavy at lower qualities and annular at higher qualities. These regimes are compatible with high slip ratios since the vapor flow area is unrestricted. The existence of bubble flows (as would probably occur in a vertical tube) is not probable, since gravitational asymmetry in the horizontal flows would tend to force liquid to the bottom of the tube except at higher qualities. The apparent inability of the Baker and Ros correlations to predict potassium flow regimes may hinge on wettability considerations, since liquid metals probably have far more affinity for metallic pipe walls than do water and oils, the liquid phases used in developing the predictive correlations. Another possible failure in the prediction methods is that they are based on two-compontne data for which the gas phase was noncondensable.

CONCLUSIONS

The results of this experimental study lead to the following conclusions:

1. Although the experimenta were run with a fluid mixture of 8 weight per cent sodium in potassium, it is believed from comparison of the properties of this mixture with those of pure potassium that the two-phase flow correlations will yield reliable values for pure potassium.
2. Although the potassium two-phase flow patterns are not exactly known, the experimental range of liquid volume fraction and velocity slip ratio suggest that flows probably were stratified or wavy at lower qualities and annular at higher qualities.

3. The two-phase frictional pressure gradient for potassium proved to be a function of total mass flow rate, quality, and system pressure. The data were correlated in terms of a two-phase friction factor, f, defined by Equation (6), as a function of quality. The correlation, developed in Figure 32 and stated by Equation (7), has a high statistical significance and behaves correctly in the all-vapor limit. This type of correlation is suitable for presentation of data from other two-phase fluid systems.
4. The well-known two-phase pressure drop correlations of Lockhart and Martinelli (35) and Bertuzzi, Tek, and Poettmann (8), when applied in the usual manner, predict potassium pressure gradients that are high by average factors of 2.5 and 4, respectively. The Bankoff variable density single fluid model (5) predicts pressure gradients which are nearly a hundred fold high.
5. The potassium two-phase frictional pressure gradient results show remarkably good agreement with mercury-nitrogen data (31). These metallic data fall much lower than values reported for flows of water-air, oil-air, and water-steam systems. The parameters which cause such strong differences between metallic and nonmetallic two-phase pressure gradients have not been determined. Surface tension and liquid viscosity may be among the most influential properties.
6. The potassium void fraction data, together with other metallic data from the literature (55, 41) have yielded a general liquid fraction correlation for single-component metallic systems. This Lockhart-Martinelli type of correlation, developed in Figure 33 and stated by Equation (12), has a high statistical significance and behaves correctly in the all-vapor limit.
7. Metallic void fractions are lower than for water-steam and water-air systems No other general correlation was found adequate in predicting metallic void fractions. The mercury-nitrogen data (31) which agreed very favorably

with the potassium two-phase pressure gradients, show large divergence with respect to void fractions. Since the mercury-nitrogen data were obtained from a glass test section, it appears that wettability may be of great effect on void fraction behavior.

8. Because of generally higher liquid-to-vapor density ratios and lower void fractions, metallic systems display much higher velocity slip ratios than nonmetallic systems. Although the scatter in the void fraction data precludes precise knowledge of slip ratios, the potassium values appear to be of the order of 10^2. Values between 1 and 10 have been observed for water-air flows at atmospheric pressure.

LIQUID METAL BOILING IN AGRAVIC FIELDS

Herman Merte, Jr.

INTRODUCTION

Test apparatus was designed and constructed to obtain data on the influence of increased body forces, up to $a/g = 20$, on nucleate boiling of liquid metals. Mercury was selected as the initial fluid, and the flat heating surface is oriented such that the body forces are perpendicular to it. The apparatus is described in detail in Reference (4).

The heater surface initially consisted of a 0.001 inch foil of 347 stainless steel attached to a copper heater block containing cartridge-type electrical heaters. The foil was attached to the copper heater by successively copper and silver plating the foil on one side, placing it in mechanical contact with the copper heater in a vacuum, and heating the copper block to approximately 1600°F with the internal cartridge heaters. This procedure was found to provide an intimate bond.

Some preliminary data obtained with the stainless steel heater surface is presented below, but difficulties arose in maintaining a sufficient degree of wetting of the surface to produce nucleate boiling. Early operation gave consistent nucleate boiling but as time progressed, the boiling mode would vary unpredictably between nucleate and film boiling on startup. Trace additives of Mg and Ti were of assistance only for short periods of time.

The stainless steel foil was removed and replaced with C-1010 carbon steel sheet 0.005 inches thick. This was assembled to the copper heater block in the same manner as the stainless steel foil. Prior to assembly the surface to be

in contact with the mercury was given a thin plating of copper to promote initial wetting by the mercury. Results of these tests are presented.

TEST CONDITIONS AND PROCEDURES

All tests reported below were conducted at nominal pressures of 75 psia at the liquid free surface. The nucleate boiling data is presented with $T_{surf} - T_{sat}$ as the independent parameter. T_{sat} is the saturation pressure at the heater surface, and corrections due to changes in hydrostatic bead with acceleration were applied. T_{surf} is the heat transfer surface temperature and is computed by extrapolating the temperature measured approximately 1/32 inch below the heater surface. Argon is used as the pressurant, and once operation began an inert atmosphere was maintained at all times.

A liquid depth of 1/2 inch was used for all tests reported here. Subcooling of the liquid could not be controlled, but generally remained constant on the order of 4-8°F. Particular values can be noted on the data plots.

Heat flux was varied from q/A = 20,000 Btu/(hr)(sq ft) to q/A = 100,000 Btu/(hr)(sq ft). The heat flux was computed in three ways: (a) from the measured electrical power input to the main heater, (b) from the enthalpy rise of the coolant, (c) from the temperature gradient within the heater block. In general, when water was used as the coolant, (a) and (b) were in excellent agreement for steady-state conditions. When air was used, (b) gave results lower than (a), most likely due to heat transfer to the connecting tubing to the point of temperature measurement. In early preliminary tests (c) gave excellent agreements with both (a) and (b), but later gave results about 2/3 that of (a). This may be a consequence of changes in uniformity of heat flux deeper in the block.

The acceleration levels covered thus far are a/g = 1, 5, 10, 15.

Test runs up through No. 18 apply to the type 347 stainless steel heating surface, whereas all later data were obtained with the carbon steel surface.

Once power had been turned on to the main and guard heaters, all temperatures were monitored continuously on a 20 point slow speed recorder for purposes of determining when steady-state conditions had been achieved. Due to the large heat capacity of the heater block and the test vessel, long periods of time were required to reach steady-state on start-up and subsequent changes in acceleration. Once steady-state was achieved, temperature data were taken with a type K-3 Leeds and Northrup potentiometer. Even with the utmost in precautions, after steady-state was seemingly present changes in heat flux or temperatures would occur at times. Where uncertainties in heat flux arise, these are indicated by ranges in the specified values. Temperature data are presented as functions of time, and any changes taking place are evident.

Figure 40 is a schematic of the test vessel identifying the location of the various thermocouples for reference in interpreting the time-temperature data to be presented.

EXPERIMENTAL RESULTS

Run No. 6. $a/g = 1$, $q/A = 23{,}000$ Btu/(hr)(sq ft)

Figure 41 shows the time-temperature data in the later heatup and steady-state stages. The bulk liquid temperature (T-3) remains constant, being about 4°F sub-cooled, while the heater surface temperature rises and then suddenly drops. The power input to the heater was constant in this period, being equivalent to a heat flux of $q/A = 23{,}000$ Btu/(hr)(sq ft) at the heat transfer surface. It is believed that at some time prior the boiling mode went directly into film boiling from natural convection, and spontaneously reverted to nucleate boiling. While in film boiling a significant portion of the power input was going into heating of the copper block, rather than in producing vapor. This is supported by the behavior of the temperature in the vapor space (T-4), which rises suddenly with nucleate boiling, and the increase in $\Delta T(1\text{-}2)$ and ΔT_{water}, which are proportional to the rate of heat transfer to the mercury.

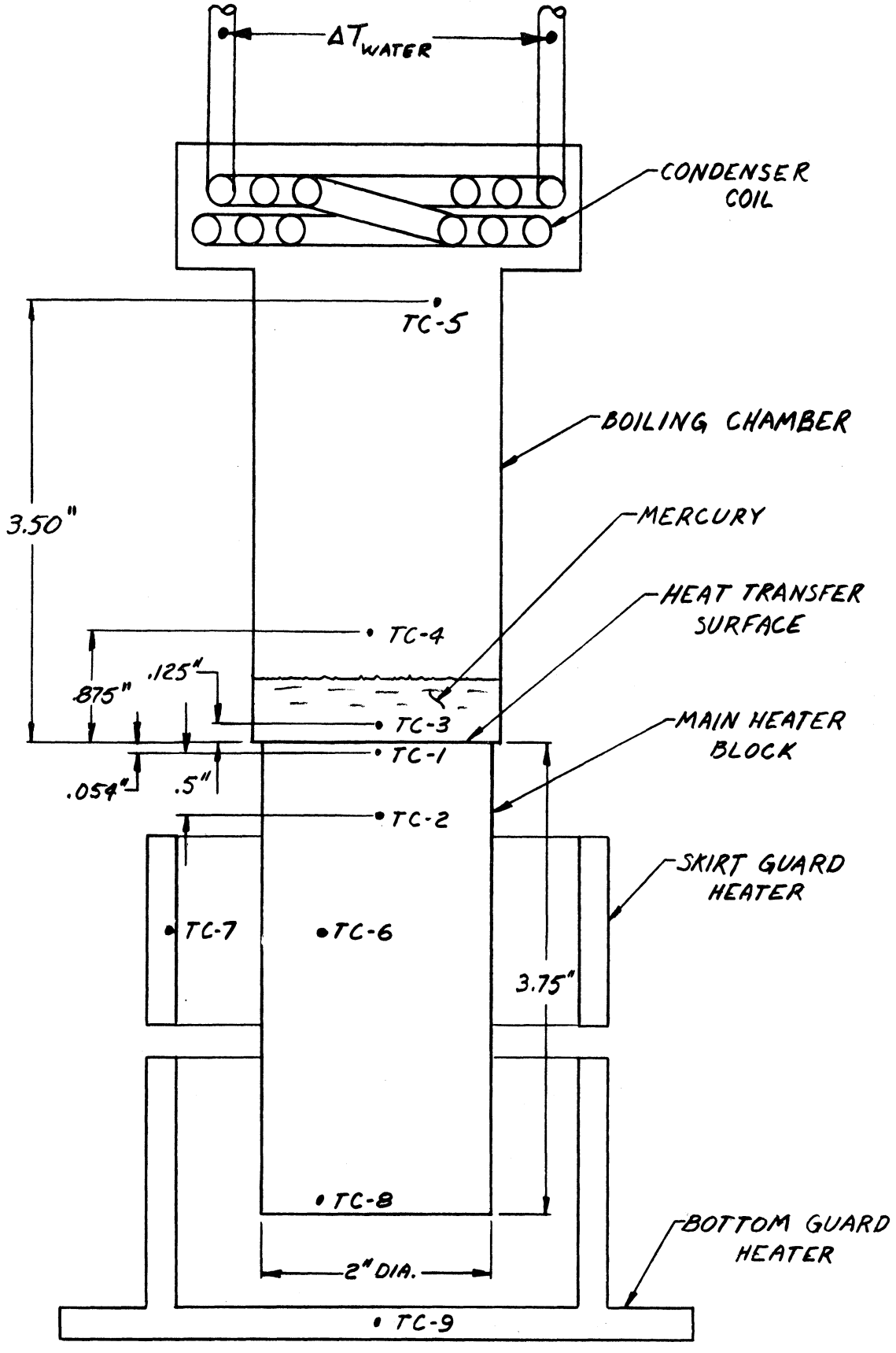

Figure 40. Thermocouple Locations for Reference

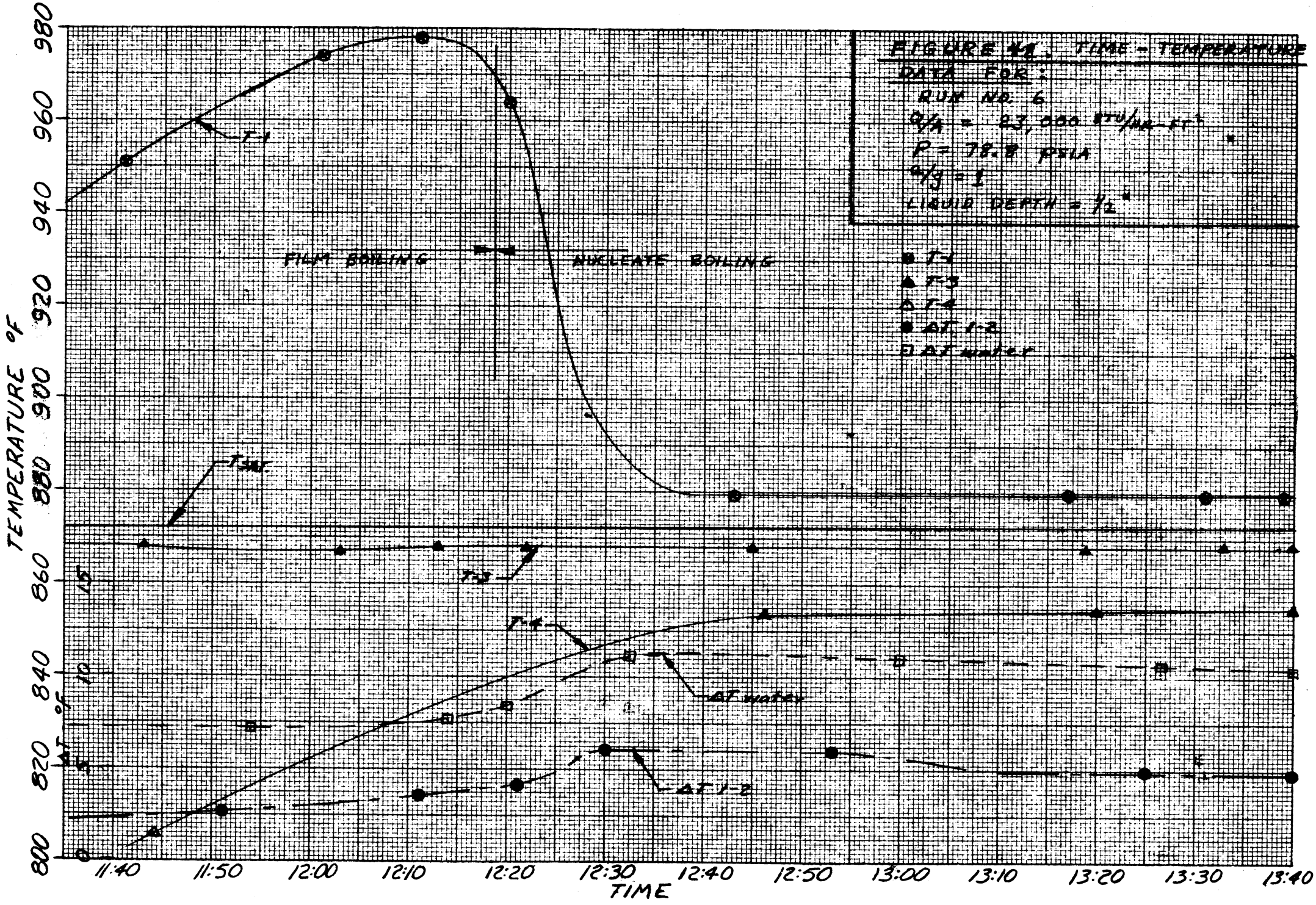
FIGURE 11. TIME - TEMPERATURE DATA FOR:
RUN NO. 6
q/A = 23,000 BTU/HR-FT²
P = 78.8 PSIA
q/J = 1
LIQUID DEPTH = 1/2"
FILM BOILING
NUCLEATE BOILING
T-1
T-3
T-4
ΔT 1-2
ΔT water
T_SAT
T-3
T-4
ΔT water
ΔT 1-2
TEMPERATURE °F
ΔT °F
TIME
980
960
940
920
900
880
860
840
820
800
15
10
5
0
11:40
11:50
12:00
12:10
12:20
12:30
12:40
12:50
13:00
13:10
13:20
13:30
13:40

Similar behavior was observed by other workers (9) where apparent premature film boiling was attributed to the non-wetting characteristics of mercury. When suitable "conditioning" of the surface had taken place, the system reverted to nucleate boiling. In Figure 41 , it appears that with the initial startup the mercury was not wetting the stainless-steel surface to a sufficient degree until after some period of operation.

The data tabulated below apply to the steady-state conditions:

Test Run No. 6. $a/g = 1$

q/A = 23,000 Btu/(hr)(sq ft)

T_{surf} = 878.8°F

T_{sat} = 872.2°F

ΔT_{sat} = 6.6°F

T-1 = 879.5°F

T-2 = 884.8°F

T-3 = 868.1°F

T-4 = 853.4°F

T-5 = 279.3°F

Subcooling = 4.1°F

P = 78.8 psia

Liquid Level = 1/2 inch

Run No. 7. $a/g = 1$, q/A = 46,900 Btu/(hr)(sq ft)

In the next consecutive test run, tabulated below, no tendency for film boiling was observed.

Test Run No. 7. a/g = 1

q/A = 46,900 Btu/(hr)(sq ft)

T_{surf} = 895.8°F
T_{sat} = 872.2°F
} ΔT_{sat} = 23.6°F

T-1 = 897.3°F

T-2 = 906.7°F

T-3 = 868.8°F

T-4 = 857.8°F

T-5 = 768.8°F

Subcooling = 3.4°F

P = 78.8 psia

Liquid Level = 1/2 inch

Run No. 8. a/g = 1, q/A = variable

The next test run was attempted at a heat flux q/A = 100,000 Btu/(hr)(sq ft). However, film boiling set in. Test Run No. 8 was then conducted to find the order of magnitude of the maximum heat flux for this system with nucleate boiling at a/g = 1. This was accomplished by raising the power level in small increments. In order to do so in a reasonable length of time it was not possible to wait for true steady state at each level. Thus some care should be exercised in comparing these results to steady-state results. Figure 42 shows the data for the entire period, along with indications of the regimes of boiling present. The transition from nucleate to film boiling, or the maximum heat flux, is fairly well defined, and is accompanied by a pronounced increase in temperature level of the heater, even with a large decrease in heat flux. The temperature measurement in the vapor region near the cooling coil (T-5) dropped off scale on the recorder, as might be expected with the decrease in vapor generation rate. To determine the approximate region of the minimum heat flux for film boiling, the heat flux was then reduced in small increments until the system reverted to nucleate boiling,

A summary of the results for periods closest to steady-state are given below:

Test Run No. 8 a/g = 1

P = 78.2 psia Mercury Depth = 1/2" T_{sat} = 871.6°F

Time	Data No. Fig. 42	q/A $\frac{BTU}{hr \cdot ft^2}$	T-1	T-3	T_{surf} °F (Estim.)	ΔT_{sat} °F	Remarks
1:01	1	48,500	890.0	868	888.6	17.0	Nucleate Boiling
1:19	2	52,000	891.3	867	889.8	18.2	Nucleate Boiling
1:34	3	58,000	898.4	867	896.8	25.2	Nucleate Boiling
1:49	4	63,000	904.0	866	902.2	30.6	Burnout occurs within this region of heat flux.
1:53		68,000	B.O. ≈910	866		B.O. ≈ 36	
2:11	5	27,000	1051.3	866	1050.7	179.1	- Stable film boiling. Transition from minimum film to nucleate.
2:19		23,000	Min. ≈1010	867		Min. ≈140	
2:27	6	23,000	876.1	867	875.6	4.0	Nucleate Boiling

The maximum heat flux occurs within the region q/A = 63,000 - 68,000 Btu/(hr)(sq ft) with $\Delta T_{sat} \approx 36°F$, and the minimum film boiling heat flux occurs within the region q/A = 23,000 - 27,000 Btu/(hr)(sq ft) with $\Delta T_{sat} \approx 140°F$. For comparison with the steady-state data of Runs 6 and 7, the data above are plotted on Figure 43.

The correlation of Noyes (42) based on Na data predicts a maximum heat flux for mercury of $(q/A)_{max} = 2.6 \times 10^6$ Btu/(hr)(sq ft) for the test conditions here. The gross discrepancy with the experimental results here may well be a consequence of the poor wetting of mercury with the type 347 stainless steel heating surface used.

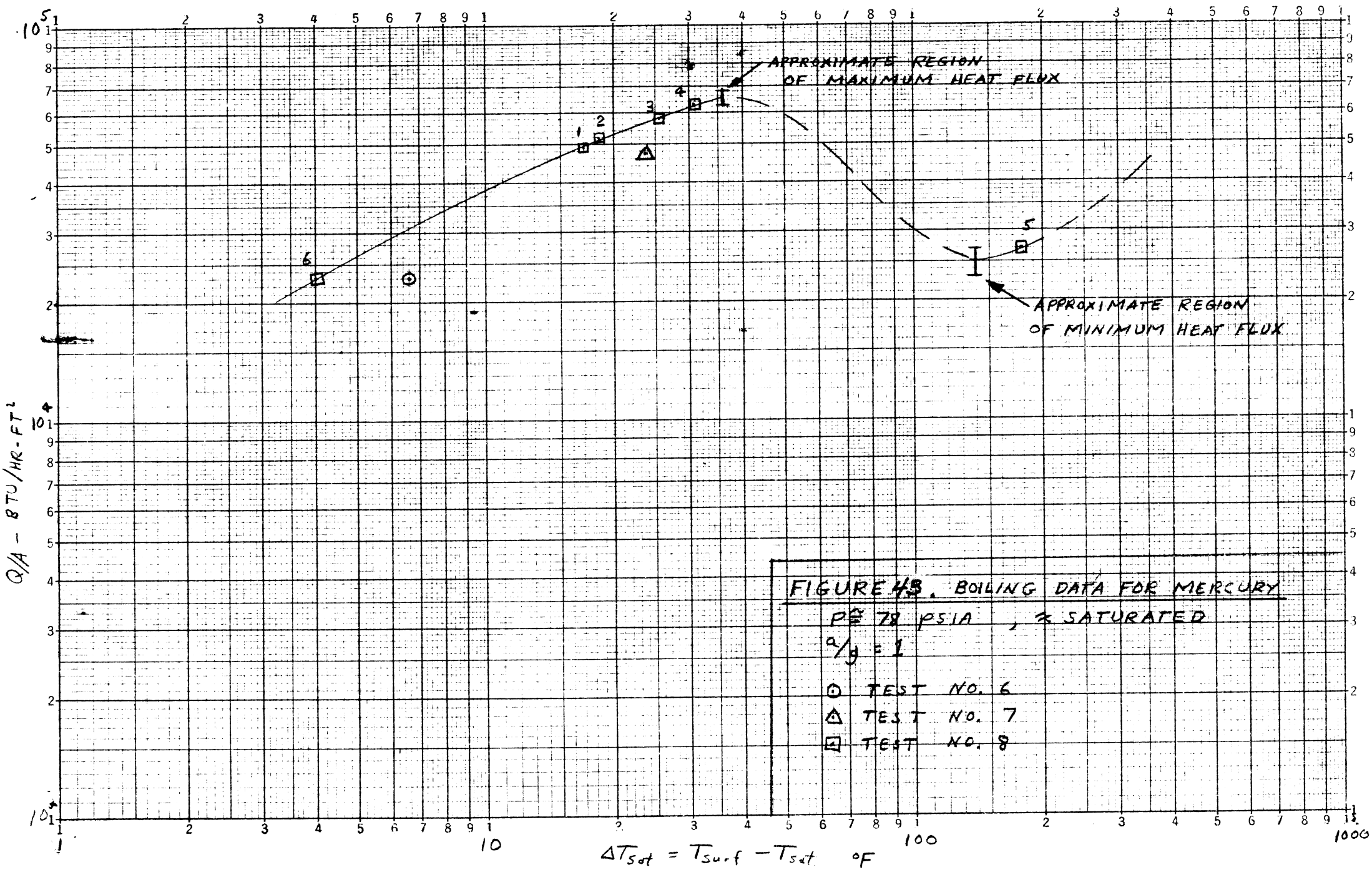

FIGURE 45. BOILING DATA FOR MERCURY
P = 78 PSIA , % SATURATED
q/q = 1
⊙ TEST NO. 6
△ TEST NO. 7
⊡ TEST NO. 8

Run No. 17. a/g = 1 and 5. q/A = 18,000 Btu/(hr)(sq ft)

With subsequent tests it was not possible to obtain nucleate boiling at all. Small amounts of Mg were added to the mercury, which was successful in producing nucleate boiling for short periods of time only. It was then planned that data for film boiling at high acceleration be obtained, with the view that this may assist in producing nucleate boiling again. The cooling system was modified to use air as well as water, so the liquid could be maintained at saturation conditions with the low heat flux associated with film boiling. The results for one run are tabulated below:

Test Run No. 17

P = 80.3 Mercury Depth = .55" q/A = 18,000 Btu/(hr)(sq ft)

	a/g = 1	a/g = 5
T_{sat} (at Heater Surface)	875.3	877.2
ΔT_{sat} - °F	282	101
T_{liq} - °F	873.7	874.8
h - Btu/(hr)(sq ft) - °F	64	178

The increase in the heat transfer coefficient by a factor of almost 3 for a 5-fold increase in a/g is noted, although any general conclusions must await the availability of more data.

Run No. 19. a/g = 1, 5. q/A = 18,500 Btu/(hr)(sq ft)

For this and subsequent tests the type 347 stainless steel heating surface was replaced by a C-1010 carbon steel surface. Figure 44 shows the time-temperature data obtained immediately after this change had been made.

It is noted that once the liquid had become saturated that the heater surface temperature continued to rise linearly with time, indicating the presence of film

boiling. The centrifuge was rotated corresponding to a/g = 5 to attempt to halt this trend, and after a period of changes further data taken. ΔT_{sat} dropped to zero under the increased body forces, indicating that no boiling existed, and continued after the system was brought back to a/g = 1. The existence of the small values of ΔT_{bulk} perhaps serve as an indication that good wetting of the carbon steel surface had been achieved at this point with the removal of the thin copper plating.

Run No. 20. a/g = 1, 10, 15. q/A = 18,000 Btu/(hr)(sq ft)

Figure 45 presents data obtained with conditions similar to the previous test with other accelerations. No boiling existed even on start-up at a/g = 1, again indicating continued good wetting. It is interesting to note that at a/g = 10 the value of ΔT_{bulk} decreased by only 0.5°F, and only about 1°F at a/g = 15. It would appear that with extremely good wetting that the buoyant forces are not controlling in the heat transfer between the solid surface and the mercury. This phenomena may also be related to the low liquid depth used, being only 1/2 inch. T-1, related to T_{surf} does decrease with increasing acceleration as a consequence of the increasing natural convective heat transfer between the mercury free surface and the cooling coils.

Run No. 21. a/g = 1, 5. q/A = 19,500 Btu/(hr)(sq ft)

The previous two runs were repeated once more to check reproducibility, and on start-up film boiling again occurred. The power level was reduced and increased, and the centrifuge rotated corresponding to approximately a/g = 2. When the centrifuge was shut down again, the value of ΔT_{sat} leveled off at 75°F as shown on the early part of Figure 46. Some change in the wetting characteristics had apparently occurred again. Upon subsequent acceleration to a/g = 5, boiling was once again suppressed completely. When rotation was stopped the system was allowed to boil for approximately 7 hours, and the final value of ΔT_{sat} was 26°F,

although at a slightly higher flux of q/A = 24,700 Btu/(hr)(sq ft).

In these three tests it is evident that the increased acceleration is having a definite effect on the nucleating characteristics of the surface. The relationship of this effect to the non-reproducibility of conditions at a/g = 1 is not clear at this point. Physical changes in the surface may be taking place, or this may be a manifestation of a "prior history" effect. Subsequent tests were conducted at consecutively higher values of heat flux.

Run No. 22. a/g = 1, 5, 10, 15. q/A = 34,000 Btu/(hr)(sq ft)

Figure 47 shows the time-temperature data for Run No. 22 at a heat flux of q/A = 34,000 Btu/(hr)(sq ft). A consistent decrease in T_{surf} and ΔT_{sat} as acceleration increases is observed. After the high acceleration conditions further data were obtained at a/g = 1 to again observe any prior history effect. In this case ΔT_{sat} is 37°F compared to the initial value of 42°F, a decrease of 5°F.

Run No. 23. a/g = 1, 5, 10, 15. q/A = 46,000 Btu/(hr)(sq ft)

Figure 48 presents the data for Run No. 23 at q/A = 46,000 Btu/(hr)(sq ft). Again a consistent decrease in ΔT_{sat} with increasing acceleration is noted, and the value changes from 65°F at a/g = 1 initially, to 57°F at the conclusion of the tests.

Run No. 24. a/g = 1, 5, 10, 15. q/A = 61,000 Btu/(hr)(sq ft)

Figure 49 shows the data for Run No. 24 at q/A = 61,000 Btu/(hr)(sq ft), and shows decreasing ΔT_{sat} with increasing acceleration. In this case ΔT_{sat} at a/g = 1 at the end reproduced the initial value of 43°F.

Run No. 25. a/g = 1, 5, 10, 15. q/A = 78,000 Btu/(hr)(sq ft)

Figure 50 presents data for Run No. 25 at q/A = 78,000 Btu/(hr)(sq ft). No data could be obtained at a/g = 1 at the conclusion of the test because of loose electrical connections which arose. For an unknown reason an abrupt change in ΔT_{sat} took place during the data taking process at a/g = 10.

Run No. 26. a/g = 1, 5, 10, 15. q/A = 98,000 Btu/(hr)(sq ft)

The data for Run No. 26 are shown in Figure 51. In obtaining the initial readings of ΔT_{sat} at a/g = 1 some instabilities in the boiling process were noted, with ΔT_{sat} sometimes increasing, sometimes decreasing, and sometimes remaining constant with no apparent regularity. With increasing acceleration stable conditions were present, with decreases in ΔT_{sat} occurring with increases in acceleration. Observing the behavior of TC-1, it is noted that a slight decrease in T_{surf} occurs in changing from a/g = 1 to a/g = 5, but thereafter no changes take place. ΔT_{sat}, however, changes because of the increase in T_{sat} with acceleration. Upon shutdown after a/g = 15, ΔT_{sat} increased and then decreased. After apparent stabilization readings were taken, and ΔT_{sat} began to rise again as noted on Figure 51. The rise thereafter became rapid, and after giving the vessel a sharp rap it decreased again. Burnout conditions may be near at this value of heat flux.

DISCUSSION

A composite of the nucleate boiling data is presented in Figure 52 with ΔT_{sat} as a function of acceleration and heat flux as a parameter. The numbers along each data point indicate the sequence in which the data were obtained. Several remarks can be made regarding this data.

Although no consistent trend in the behavior of ΔT_{sat} with heat flux at a/g = 1 is present, again perhaps due to prior history effects or physical changes in the boiling surface, increasing acceleration does produce a definite decrease in ΔT_{sat}; the decrease becoming smaller as heat flux increases. Similar effects were obtained with water (38). In the case of water at the higher heat flux, ΔT_{sat} actually increased with increasing acceleration. With mercury, heat fluxes higher than those used thus far might produce a similar effect.

For future efforts it is planned that three of the tests reported here be repeated to verify reproducibility of the effect of acceleration, if not the absolute levels of ΔT_{sat}. The series will then be repeated at a low level and high level of pressure, on the order of 20 psia and 300 psia.

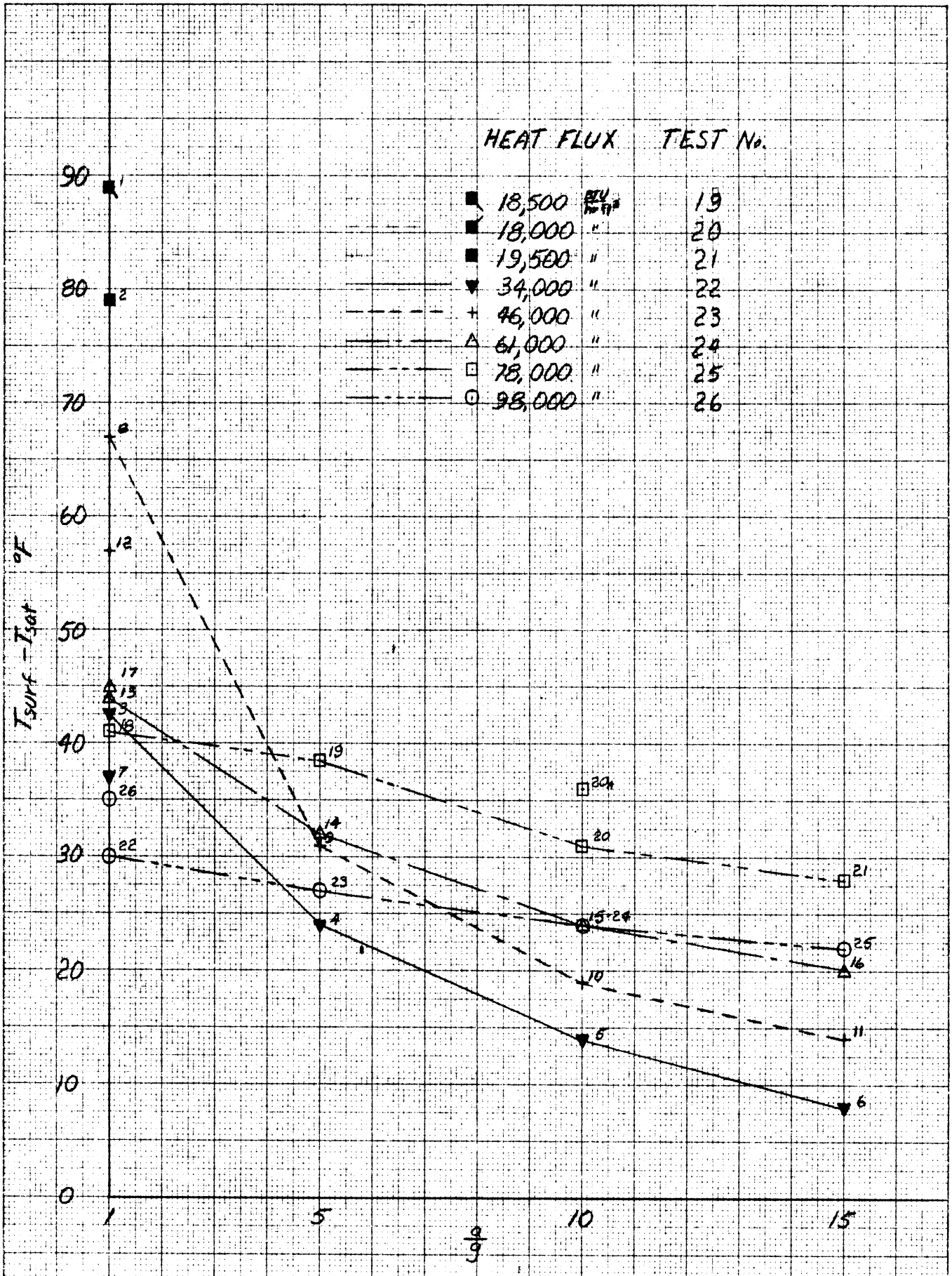

FIGURE 52. COMPOSITE OF BOILING MERCURY DATA UNDER HIGH ACCELERATION FOR NOMINAL P = 75 PSIA.

BIBLIOGRAPHY

1. Addoms, J. N. Sc.D. Thesis in Chemical Engineering, Massachusetts Institute of Technology. 1948.

2. Anderson, G. H. and Mantzouranis, B. G. "Two-Phase (Gas-Liquid) Flow Phenomena--I. Pressure Drop and Holdup for Two-Phase Flow in Vertical Tubes." Chemical Engineering Science. Vol. 12, 1960, p. 109.

3. Baker, O. "Simultaneous Flow of Oil and Gas." Oil and Gas Journal. Vol. 52, No. 14, 1954, p. 185.

4. Balzhiser, R. E. et al. "Investigation of Liquid Metal Boiling Heat Transfer." United States Air Force Systems Comman, Wright-Patterson Air Force Base, Ohio, Report RTD-TDR-63-4130, November 1963.

5. Bankoff, S. G. "A Variable Density Single Fluid Model for Two-Phase Flow with Particular Reference to Steam-Water Flow." Journal of Heat Transfer. Vol. 82, 1960, p. 265.

6. Baroczy, C. J. "Correlation of Liquid Fraction in Two-Phase Flow with Application to Liquid Metals." NAA-SR-8171. Atomics International, Div. of North American Aviation, Inc., Canoga Park, California. April 15, 1963.

7. Berenson, P. J. and Killackey, J. J. "An Experimental Investigation of Forced-Convection Vaporization of Potassium." Presented at Third Annual High-Temperature Liquid Metal Heat Transfer Technology Conference, Oak Ridge National Laboratory, September 4-6, 1963. Proceedings to be published.

8. Bertuzzi, A. F., Tek, M. R. and Poettmann, F. H. "Simultaneous Flow of Liquid and Gas Through Horizontal Pipe." Journal of Petroleum Technology. Vol. 8, January 17, 1956.

9. Bonilla, C. F. et al. "Reactor Heat Transfer Conference of 1956." TID-7529 Part 1, Book 2, November 1957, pp. 324-341.

10. Brooks, R. D. and Bonilla, C. F. "Liquid Metal Heat Transfer Nucleonics, Vol. 22, No. 3, March 1964.

11. Calvert, S. and Williams, B. "Upward Cocurrent Annular Flow of Air and Water in Smooth Tubes." AIChE Journal. Vol. 1, 1955, p. 78.

12. Carbon, M. W. AEC and University of Wisconsin, Report, May 30, 1964.

13. Colver, C. P. "A Study of Saturated Pool Boiling Potassium up to Burnout Heat Fluxes." Ph.D. Thesis in Chemical Engineering, The University of Michigan, September, 1963.

14. Deissler, R. G. "Analytical and Experimental Investigation of Adiabatic Turbulent Flow in Smooth Tubes." NACA TN2138, 1950.

15. Deissler, R. G. and Eian, C. S. "Analytical and Experimental Investigation of Fully Developed Turbulent Flow of Air in a Smooth Tube with Heat Transfer with Variable Fluid Properties." NACA TN2629, 1952.

16. Deissler, R. G. "Analysis of Fully Developed Heat Transfer at Low Peclet Numbers in Smooth Tubes with Application to Liquid Metals." NACA RME52F05, 1952.

17. Deissler, R. G. "Analysis of Turbulent Heat Transfer and Flow in Entrance Regions of Smooth Passages." NACA TN3016, 1953.

18. Dukler, A. E. "Fluid Mechanics and Heat Transfer in Vertical Falling Film Systems." ASME-AIChE Third National Heat Transfer Conference. August, 1959.

19. Dzhelepov. B. S. and Peker, L. K. Decay Schemes of Radioactive Nuclei. Pergamon Press, New York, New York, 1961, pp. 497-499.

20. Fisher, C. R. "Heat Transfer and Pressure Drop Characteristics for Boiling Rubidium in Forced Convection." Presented atThird Annual High-Temperature Liquid Metal Heat Transfer Technology Conference, Oak Ridge National Laboratory, September 4-6, 1963. Proceedings to be published.

21. Goldmann, D. "Selected Parameters for Two-Phase Flow of Sodium." Presented at Third Annual High Temperature Liquid Metal Heat Transfer Technology, Oak Ridge National Laboratory, September 4-6, 1963. Proceedings to be published.

22. Govier, G. W. and Omer, M. M. "The Horizontal Pipeline Flow of Air-Water Mixtures." Canadian Journal of Chemical Engineering. Vol. 40, 1962, p. 93.

23. Herrick, R. "Liquid Metal Heat Transfer by Forced Convection - A Literature Survey." United Kingdom Atomic Energy Authority, TRG Report 546 (R), 1964.

24. Hewitt, G. F., King, I. and Lovegrove, P. C. "Holdup and Pressure Drop Measurements in the Two-Phase Annular Flow of Air-Water Mixtures." British Chemical Engineering. Vol. I, 1963, p. 311.

25. Hoffman, H. W. "Recent Experimental Results in ORNL Studies with Boiling Potassium." Presented at Third Annual High-Temperature Liquid Metal Heat Transfer Technology Conference, Oak Ridge National Laboratory, September 4-6, 1963. Proceedings to be published.

26. Howell, J. R. and Bell, K. J. "Chemical Engineering Progress Symposium Series." No. 41, Vol. 59, 1963, pp. 88-95.

27. Isbin, H. S., Moen, R. H. and Mosher, D. R. "Two-Phase Pressure Drops." United States Atomic Energy Commission, Report AECU-2994, November 1954.

28. Isbin, H. S., Sher, N. C. and Eddy, K. C. "Void Fractions in Two-Phase Steam-Water Flow." AIChE Journal. Vol. 3, 1957, p. 136.

29. Johnson, H. A. and Abou-Sabe, A. H. "Heat Transfer and Pressure Drop for Turbulent Flow of Air-Water Mixtures in a Horizontal Pipe." ASME Transactions. Vol. 74, 1952, p. 977.

30. Kazakova, E. A. "The Influence of Pressure on the First Crisis in Boiling Water From a Flat Surface." G.E.I., Moscow, 1953.

31. Koestell, A. Thompson-Ramo-Wooldridge, Inc., Cleveland, Ohio. Tabulated data which had been previously published in TRW, Report ER-4104, June, 1960. Private Communication, January 1964.

32. Kutateladze, S. S. et al. Liquid Metal Heat Transfer Media. Atomaya Energiia, Supplement No. 2. Translated by Consultants Bureau, Inc., New York, New York, 1959.

33. Levy, S. "Prediction of Two-Phase Pressure Drop and Density Distribution From Mixing Length Theory." Journal of Heat Transfer. Vol. 85, May, 1963, p. 137.

34. Linning, D. L. "The Adiabatic Flow of Evaporating Fluids in Pipes of Uniform Bore." Institution of Mechanical Engineers. London. Proceedings (B). 1952, p. 64.

35. Lockhart, R. W. and Martinelli, R. C. "Proposed Correlation of Data for Isothermal Two-Phase, Two-Component Flow in Pipes." Chemical Engineering Progress. Vol. 45, 1949, p. 39.

36. Martinelli, R. C. "Heat Transfer to Molten Metals." Transactions ASME. Vol. 69, No. 8, November, 1947, pp. 947-59.

37. Martinelli, R. C. and Nelson, D. B. "Prediction of Pressure Drop During Forced-Circulation Boiling of Water." Transactions ASME. Vol. 70, 1948, p. 695.

38. Merte, H. and Clark, J. A. "Pool Boiling in an Accelerating System." Journal of Heat Transfer. Transactions ASME. Series C. Vol. 83, August, 1961, pp. 223-242.

39. Neal, L. G. and Bankoff, S. G. "A High Resolution Resistivity Probe for Determination of Local Void Properties in Gas-Liquid Flow." Presented at 55th Annual Meeting of AIChE. Chicago. December 2-6, 1962.

40. Neal, L. G. "Local Parameters in Cocurrent Mercury-Nitrogen Flow." ANL-6625. January, 1963.

41. Noyes, R. C. "Summary of Recent Results of Sodium Boiling Studies." Presented at Third Annual High-Temperature Liquid Metal Heat Transfer Technology Conference, Oak Ridge National Laboratory. September 4-6, 1963. Proceedings to be published.

42. Noyes, R. C. "An Experimental Study of Sodium Pool Boiling Heat Transfer." Journal of Heat Transfer. Transactions ASME. Series C. Vol. 85, May, 1963, p. 125.

43. Noyes, R. C. and Lurie, H. "Boiling Studies for Sodium Reactor Safety." Part II., NAA-SR-9477, October, 1964.

44. Pike, R. W. "The Adiabatic, Evaporating, Two-Phase Flow of Steam and Water in Horizontal Pipe." Ph.D. Thesis, Georgia Institute of Technology. 1962.

45. Poppendiek, H. F., Greene, N. D., MacDonald, F. R., Sabin, C. M., Livett, R. K. and Thompson, A. S. "Annual Technical Report on High Acceleration Field Heat Transfer for Auxiliary Space Nuclear Power Systems." (AEC Contract No. AT(04-3)-409). September 1, 1962.

46. "Proceedings of the 1962 High-Temperature Liquid-Metal Heat Transfer Technology Meeting." Brookhaven National Laboratory, Upton, New York. Report BNL-756 (c-35). May 17-18, 1962.

47. Reid, R. C., Reynolds, A. B., Diglio, A. J., Spiewak, I. and Klipstein, D. H. "Two-Phase Pressure Drops in Large-Diameter Pipes." AIChE Journal. Vol. 3, 1957, p. 321.

48. Richardson, B. L. "Some Problems in Horizontal Two-Phase, Two-Component Flow." ANL-5949. December, 1958.

49. Rohsenow, W. M. and Griffith, P. "Correlation of Maximum Heat Flux Data for Boiling of Saturated Liquids." Chap. 9 of Heat, Mass and Momentum Transfer. W. M. Rohsenow and H. Y. Choi. Prentice-Hall, New York, New York. 1961.

50. Ros, N. C. J. "Simultaneous Flow of Gas and Liquid as Encountered in Well Tubing." Transactions Soc. Pet. Eng. of AIME. Vol. 222, 1961, p. 1037.

51. Rouse, H., Editor. Advanced Mechanics of Fluids. Wiley, New York, 1959. Chapter 1.

52. Smith, C. R., Tang, Y. S. and Walker, C. L. "Slip Velocity in Two-Phase Metallic Fluids." Allison Division, General Motors Corporation. Indianapolis, Indiana. Engineering Department Report No. 2809. May 25, 1962.

53. Smith, L. R. "A Study of Pressure Drops and Void Fractions in Horizontal Two-Phase Flows of Potassium (8 per cent Sodium)." Ph.D. Thesis, The University of Michigan. April, 1964.

54. Subbotin, V. I. et al "Heat Transfer from the Turbulent Flow of Liquid Metals in Tubes." Atomnaya Energiya, II. No. 2, August, 1961, pp. 133-139.

55. Tang, Y. S., Smith, C. R. and Ross, P. T. "Potassium-Mercury Amalgam Boiling Heat Transfer, Two-Phase Flow, and Properties Investigation." Allison Division, General Motors Corporation. Indianapolis, Indiana. Engineering Department Report No. 3549. September 16, 1963.

56. Tek, M. R. The University of Michigan. Department of Chemical and Metallurgical Engineering. Private communication, January 1964.

57. Van Wijk, et al. Chemical Engineering Science. Vol. 5, 1956, pp. 68-80.

58. Volk, Wm. Applied Statistics for Engineers. McGraw-Hill, New York, 1958, Chapter 8.

59. Weatherford, W. D., Tyler, J. C. and Ku, P. M. "Properties of Inorganic Energy-Conversion and Heat Transfer Fluids for Space Applications." United States Air Force, WADD Technical Report 61-96. November, 1961.

60. Zuber, N. and Tribus, M. "Further Remarks on the Stability of Boiling Heat Transfer." AECU-3631. January, 1958.